

Electroforming and switching of organic-inorganic resistive memories

Citation for published version (APA):

Bory, B. F. (2014). *Electroforming and switching of organic-inorganic resistive memories*. [Phd Thesis 1 (Research TU/e / Graduation TU/e), Chemical Engineering and Chemistry]. Technische Universiteit Eindhoven. <https://doi.org/10.6100/IR766435>

DOI:

[10.6100/IR766435](https://doi.org/10.6100/IR766435)

Document status and date:

Published: 01/01/2014

Document Version:

Publisher's PDF, also known as Version of Record (includes final page, issue and volume numbers)

Please check the document version of this publication:

- A submitted manuscript is the version of the article upon submission and before peer-review. There can be important differences between the submitted version and the official published version of record. People interested in the research are advised to contact the author for the final version of the publication, or visit the DOI to the publisher's website.
- The final author version and the galley proof are versions of the publication after peer review.
- The final published version features the final layout of the paper including the volume, issue and page numbers.

[Link to publication](#)

General rights

Copyright and moral rights for the publications made accessible in the public portal are retained by the authors and/or other copyright owners and it is a condition of accessing publications that users recognise and abide by the legal requirements associated with these rights.

- Users may download and print one copy of any publication from the public portal for the purpose of private study or research.
- You may not further distribute the material or use it for any profit-making activity or commercial gain
- You may freely distribute the URL identifying the publication in the public portal.

If the publication is distributed under the terms of Article 25fa of the Dutch Copyright Act, indicated by the "Taverne" license above, please follow below link for the End User Agreement:

www.tue.nl/taverne

Take down policy

If you believe that this document breaches copyright please contact us at:

openaccess@tue.nl

providing details and we will investigate your claim.

Electroforming and switching of organic-inorganic resistive memories

PROEFSCHRIFT

ter verkrijging van de graad van doctor aan de Technische Universiteit Eindhoven, op gezag van de rector magnificus prof.dr.ir. C.J. van Duijn, voor een commissie aangewezen door het College voor Promoties, in het openbaar te verdedigen op dinsdag 4 maart 2014 om 16:00 uur

door

Benjamin François Bory

geboren te Grenoble, Frankrijk

Dit proefschrift is goedgekeurd door de promotoren en de samenstelling van de promotiecommissie is als volgt:

voorzitter:	prof.dr.ir. J.C. Schouten
1 ^e promotor:	prof.dr.ir. R.A.J. Janssen
2 ^e promotor:	prof.dr. D.M. de Leeuw (Max Planck Institute)
copromotor:	dr. S.C.J. Meskers
leden:	prof.dr.ir. W.A. Groen (Technische Universiteit Delft)
	dr. H.L. Gomes (Universidade do Algarve)
	prof.dr. G. de With

Printed by Gildeprint Drukkerijen, The Netherlands

A catalogue record is available from the Eindhoven University of Technology Library
ISBN: 978-90-386-3565-1

This research forms part of the research programme of the Dutch polymer
institute (DPI), project #704

Table of Contents

1. Introduction.....	9
1.1 The memory challenge.....	10
1.2 Current state-of-the-art NAND flash	10
1.3 Alternative ReRAM and memristor technology	11
1.3.1 Wide bandgap inorganic semiconductors	12
1.3.2 Organic semiconductors	13
1.4 Organic-inorganic junctions for memristors	14
1.4.1 Ohmic contacts in organic electronic devices	14
1.5 Technological potential of organic memristors	15
1.6 Aim and outline of the thesis	16
1.7 References.....	18
2. Electroforming and resistive switching in unipolar memristors	21
2.1 Introduction.....	22
2.2 Memory structure.....	24
2.3 Electroforming	24
2.3.1 Early stage: charge trapping and tunneling	26
2.3.2 Reversible dielectric breakdown.....	29
2.3.3 Memristor formation	35
2.4 Filamentary conduction	36
2.5 Switching dynamics.....	39
2.6 Operation mechanism	43
2.7 Practical consequences.....	50
2.8 Summary and conclusion.....	52
2.9 References.....	53
3. Trapping of electrons in metal oxide-polymer memory diodes in the initial stage of electroforming	57
3.1 Introduction.....	58
3.2 Experimental	58
3.3 Results.....	59
3.4 Discussion.....	61

3.5 Conclusion	62
3.6 References.....	63
4. Accumulation of charge at the LiF/organic semiconductor interface in the early stage of electroforming	65
4.1 Introduction.....	66
4.2 Experimental	68
4.2.1 Materials and device fabrication.....	68
4.2.2 Thickness characterization.....	68
4.2.3 Opto-electrical measurements	69
4.3 Results and discussion	69
4.4 Conclusion	84
4.5 References.....	85
5. Role of hole injection in electroforming of LiF/polymer memory diodes.....	87
5.1 Introduction.....	88
5.2 Experimental	88
5.3 Results and discussion	89
5.4 Conclusion	96
5.5 References.....	97
6. Electroforming in MIM diodes containing alkali halide-poly(spirofluorene) bilayer as insulator involves hole injection	99
6.1 Introduction.....	100
6.2 Materials and device fabrication	101
6.3 Results and Discussion	102
6.3.1 Electrical characterization.....	102
6.3.2 Optical characterization.....	105
6.3.3 Metal/CsI/metal diodes.....	107
6.3.4 Correlation between defect formation and electroforming.....	109
6.3.5 Electroluminescence characterization	111
6.4 Conclusion	113
6.5 References.....	114

7. Lithium fluoride injection layers can form quasi-Ohmic contacts for both holes and electrons.....	115
7.1 Introduction.....	116
7.2 Experimental.....	116
7.3 Results and discussion	117
7.4 Conclusion	129
7.5 References.....	130
Summary.....	131
Samenvatting.....	135
Résumé.....	139
Curriculum Vitae.....	143
List of publications.....	145
Acknowledgements	147

Chapter 1

Introduction

Abstract

The continuing growth of the amount of information people want to store raises a demand for efficient and cheap data storage technology. To meet this demand, research and development of next-generation memory technology is currently undertaken by industry and academia. A brief description of emerging technologies for data storage based on resistive memory is presented. The opportunities and possible advantages of organic semiconducting materials in resistive random access memories (ReRAM), also called memristors, are discussed. The aim and outline of the thesis are then described.

1.1 The memory challenge

Since information technology has progressively moved from analog to digital, the need for digital information storage has exploded. From 1986 to 2007, the capacity installed to store information increased by a factor of 100 to reach 290 exabytes. This corresponds to a growth of stored data per capita from half a GB to about 45 GB.^[1] In the same time interval, the digital to analog storage ratio went from less than 1% up to 94%. Magnetic-based devices such as hard disk drives (HDD) and optical media such as CDs, DVDs, and Blu-Ray, represent more than two-thirds of the total storage capacity. Today, with the improvement of the capacity to telecommunicate information on mobile devices, the demand for data storage capacity in mobile devices has grown considerably.^[2,3] Mobile phones, smartphones, digital cameras, and tablets make use of high-density data storage and require low-power, low-weight, thin, and robust memories.^[3] Solid-state memories based on silicon floating-gate transistors, also called NAND-flash in computational logic, are the standard for mobile devices.^[2] The motivation for NAND-flash development has been the cost reduction through scaling down of the component size. The price per MB has decreased by 7 orders of magnitude during the past 2 decades.^[4] However the continuing down scaling seems to approach a limit^[5,6] due to parasitic effects between the cells because of their close proximity.^[7] This opens a new challenge for both academic and industrial researchers in order to replace floating gate transistor memories by an alternative technology with even better performances and characteristics.^[4] NAND-flash relies on the storage of charges. For new technologies, researchers are focusing on electric field induced changes in ferroelectric polarization, magnetization, phase, and electrical resistance. Devices involving voltage induced changes in resistance are also referred to as resistive random-access memories (ReRAM).^[4] ReRAM is based on two-terminal cells which have a resistance determined by their operation history and are also referred to as memristors.^[8]

In the next sections of this introduction, the current standard floating-gate transistor will be discussed in more detail, including its limitations and problems. Alternative ReRAM technologies are then described. Emphasis is put on opportunities for molecular materials in the development of memories.

1.2 Current state-of-the-art NAND flash

Floating-gate transistors are the basic building blocks for solid-state NAND-flash digital information storage (Fig. 1.1a) and were first reported by Sze in 1967.^[9] They are transistors that contain a macroscopic trap for charge carriers, the floating gate. The floating gate is embedded in the gate insulator, usually a metal-oxide dielectric. Floating-gate transistors can be programmed into different states by application of a bias voltage between source and gate. Because of the high electric field, electrons can tunnel between the gate and the floating gate. At low applied bias, the charge on the floating gate remains

trapped. In the floating-gate transistor, the electrical conductivity between the source and drain is modulated by the amount of charge that is trapped on the *floating gate*. Read-out of the transistor is non-destructive and data retention times are long. Doped silicon is used as semiconductor and silicon oxide serves as insulating material for the floating gate to be electrically insulated from the electrical contacts.

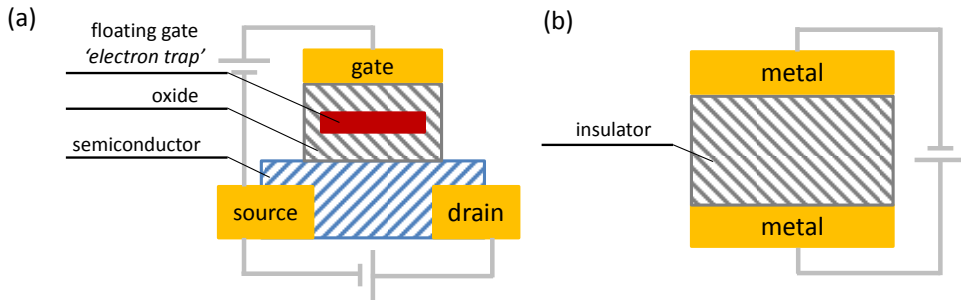


Figure 1.1: Schematic representation of (a) a floating-gate transistor structure and (b) a memristive diode structure.

Improvements in storage density and lowering the costs together with the power consumption have been achieved by downscaling. The effective area per stored bit for floating-gate transistor technology was $2 \times 10^5 \text{ nm}^2$ in 2000 and is expected to go down to about $2 \times 10^2 \text{ nm}^2$ by 2020.^[4] However, downscaling is limited by the minimum distance needed between two floating gates to avoid crosstalk or floating-gate interference.^[2] Actual silicon based floating-gate transistors can hardly tolerate a gate-to-gate spacing less than 40 nm.^[7] The use of high-*k* dielectrics as insulating material allows for further improvement but does not remove the basic limitations.^[10] The increase in number of bit errors due to floating-gate interferences resulting from downscaling can, to some extent, be compensated by the use of error correction algorithms in the software driving the memory array.^[11]

1.3 Alternative ReRAM and memristor technology

The search for new technologies for the next generation of solid-state memories has led to the development of memory cells featuring a programmable electrical resistance. This new class of memories is referred to as ReRAM or memristor.^[12] A memristor has two electrical terminals and is a resistor whose resistance depends on its operation history.^[8] Memristors with non-volatile change of resistance and non-destructive read-out can be used to store information.^[13]

Typically, memristors have a metal/insulator/metal (MIM) structure (Fig. 1.1b). The MIM diode can be switched between states of high and low resistance by applying voltage pulses of selected amplitude and polarity. Changing the resistance by application of voltage is also called resistive switching. For some memristors, pulses to raise and

lower the resistance can be of the same sign (unipolar memristor). Bipolar memristors require voltage pulses of different polarity to switch the resistance.^[13] We note that unipolar memristors require a decrease in current density with increasing voltage in the voltage range for switching. The decrease of current density with increasing voltage is referred to as negative differential resistance (NDR).

Many mechanisms can lead to resistive switching. Proposed mechanisms include *e.g.* thermal, chemical, and electrostatic/electronic effects.^[14] Properties of the insulator material in the MIM stack are crucial. It has been found that an astonishingly large variety of insulating materials can give rise to memristive effects. Below we discuss two main classes of materials that have been utilized.

1.3.1 Wide bandgap inorganic semiconductors

Many of the insulator materials in memristors are wide bandgap oxides. In the MIM stack, these materials are usually highly insulating because the conduction band (CB) and valence band (VB) edges do not match with commonly used metals. However, by growing layers of Al_2O_3 , Ta_2O_5 , ZrO_2 , or TiO_2 anodically, MIM diodes showing NDR properties could be prepared in a reproducible manner.^[15] Also evaporated SiO_x could be used. In 1967, Simmons and Verderber demonstrated experimentally that SiO_x MIM diodes showing NDR also feature non-volatile memory effects in their electrical conductivity.^[16] Following the prediction of Hickmott, that NDR may be observed in MIM diodes with an alkali halide insulator, Biedermann could demonstrate NDR and resistive switching memory characteristics for lithium fluoride (LiF).^[17]

Many studies have shown that resistive switching behavior in MIM diodes requires electroforming. The electroforming involves applying a high bias voltage to the MIM diode such that the insulator is close to dielectric breakdown.^[18]

Electroforming of metal-oxide memristors results in the formation of large numbers of defects in the dielectric and is also referred to as ‘soft breakdown’.^[19] Clustering of defects in filaments seems necessary to reach resistive switching properties.^[20] Resistive switching seems to be associated with redistribution of the defects leading to disruption of the conducting filament. It is not clear whether the disruption occurs at the interface between insulator and metal or in the bulk of the insulator. The mechanism of electroforming is not completely understood, may vary for different materials and may depend on the metal electrodes used.

Control over the electroforming process is of great practical importance. The yield of functioning memristor devices essentially relies on the success of the electroforming step of the fabricated two-terminal cells. The metal-oxide MIM diodes are susceptible to permanent shorting (hard breakdown). This may result from *e.g.* overheating and migration of metal during electroforming or memory operation. During operation and electroforming, currents through oxide-memristors have to be tightly controlled.

1.3.2 Organic semiconductors

Organic semiconductors are carbon rich materials. Organic molecules with alternation of single and double bonds feature delocalized π -orbitals for electrons. The semiconducting properties of the organic semiconductors originate from electrons in delocalized π -orbitals. The extended orbitals permit electron transport along the conjugated backbone. Overlap of orbitals on neighboring molecules allows for hopping of carriers between molecules. Important for opto-electronic properties are the highest occupied molecular orbital (HOMO) and the lowest unoccupied molecular orbital (LUMO) as illustrated in Fig. 1.2a. The HOMO is involved in transport of holes and the LUMO in the transport of electrons. Combination of an electron in the LUMO with a hole in the HOMO of the same molecule gives rise to excited states (excitons) that can emit light. Oxygen and water impurities form trap sites for electrons. As a consequence, electron transport in organic semiconductors is often trap limited.^[21] Transport of holes in purified organic semiconductors is often less affected by extrinsic traps and is often limited by space-charge effects.^[22]

In Fig. 1.2 we show polymeric organic semiconductors that are used in this thesis. Poly(3-hexylthiophene) shown in Fig. 1.2b has an energy gap between the HOMO and LUMO of $E_g = 1.9$ eV.^[23] Spirofluorene polymers (Fig 1.2c) have larger bandgaps: $E_g = 2.8$ eV.

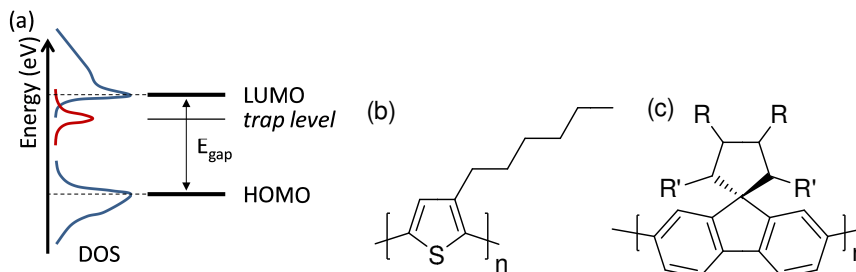


Figure 1.2: (a) Schematic representation of the density of states for a semiconducting polymer, showing the HOMO, LUMO and trap level within the bandgap. Chemical structure of (b) poly(3-hexylthiophene) and (c) poly(spirofluorene).

A large variety of organic semiconductors has been used as insulator in memristors with MIM configuration. No clear correlation between resistive switching properties and molecular structure could be found. A number of studies have indicated the importance of interfaces and interlayers in the resistive switching of memristors incorporating organic semiconductors.^[18,24] Deliberate insertion of metal-oxide interlayers, metal nanoparticles, or metal layers in the MIM structure, has been found to give reproducible and reliable resistive switching properties.^[25]

1.4 Organic-inorganic junctions for memristors

A number of studies, ^[26,27] including the work by Verbakel in our laboratory, ^[28] have shown that very reliable and reproducible resistive memories can be obtained by combining organic and wide bandgap inorganic materials as insulators in the MIM stack (Fig. 1.3b).

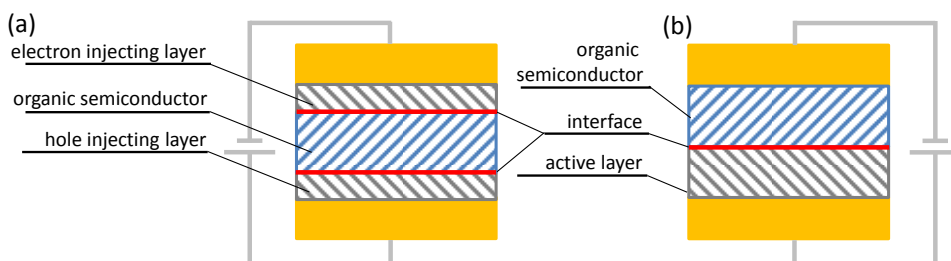


Figure 1.3: (a) Typical structure of an organic-inorganic diode. (b) Typical structure of an organic-inorganic memristor.

It has been argued that resistive switching involves defects in the oxide and that the organic semiconductor is important in limiting the current densities to prevent hard breakdown. In this thesis we follow this lead and study electroforming and resistive switching involving organic/metal oxide and organic/alkali halide junctions. Our hypothesis is that resistive switching and electroforming involve processes occurring at the interface of organic and inorganic materials. Alkali halides provide a series of ionic bandgap semiconductors that can be used for systematic variation of the electron energy levels at the organic/inorganic junction. We find that accumulation of defects in the alkali halide can lead to formation of quasi-Ohmic contacts in the memristor. Formation of Ohmic contacts involving organic semiconductor and metal-oxides or alkali halides has been studied intensively in the context of organic electronics. Below we give a brief overview on this topic.

1.4.1 Ohmic contacts in organic electronic devices

Organic semiconductors can be used as active material in light-emitting diodes, photovoltaic cells, and transistors.^[29] The electrical contact with the organic semiconductor is crucial in determining efficiency and stability. In fact, organic electronic devices require Ohmic contacts for their utmost performances. An Ohmic contact can, in theory, provide an unlimited number of charge carriers without energy dissipation. An Ohmic contact may be realized by the incorporation of specific interlayers. The interlayer between organic semiconductor and metal electrode can allow for efficient injection and

collection of electrons (e.g. LiF^[30], ZnO,^[31] TiO₂^[32]) or holes (e.g. Poly(3,4-ethylenedioxythiophene) poly(styrenesulfonate) (PEDOT:PSS)^[31], MoO₃^[32], V₂O₃^[32]) see Fig. 1.3a. As will become clear in this thesis, there is a close link between formation of an Ohmic contact between organic semiconductors and inorganic interlayers and electroforming in organic/inorganic hybrid MIM diodes.

The formation of an Ohmic contact between organic and inorganic layers may be explained in terms of doping of the layers, as observed for e.g. PEDOT:PSS and ZnO. High doping densities are required. Interestingly, the formation of Ohmic contacts is also reported after electroforming. Therefore it seems, apart from relying on spontaneous doping of the semiconductors used, that also electroforming of interlayers may be used to establish an Ohmic contact.^[33]

1.5 Technological potential of organic memristors

The performance of memristors incorporating organic semiconductors in combination with inorganic materials has been assessed by several research groups. Table 1.1 shows a selection of state-of-the-art characteristics and projections for such organic memristors and for conventional NAND-flash memory elements.

Table 1.1: Selected characteristics and projections of NAND-flash memory elements compared with the memristor incorporating organic materials.

	NAND-flash ^[34]		Memristor incorporating organic materials	
	2011	2024	2013	Best projected
Feature size (nm)	22	8	5 ^[26]	5
Read voltage (V)	1.8	1	0.2 ^[35]	< 0.1
Write voltage (V)	15	15	1.4 ^[35]	1
W/E time	1 / 0.1 ms	1 / 0.1 ms	15 ns ^[36]	< 10 ns
Write cycles	10⁴	5 × 10³	>10⁵ ^[37]	>10⁵
Write energy (J/bit)	2 × 10⁻¹⁶	2 × 10⁻¹⁷	1 × 10⁻¹⁴ ^[30,38]	1 × 10⁻¹⁶ ^[26]

Table 1.1 highlights drawbacks of NAND-flash technology. The individual memory cells still have relatively large feature size, require long write/erase time, and use high voltage for writing. The organic memristor technology shows promising characteristics with respect to feature size and operation voltages. Excellent cycle endurance can be achieved and time intervals for single writing and erasing events are short.^[36] We note that repeated writing and erasing may be limited by processes with characteristic times much longer than indicated in Table 1.1 (ms).^[39]

In order to be a viable alternative technology for floating-gate transistors

memories, organic memristors will have to show superior characteristics with respect to size, speed, and cost per bit.^[4] A major drawback of the memristor technology is the initial electroforming step that is required before switching occurs.^[40] The fabrication of memristive devices is compatible with the use of standard lithography technologies.^[41] Key opportunities for hybrid organic resistive memory list low cost of raw materials and of deposition methods, e.g. printing and coating. Integration of memory cells into 3D stacks has been accomplished.^[42] Furthermore, memory cells incorporating environmentally friendly materials can be realized. This primes application and integration in low-end, disposable electronics on e.g. flexible substrate such as paper or plastic.

1.6 Aim and outline of the thesis

The aim of the thesis is to understand the electroforming in metal/ inorganic semiconductor/ organic semiconductor/ metal devices. The hypothesis that the organic/inorganic interface plays an active role in the electroforming and memory operation, is investigated throughout the thesis.

The role of the different layers will be addressed by varying the thickness of the layers and their chemical composition. Electrical and optical characterization techniques are utilized to identify any changes in conductivity, capacitance, absorption, and luminescence during electroforming. Changes in electrical and optical characteristics will be interpreted in terms of modifications to the electronic structure of the materials due to formation of defects with electronic levels within the electronic gap of the materials.

An explanation of electroforming and the related electronic memory effects will be attempted in terms of density, distribution, and ionization state of defects within the memristor. Based on experimental evidence, we will divide the electroforming into sub-processes that follow each other up in time and involve different types of charge carriers, defects, and energy levels. Also the memristive effect is eventually interpreted in terms of sub-processes that follow each other up in time in a conditional sequence determined by the mutual interactions between charge carriers involved and the applied potential. The thesis is organized as follows:

Chapter 2 is an explanatory account of research done on the electroforming and switching of unipolar memristors. The overview described in this chapter is based on a collaborative research effort on Al_2O_3 / polymer memories. The focus on unipolar operation is motivated by the fact that this type of switching is observed in all hybrid organic memory diodes investigated in this thesis. Experimental evidence for defect formation in the inorganic material and the crucial role of the organic/inorganic interface in memory operation are summarized.

In Chapter 3, devices with Al_2O_3 in combination with a blue-light emitting semiconducting polymer are studied using quasi-static capacitance voltage measurements. We identify accumulation and trapping of electrons at the Al_2O_3 /polymer interface as an

initial step of the electroforming process. Chapter 4 also focuses on the early stage of the electroforming in which quasi-reversible charging and discharging processes of the LiF/polymer interface occurs. Spectroscopic methods are used to study trapping of electrons at the LiF/polymer interface. Current transients indicate the formation of a highly doped region in the LiF near the LiF /polymer interface with a width of about 10 nm.

While Chapter 4 focuses on the initial stages of electroforming, in Chapter 5 we discuss the final stage of electroforming in metal/ LiF/ polymer/ Ba/ Al diodes. The observation of electroluminescence marks a dramatic change in transport characteristics of the LiF layer. While LiF is commonly used as electron injection/collection layer, our measurements indicate that upon electroforming, LiF can turn into a quasi-Ohmic contact for holes.

Chapter 6 extends the investigations of Chapter 5 to other alkali-halide materials. We identify corresponding electrical processes in various alkali halides and investigate the formation of defects. Voltages required for electroforming and induction of defects in a series of alkali halides correlate with the energy of the valence band edge.

Chapter 7 shows that the electroforming process can be used to establish quasi-Ohmic injecting contacts for both holes and electrons from LiF into organic semiconductors. The formation of defects in LiF induced by electrical bias appears to be crucial. Depending on the ionization state of the defects, either positive or negative charge carriers can be injected. As a result, metal/ LiF/organic semiconductor/LiF/metal diodes show electroluminescence for both positive and negative applied bias voltages. This chapter establishes a link between electroforming and Ohmic contact in organic diodes.

1.7 References

- [1] M. Hilbert and P. Lopez, *Science* **2011**, 332, 60.
- [2] T. Mikolajick, N. Nagel, S. Riedel, T. Mueller, and K.-H. Kusters, *Mater.-Sci.-Poland* **2007**, 25, 33.
- [3] C.-G Hwang, *P. IEEE* **2003**, 91, 1765.
- [4] G. W. Burr, B. N. Kurdi, J. C. Scott, C. H. Lam, K. Gopalakrishnan, and R. S. Shenoy, *IBM J. Res. Dev.* **2008**, 52, 449.
- [5] K. Prall, *P. IEEE NVSMW* **2007**, 2, 5.
- [6] Y. Fujisaki, *Jap. J. Appl. Phys.* **2013**, 52, 040001.
- [7] J.-D. Lee, S.-H. Hur, and J.-D. Choi, *IEEE Electr. Device L.* **2002**, 23, 264.
- [8] L. Chua, *Appl. Phys. A* **2011**, 102, 765.
- [9] D. Kahng and S. M. Sze, *AT&T Tech. J.* **1967**, 46, 1288.
- [10] K. Mistry, C. Allen, C. Auth, B. Beattie, D. Bergstrom, M. Bost, M. Brazier, M. Buehler, A. Cappellani, R. Chau, C.-H. Choi, G. Ding, K. Fischer, T. Ghani, R. Grover, W. Han, D. Hanken, M. Hattendorf, J. He, J. Hicks, R. Huessner, D. Ingerly, P. Jain, R. James, L. Jong, S. Joshi, C. Kenyon, K. Kuhn, K. Lee, H. Liu, J. Maiz, B. McIntyre, P. Moon, J. Neiryneck, S. Pae, C. Parker, D. Parsons, C. Prasad, L. Pipes, M. Prince, P. Ranade, T. Reynolds, J. Sandford, L. Shifren, J. Sebastian, J. Seiple, D. Simon, S. Sivakumar, P. Smith, C. Thomas, T. Troeger, P. Vandervoorn, S. Williams, and K. Zawadzki, *IEEE IEDM* **2007**, 247-250.
- [11] S. Tanakamaru, A. Esumi, M. Ito, L. Kai, and K. Takeuchi, *P. IEEE IMW* **2010**, 1, 16.
- [12] D. B. Strukov, G. S. Snider, D. R. Stewart, and R. S. Williams, *Nature* **2008**, 453, 80.
- [13] C. Kuegeler, R. Rosezin, E. Linn, R. Bruchhaus, and R. Waser, *Appl. Phys. A* **2011**, 102, 791.
- [14] R. Waser, R. Dittman, G. Staikov, and K. Szot, *Adv. Mat.* **2009**, 21, 2632.
- [15] T. W. Hickmott, *J. Appl. Phys.* **1962**, 33, 2669.
- [16] J. G. Simmons and R. R. Verderber, *Proc. R. Soc. London, Ser. A* **1967**, 301, 77.
- [17] H. Biederman, *Vacuum* **1976**, 26, 513.
- [18] F. Verbakel, S. C. J. Meskers, R. A. J. Janssen, H. L. Gomes, M. Cölle, M. Büchel, and D. M. de Leeuw, *Appl. Phys. Lett.* **2007**, 91, 192103.
- [19] T. W. Hickmott, *J. Appl. Phys.* **2012**, 112, 073717.
- [20] R. Waser and M. Aono, *Nat. Mater.* **2007**, 6, 833.
- [21] H. T. Nicolai, M. Kuik, G. A. H. Wetzelaer, B. de Boer, C. Campbell, C. Risko, J. L. Brédas, and P. W. M. Blom, *Nat. Mater.* **2012**, 11, 882.
- [22] C. Tanase, E. J. Meijer, P. W. M. Blom, and D. M. de Leeuw, *Phys. Rev. Lett.* **2003**, 91, 216601.
- [23] R. Kroon, M. Lenes, J. C. Hummelen, P. W. M. Blom and B. de Boer, *Polymer Reviews* **2008**, 48, 531.
- [24] Y. Yang, J. Ouyang, L. Ma, R. J.-H. Tseng, and C.-W. Chu, *Adv. Funct. Mater.* **2006**, 16, 1001.
- [25] J. C. Scott, and L. D. Bozano, *Adv. Mater.* **2007**, 19, 1452.
- [26] C.-L. Tsai, F. Xiong, E. Pop, and M. Shim, *ACS Nano* **2013**, 7, 5350.
- [27] P. Siebeneicher, H. Kleemann, K. Leo, and B. Lüssem, *Appl. Phys. Lett.* **2012**, 100, 193301.

-
- [28] F. Verbakel Resistive switching in polymer - metal oxide diodes, Ph.D. Thesis, TU/e (2008).
- [29] S. R. Forrest, *Nature* **2004**, *428*, 911.
- [30] L. S. Hung, C. W. Tang, and M. G. Mason, *Appl. Phys. Lett.* **1997**, *70*, 152.
- [31] R. Steim, F. R. Kogler, and C. J. Brabec, *J. Mater. Chem.* **2010**, *20*, 2499.
- [32] M. T. Greiner, M. G. Helander, W.-M. Tang, Z.-B. Wang, J. Qiu, and Z.-H. Lu, *Nat. Mater.* **2012**, *11*, 76.
- [33] F. Verbakel, S. C. J. Meskers, and R. A. J. Janssen, *J. Appl. Phys.* **2007**, *102*, 083701.
- [34] ITRS PIDS chapter, Tables PIDS7&8 **2011**.
- [35] Y.-C. Lai, D. Y. Wang, I-S. Huang, Y. T. Chen, Y.-H. Hsu, T.-Y. Lin, H.-F. Meng, T. C. Chang, Y. J. Yang, C. C. Chen, F.-C. Hsu, and Y.-F. Chen, *J. Mater. Chem. C* **2013**, *1*, 552.
- [36] Y. B. Kuang, R. Huang, Y. Tang, W. Ding, L. J. Zhang, and Y. Y. Wang, *IEEE Electr. Device. L.* **2010**, *31*, 758.
- [37] S.-H. Liu, W.-L. Yang, C.-C. Wu, T.-S. Chao, M.-R. Ye, Y.-Y. Su, P.-Y. Wang, and M.-J. Tsai, *IEEE Electr. Device L.* **2013**, *34*, 123.
- [38] W. Bai, R. Huang, Y. Cai, Y. Tang, X. Zhang, and Y. Wang, *IEEE Electr. Device L.* **2013**, *34*, 223.
- [39] F. Verbakel, S. C. J. Meskers, R. A. J. Janssen, H. L. Gomes, A. J. M. van den Biggelaar, and D. M. de Leeuw, *Org. Electron.* **2008**, *9*, 829.
- [40] Y. V. Pershin and M. Di Ventra, *Adv. Phys.* **2011**, *60*, 145.
- [41] S. H. Jo and W. Lu, *Nano Letters* **2008**, *8*, 392.
- [42] S. Song, B. Cho, T.-W. Kim, Y. Ji, M. Jo, G. Wang, M. Choe, Y. H. Kahng, H. Hwang, and T. Lee, *Adv. Mater.* **2010**, *22*, 5048.

Chapter 2

Electroforming and resistive switching in unipolar memristors

Abstract

Memristors are two-terminal bistable resistors that are envisaged to have broad application in data storage, reconfigurable logic and neuromorphic computing. Materials for memristors include common oxides such as Al_2O_3 or SiO_2 . Electronic memory properties of the oxide are induced by electroforming. Electroforming can be induced by applying bias voltage stress close to the limit for dielectric breakdown. Tight control over electroforming under these near-critical conditions is crucial for the success of memristive memory as a device technology. Al_2O_3 and SiO_2 show unipolar switching, i.e. their resistance can be switched between high and low values using voltage pulses of the same polarity. Currently the mechanism for unipolar switching and its electroforming are still largely unknown. In this feature, results on unipolar switching in bilayer memristors involving a layer of Al_2O_3 and semiconducting polymer are summarized. The bilayer architecture allows for reliable electroforming involving charge trapping and defect formation at the polymer / oxide interface. A qualitative description of the filamentary conduction and switching dynamics after electroforming are presented.

2.1 Introduction

Many metal-insulator-metal (MIM) systems show electrically induced resistive switching and, therefore, have been proposed to replace the standard NAND-flash non-volatile circuitry.^[1] There are many physical phenomena that can lead to resistive switching and memory effects. The mechanisms have been classified, based on thermal, chemical, and electronic/electrostatic effects.^[2]

A large variety of materials and materials combinations can give rise to resistive switching.^[3-6] This poses a challenge to the materials scientist to find/design materials with ultimate properties regarding operation, availability and compatibility with existing and future technology and regulations. To illustrate the potential for technological innovation, we mention recent reports on memristors on flexible substrate^[7] and their 3D integration.^[8]

In their pristine state, the materials in the MIM diodes are usually high resistivity insulators. Before the diodes show memory properties they have to be electroformed by applying a high electric field in a current-voltage sweep with an appropriate current compliance. This induces a so-called ‘soft-breakdown’. The electroformed device can be switched between a high conductance on-state and a low conductance off-state. The resulting bistable current-voltage (I - V) characteristics can be applied as a non-volatile memory.

The electric fields needed to induce the electroforming are usually close to the critical field for dielectric breakdown. In practice the electroforming needs to be tightly controlled by e.g. programming a current compliance limit in the external circuit, in order to avoid permanent shorting and breakdown of the MIM diodes. The yield of active memory cells in the electroforming step is crucial for the success of memristors as a device technology. A detailed understanding of processes happening during electroforming is therefore of paramount importance.

Resistive switching was first reported in 1962 when Hickmott described a hysteretic I - V characteristic in thin anodic films.^[9] A large negative resistance was observed for thin films of SiO_x , Al_2O_3 , Ta_2O_5 , ZrO_2 , and TiO_2 . Resistive switching has subsequently been reported in a wide variety of MIM structures composed of binary oxides such as SiO ^[10] and NiO .^[11] Early research up to the 1980s has been thoroughly reviewed by Dearnaley *et al.*,^[12] Oxley,^[13] and by Pagnia and Sotnik.^[14] In the 1990s attention shifted from binary oxides to complex metal oxides after a report on resistive switching in $\text{Pr}_{0.7}\text{Ca}_{0.3}\text{MnO}_3$.^[15] The research on these perovskite-type manganites and titanates has been reviewed by Sawa^[16] and by Waser and Aono.^[17]

The devices are called memristors after the theoretical prediction of Leon Chua^[18] in 1971. He showed from symmetry arguments that apart from a resistor, capacitor, and inductor, a fourth passive circuit element should exist, which he termed a memristor, short for memory resistor. In 2008, this theoretical prediction was connected to the vast amount of literature on resistive switching.^[19] Since then, the name memristor has

become the generic abbreviation for resistive switching memories.

The switching mechanism of memristors can be unipolar or bipolar depending on the type of oxide and the electroforming procedure applied.^[20,21] In unipolar switching, the switching direction depends on the magnitude of applied bias but not on the polarity. The I - V curves of both the on-state and the off-state are symmetric and the type of electrode is relatively unimportant. This type of switching is operative in highly insulating oxides. The microscopic mechanism is not yet known. Most mechanisms suggested, such as forming and dissolution of metallic filaments, the so-called fuse-antifuse mechanism, do not comply with the unipolarity.

In contrast, the switching is called bipolar or anti-symmetric when the set voltage for the on-state occurs at one voltage polarity while the reset to the off-state occurs at the reversed polarity. The I - V curves are asymmetric and depend on the type of electrode. Bipolar switching is operative in semiconducting binary oxides and complex perovskites. The origin depends on the type of oxide system and could be as diverse as modulation of a Schottky barrier,^[22] electrochemical migration of oxygen vacancies, or a Mott transition induced by carrier doping at the interface.^[16]

Here we focus on unipolar switching in Al_2O_3 memristors. In order to fabricate reproducible memories, a bilayer comprised of a thin insulating Al_2O_3 layer in series with a semiconducting layer is needed. The yield of memories made with only an Al_2O_3 layer is extremely low. Electroforming then almost inevitably leads to hard shorts, irrespective of the set current compliance or of the type of forming *e.g.* pulsed or voltage sweep. The electrodes melt or even evaporate. Already for the memories made in the 1960s and 1970s it turned out that an unidentified layer of carbon enhances the reproducibility. Diodes made in high vacuum did not show switching. Oil vapor contamination from a rotary pump was needed to make reliable memories.^[14]

Reproducible memories with a yield of about unity could be fabricated by adding a well-defined thin layer of a semiconducting polymer.^[23] The devices therefore are often called polymer RRAMs. The type of electrodes turned out to be irrelevant. After electroforming, the I - V characteristics are symmetric. A narrow voltage region with a negative differential resistance (NDR) is observed in both polarities. The device can be switched between a high conductance on-state and a low conductance off-state at biases corresponding to the top and bottom of the NDR. The switching is unipolar and due to the Al_2O_3 . The distributed series resistance of the polymer prevents thermal runaway when a local filament is turned on. Polymer / metal oxide diodes are then expected not only to exhibit a better control of the switching properties but also to have superior endurance as compared to metal oxide-only based memristors. The semiconducting polymer not only acts as a current limiting series resistance, but also plays a crucial role by providing a charged layer of trapped electrons at the polymer / metal oxide interface. This charge layer enhances the tunneling across the metal oxide and tunes the formation of electrically bistable defects.

This chapter is an explanatory account of electroforming and unipolar switching

in memristors with an internal bilayer structure consisting of Al_2O_3 and a semiconducting polymer and is organized as follows. The overview compiled in this chapter is based on results from the collaborative research effort on Al_2O_3 /polymer memories by Philips Research, the University of Algarve, and the Eindhoven University of Technology. Results presented were obtained by various researchers involved in the collaboration, including the author of this thesis. Contributions from researchers other than the author are indicated as such in the text.

The physical structure of the memory diodes is briefly described in section 2.2. Electroforming to transform pristine capacitors into memristors is discussed in section 2.3. The filamentary conduction and switching dynamics are analyzed in sections 2.4 and 2.5. The operation mechanism and a qualitative interpretation of unipolar switching characteristics is presented in section 2.6. Practical design consequences due to the internal bilayer structure of the memristor are analyzed in section 2.7 and a summary is presented in section 2.8.

2.2 Memory structure

The nominally electron-only diodes investigated consist of an Al bottom electrode thickness (30 nm), a thin sputtered Al_2O_3 layer (controlled thickness varying from 2-50 nm), a spincoated layer of a spirofluorene semiconducting polymer^[24] (80 nm), and a Ba/Al top electrode. The layout of the metal-insulator-semiconductor diodes is shown in Fig. 2.1a and the schematic flat band diagram is shown in Fig. 2.1b. The glass substrate holds 6 devices with active areas between 1 and 9 mm^2 , and is capped with a stainless steel cap. A getter was placed under the stainless steel cap to exclude H_2O . A picture of a module is shown in Fig. 2.1c.

2.3 Electroforming

The pristine capacitors are highly insulating: direct currents are very low. An electroforming step^[23,25] is required to obtain electrical bistability. Electroforming can be performed by applying a short high voltage pulse or by increasing the bias and set the current compliance. Memristors can also be formed by constant current stress where the current value is set and the voltage is monitored over time.^[26] In this way electroforming can be investigated at low power consumption.

After electroforming, the diodes show electrical bistability and feature a low resistance on-state and the high resistance off-state. Typical I - V characteristics in the on- and off-state are presented in Fig. 2.1d. The currents scale with the device area. The current is Ohmic at low bias, below ~ 2 V, and superlinear at higher bias. The on-state shows a clear voltage controlled negative differential resistance (NDR) region. Reliable switching is obtained under pulse bias conditions that correspond to the top and bottom of the NDR.^[27] Those are the optimized SET and RESET values for practical memories.

Programming cycle endurance and data retention are excellent.^[28] The yield of memristors is about unity.^[23] In addition, due to the encapsulation, both pristine devices as well as electroformed memristors are stable for years.

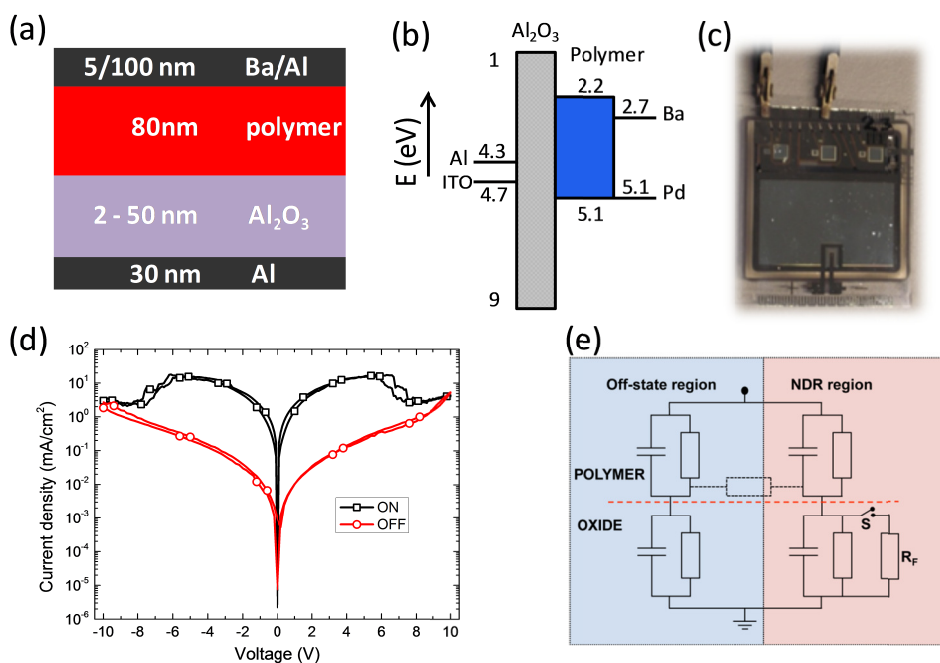


Figure 2.1: Memristor layout. (a) Typical nominal e-only metal-insulator-semiconductor-metal diode layout where the Al₂O₃ thickness is varied. (b) Flatband energy diagram where numbers are in eV. (c) Photograph of a module containing several memristors. The devices with an active area between 1 mm² and 9 mm² were encapsulated to exclude H₂O. (d) J - V characteristics after forming showing a pronounced negative differential resistance. (e) Equivalent circuit representing the electroformed diode in the on-state. The NDR branch is highly localized and connected to the electroformed off-state region via the distributed resistance of the polymer layer, represented by the dotted resistor. When the switch S is closed, a conducting filament of resistance R_F shunts the normally high local oxide resistance. (e) Reprinted from Ref. [61]. Copyright 2013, AIP Publishing LLC.

The electroforming process can be subdivided into three steps. First, at low bias, electrons get trapped at the semiconductor / oxide interface. The electron density increases with increasing bias and reaches a density high enough to induce tunneling through the oxide. In this second stage holes are trapped in the oxide. Then, upon further increasing of the applied voltage, the oxide breaks down. However, when using a low current compliance, the breakdown is still reversible. The state formed is metastable and the

diodes recover to their insulating pristine state. Finally in the third stage at high bias, irreversible dielectric breakdown occurs forming the memristor: a bistable switching resistor. These three stages are discussed in detail below.

2.3.1 Early stage: charge trapping and tunneling

The mechanism of electroforming at low applied bias has been investigated with current density-voltage (J - V), quasi-static capacitance-voltage (QSCV) measurements^[30] and by optical detrapping investigations.^[29] From the measurements, the position of traps and the number of trapped charges can be derived. Sequential J - V characteristics for a nominal e -only diode consisting of an Al/Al₂O₃/poly(spirofluorene)/Ba/Al stack are reproduced^[30] in Fig. 2.2a. The cyclic J - V scans were measured upon stepwise increase of the maximum bias. The arrows indicate the direction of the voltage scans starting at 0 V, scanning forward and then backward to 0 V. Fig. 2.2a shows three stages in the electroforming process. This section describes charge trapping (I) and tunneling (II).

For voltages in the range between 0 and 8 V, a pronounced hysteresis in the J - V characteristics has been observed. In the forward scan, the current increases with bias. However in the backward scan the current is negligible. Actually the current level on the return scan is approximately equal to the displacement current associated with the device geometrical capacitance, C_0 , assuming that both oxide and polymer layers are insulators. If the subsequent J - V loop is recorded using the same bias conditions, the hysteresis is not present and the measured current equals the displacement current. Then, scanning forward to a higher bias voltage that has not been applied before, the current shows a large increase. Backward scans give the same low current value, independent of the previous scans. The hysteresis in the J - V measurements shows that the electrons are trapped. With small signal impedance spectroscopy or capacitance transients, the trapping cannot be observed, hence the trap levels must be deep. This is confirmed by the fact that under short-circuit conditions it takes days to discharge. Once emptied, identical J - V traces are measured; charging in region I is reversible.

In the second stage of electroforming, region II, for biases of 8 to 14 V, the current is due to tunneling of electrons through the oxide. The tunneling current gets much larger than the trapping current; hence the amount of hysteresis decreases with increasing bias. The magnitude and voltage dependence of the current could tentatively be modeled as being due to Fowler-Nordheim tunneling through the oxide^[31] using a barrier height of approximately 1 eV and assuming a potential drop over the oxide layer equal to the applied bias. Although a good agreement was obtained, the barrier height is unrealistically low. The low barrier for injection may be explained by accumulation of positively charged defects in the oxide^[32] (see section 2.3.2).

To quantify the number of trapped electrons and to locate their position we used both the voltage-step QSCV method^[33,34] and optical detrapping experiments. The QSCV method is ideally suited to study traps that fill quickly but empty slowly. Fig. 2.2b shows

the cyclic QSCV scans under the same bias conditions as for the J - V scans. Scanning in the reverse bias ($V < 0$), a practically constant capacitance of 30 nF/cm^2 is recorded which we interpret as the geometrical capacitance, C_0 . The hysteresis is due to a small leakage current.

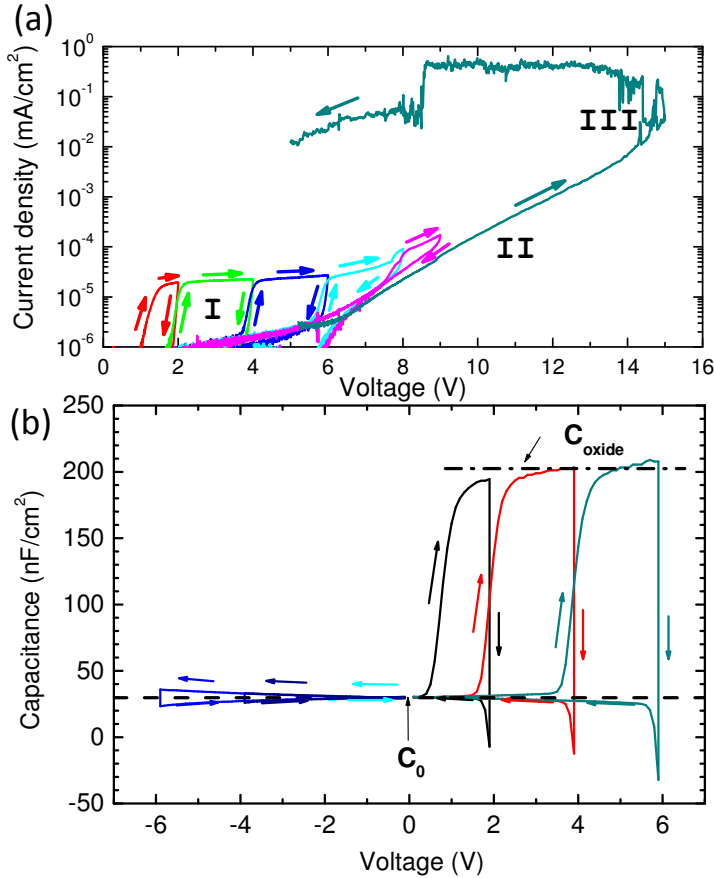


Figure 2.2: Electroforming. (a) Sequential J - V characteristics of a pristine Al/Al₂O₃ (20 nm)/polymer/Ba/Al diode. J - V sweeps were recorded with 10 mV step and 40 ms integration time. The diode layout showing the poly(spirofluorene) and oxide sandwiched in between Al and Ba/Al electrodes is presented in Fig.1a. (b) Sequential QSCV characteristics for a Al/Al₂O₃ (40 nm)/ polymer/ Ba/Al diode measured using an integration time of 4 s and a voltage step of 100 mV. Reprinted from Ref [30]. Copyright 2010, AIP Publishing LLC.

We consider the pristine capacitor as a double-layer structure comprised of an oxide layer, with capacitance C_{oxide} , in series with a polymer layer, with capacitance C_{polymer} . As expected, the experimental capacitance as obtained from QSCV near zero bias, C_0 , follows accurately the calculated geometrical capacitance $1/C_0 = 1/C_{\text{oxide}} +$

$1/C_{\text{polymer}}$. $1/C_0$ is weakly dependent on the oxide thickness, but strongly varies with polymer thickness, because C_{oxide} is much higher than C_{polymer} . In contrast, the high capacitance from QSCV, C_{high} , varies strongly with oxide thickness but is virtually independent of polymer thickness. Moreover C_{high} is essentially the same as the capacitance measured with QSCV on devices without polymer layer, and matches with the calculated C_{oxide} .

The equality C_{high} and C_{oxide} follows directly from the equivalent circuit shown as the left side of the equivalent circuit of Fig. 2.1e. Under sufficient forward bias, electrons are injected via the Ba/Al electrode, drift through the polymer and get trapped at the polymer/oxide interface. The injection of mobile carriers lowers R_{polymer} sufficiently to shunt C_{polymer} , and raises the bilayer capacitance to C_{oxide} . Trapping of electrons at the interface explains why C_{oxide} is only observed using the QSCV method under forward bias that is applied for the first time. For instance, in the return path of the cyclic QSCV scan, there is no discharging current because of the trapping and the two layers behave again as pure insulators with the overall capacitance equal to the geometric device capacitance C_0 . In a second scan, new electrons can only be injected into the polymer when the bias voltage applied exceeds the built-in voltage resulting from the trapped electrons. Hence C_{oxide} is observed only if the applied bias voltage exceeds the maximum voltage of the previous scan.

From the observation that C_{high} matches with C_{oxide} for bias voltages up to 6 V, we conclude that the number of electrons stored at the oxide-polymer interface is determined by the capacitance of the oxide layer and the applied bias V_{appl} . This implies a density of trap states for electrons at the interface exceeding $C_{\text{oxide}}V_{\text{appl}}/q_e = 3 \times 10^{17} /\text{m}^2$ with q_e the electron charge and using the measured value for C_{oxide} of 800 nF/cm² for 10 nm thick oxide. The QSCV technique and results are further described in Chapter 3.

To accurately determine the density of trapped electrons, Chen *et al.* performed optical detrapping experiments.^[29] The trapped charge in region I can be neutralized by photo-generated charge carriers. Under illumination, transient discharge currents were observed on the time scale of hundreds of seconds. Optical detrapping was only observed for light with photon energies higher than the polymer band gap (3.1 eV), showing that the charge carriers inducing the neutralization are generated in the polymer. Furthermore, detrapping transients were faster for higher optical power, in agreement with first order kinetics. Once the traps have been emptied optically, the filling of the traps could be repeated. Charging and optical discharging were found to be fully reversible processes.

To determine the amount of trapped charge, Chen *et al.* performed a series of trap filling and emptying cycles with increasing voltage from 1 V up to 6 V in steps of 1 V. Charging J - V sweeps are shown in Fig. 2.3a, and the corresponding optical discharging transients recorded after the sweeps and under the same optical power are shown in Fig. 2.3b. From the discharge transient, the density of trapped charge was calculated from the area under the optically induced current transient. The inset in Fig. 3b shows the total amount of charge released upon illumination as a function of the maximum applied

charging voltage in the preceding charging J - V sweep. The amount of charge released depends linearly on the applied maximum charging voltage. Extrapolation to the voltage necessary to fully electroform the device, *cf.* region III in Fig. 2.2, predicts that a total amount of $8 \times 10^{17}/\text{m}^2$ charges must be stored in the device before soft-breakdown occurs. This value is in good agreement with the number extracted from QSCV measurements described in chapter 3. This charge density corresponds to a critical electric field strength for electroforming of 1.5×10^9 V/m, which is close to the breakdown field strength of Al_2O_3 , *viz.* 10^9 V/m.^[35,36] When the oxide thickness was varied, the amount of stored charge for the same applied bias voltage varied linearly with oxide thickness, showing that the critical electrical field strength for electroforming is thickness independent.^[29,30]

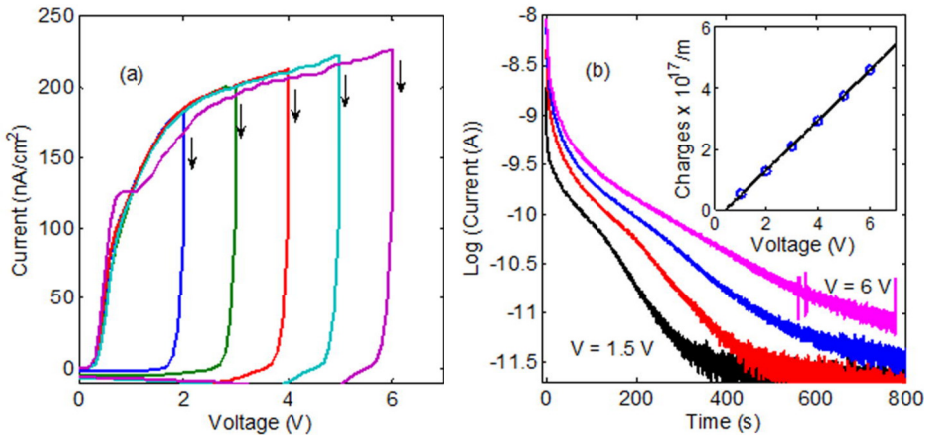


Figure 2.3: Density of trapped electrons. (a) Trapping J - V loops with increasing maximum filling voltages. After each trapping loop, optically induced discharge transients were recorded as shown in (b). The number of detrapped electrons is calculated from the area under each current transient. The inset of (b) shows the number of detrapped charges as a function of the filling voltage (1 V to 6 V). Reprinted from Ref. [29]. Copyright 2011, AIP Publishing LLC.

2.3.2 Reversible dielectric breakdown

In the early stage of electroforming electrons are trapped at the polymer/oxide interface. At slightly higher fields the electrons can tunnel through the oxide. Both processes are fully reversible. At still higher fields, the oxide in the capacitor breaks down. A new state is formed, with properties which depend on the power dissipated during the forming process.

Chen *et al.* have investigated the dielectric breakdown under constant current stress.^[26] A current value is set and the voltage is followed in time. The dissipated power can be varied by varying the set current value. At low power, around 0.1 mW/cm², the

electroforming is fully reversible. The state is metastable, the post-breakdown conduction decays in a power law with time. The capacitors recover to their original insulating properties, hence this state is self-healing. At high dissipated power, typically 10 mW/cm², the electroforming is irreversible, presumably due to Joule heating, and a non-volatile memristor is obtained. Here the reversible, self-healing breakdown is discussed.

Fig. 2.4 shows dielectric breakdown under constant low current stress. Initially, the rate (dV/dt) at which the bias increases reflects changes in capacitance since $C = I/(dV/dt)$ with the current, I , kept constant. The extracted capacitance is presented as the inset in Fig. 2.4. Initially, the oxide-polymer bilayer acts as a combined dielectric for which the expected capacitance would be ~ 30 nF/cm². In the first few milliseconds the voltage rises rapidly and at voltages exceeding the built-in potential of the diode (~ 2 V), electrons can be injected into the semiconducting polymer and the measured capacitance (149 nF/cm²) exceeds the value for the bilayer but is still below the capacitance expected for only the oxide layer ($C_{\text{oxide}} \sim 400$ nF/cm² for 20 nm oxide thickness). As time progresses, electrons are injected by the Ba/Al electrode, drift through the polymer and get trapped at the polymer/oxide interface. As discussed for the QSCV measurements of Fig. 2.2, the injection of electrons lowers R_{polymer} sufficiently to shunt C_{polymer} , and raises the bilayer capacitance to C_{oxide} . After 10 ms the capacitance exceeds 400 nF/cm² corresponding to the estimated oxide capacitance C_{oxide} . The apparent capacitance keeps rising gently with time to almost 900 nF/cm² just before breakdown. This capacitance value is no longer accurate because with increasing bias, the tunneling current through the oxide increases, *cf.* region II in Fig. 2.2, and distorts the slope of the voltage-time curve. The corresponding estimated oxide capacitance is artificially higher than expected. Finally at high bias, corresponding to the maximum dielectric field strength of the oxide, the capacitor breaks down. Current paths are formed through the oxide, and the bias needed to sustain the current falls dramatically.

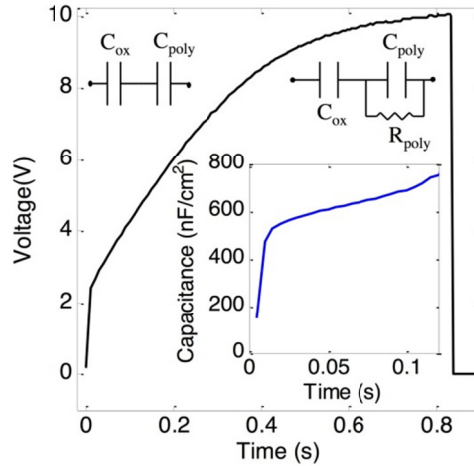


Figure 2.4: Breakdown under constant current stress. The voltage across the Al/Al₂O₃(20 nm)/poly(spirofluorene) (80 nm)Ba/Al capacitor as a function of time under a constant current stress of 1 $\mu\text{A}/\text{cm}^2$. An abrupt voltage drop is observed at 10 V. The inset shows the corresponding change in capacitance estimated from the change in slope of the voltage. The layout of the capacitor and the schematic flat band diagram for the dielectric layers are presented in Fig. 2.1a,b. Reprinted from Ref. [26]. Copyright 2013, AIP Publishing LLC.

The increased conduction after breakdown when using a low set current value was found to be a transient effect. The electroformed state is metastable and slowly returns to the pristine state. This self-healing process is accelerated by an applied electric field. The conductivity of the electroformed state as a function of time is presented on a double logarithmic scale in Fig. 2.5a. The capacitor is held at a constant forward bias. The conduction is probed intermittently at a bias of 0.5 V. Straight lines are obtained showing that the conduction decreases as a power law of time, $\sim (1/t)^\alpha$. The inset shows that the value of the exponent α increases with applied bias. To demonstrate that the self-healing is driven by the applied electric field and not by the applied bias, the recovery at constant forward bias as a function of oxide thickness was measured. Fig. 2.5b shows that the recovery for thicker oxides is slower. The inset shows that the value of the exponent α is directly proportional to the reciprocal oxide thickness, meaning that the recovery is driven by the electric field across the oxide.

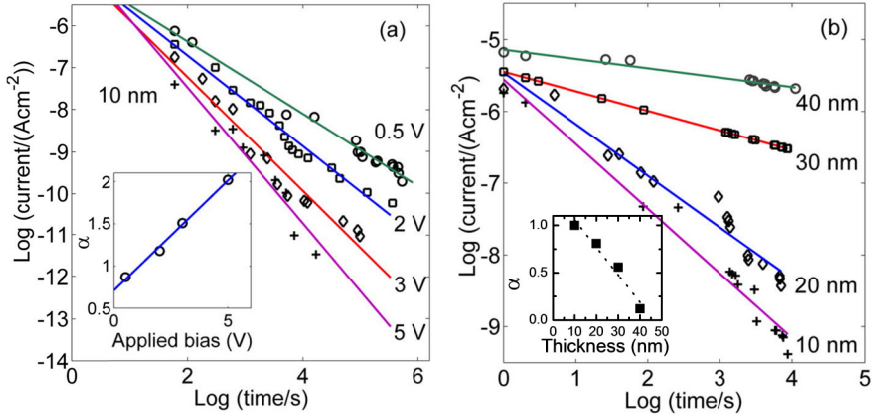


Figure 2.5: Self-healing. (a) Decay of current as function of time for different voltage biases (0.5 to 5 V) applied after electroforming by constant current stress. The current is measured at 0.5 V and follows a power-law decay with time: $t^{-\alpha}$. The inset illustrates the proportionality of the power α to bias voltage. (b) Thickness dependence of current decay monitored by voltage ramp (1 V) after forming by constant current stress. The inset shows the power α of current decay is as function of oxide thickness. The kinetics of the current decay should not be disturbed by the measurement procedure. For this reason, only one reading was done per data point and the reading voltage (0.5 V) was applied for a short period of time, about 1 s. Reprinted from Ref. [26]. Copyright 2013, AIP Publishing LLC.

Recovery after breakdown was recently also reported for HfO_2 ^[37] and SiO_2 ^[38,39]. Comparable phenomena were reported for $\text{Al}/\text{Al}_2\text{O}_3$ diodes and named “unforming”,^[40] tentatively explained as the neutralization of positive charges in the oxide by mobile injected electrons. It has also been proposed that the recovery is due to the melting of metallic filaments by Joule heating^[41] or to annihilation of oxygen vacancies^[42] formed during breakdown. The dissipated power during recovery is low, hence we disregard melting of filaments and we focus on annihilation of oxygen vacancies. A tentative mechanism for the recovery is elucidated in Fig. 2.6, where the Al_2O_3 / polymer interface is schematically presented. Application of a forward bias voltage to the capacitor before breakdown, results in injection of electrons into the polymeric semiconductor. The electrons get trapped at the oxide/polymer interface, *cf.* region I in Fig. 2.2. Consequently, the potential difference over the oxide layer becomes equal to the applied bias. In flat band condition, when the applied bias voltage approaches the band-gap of the aluminum oxide, positive charge carriers (holes) can be injected into the oxide, *cf.* region II in Fig. 2.2. The holes get trapped in the oxide. The potential over the oxide layer increases, thereby inducing the formation of oxygen vacancies. Two oxygen ions dimerize into an O_2 molecule, whereby the electrons are annihilated by the trapped holes. The O_2 molecules may diffuse into the polymer layer, escape from the electroformed device, or even form oxygen interstitials, depending on the dissipated power used in the

electroforming. The oxygen vacancies, also referred to as F-centers,^[43] can exist in a charge neutral state where an electron occupies the empty space left by the oxygen anion. When the electron leaves the vacancy, the F-center is ionized (F^+). The ionized F^+ center can be regarded as a trapped hole.

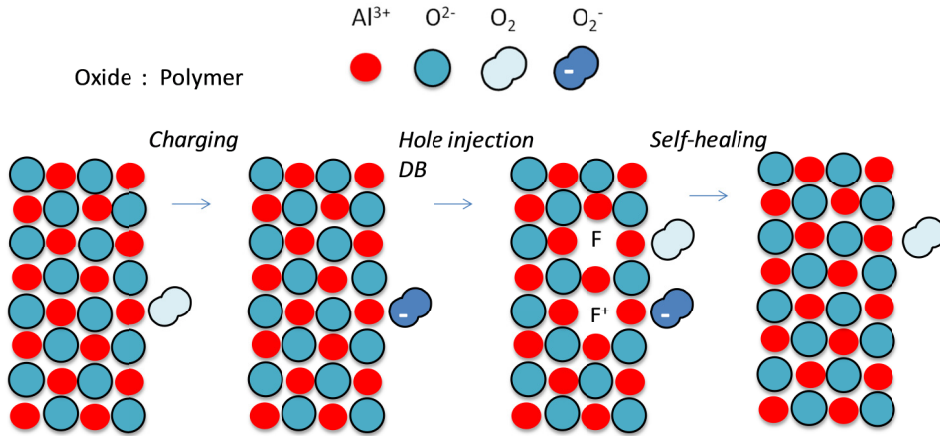


Figure 2.6: Self-healing mechanism. The red and blue spheres represent Al^{3+} and O^{2-} ions of the Al_2O_3 lattice. Neutral oxygen, O_2 , and the superoxide ion, O_2^- are presented by the lemniscates. First electrons are trapped at the polymer / oxide interface. When the bias is larger than the flat band voltage holes are injected into the oxide, and a highly polarized electric double-layer is formed at the polymer/oxide interface. In dielectric breakdown oxygen vacancies, F-centers, are formed. In self-healing, superoxide ions, O_2^- , react with a neutral and charged oxygen vacancy to re-form a defect-free Al_2O_3 lattice.

When the O_2 molecules are still present at the interface, the breakdown is reversible. Due to their large electron affinity, the O_2 molecules trap electrons. The formed superoxide ions, O_2^- , react with a neutral and charged oxygen vacancy to a defect-free Al_2O_3 lattice, indicated by the open square, as:



Due to this reaction, the breakdown state is self-healing and recovers with time towards the original, pristine state.

The positively charged defects are in the oxide while the superoxide ions are located in the polymer. At the oxide-polymer interface, a highly polarized double layer is formed. Because of this asymmetry, the Gibbs free energy of the reaction Eq. (2.1) depends on the applied electric field. Application of a forward bias raises the energy of the reactants with respect to that of the product and, therefore, enhances the self-healing rate. From electrostatics and by assuming a bimolecular recombination between trapped holes and electrons, *e.g.* described as Shockley-Reed-Hall (SRH) recombination, an implicit

relation for the time dependence of hole density has been derived.^[26] Taking the conductivity proportional to the hole density, the measured power-law dependence on time and electric field, $\sim (1/t)^\alpha$, is qualitatively reproduced.^[26]

This interpretation is corroborated by optical detrapping experiments. As shown in Fig. 2.3, trapped electrons can optically be released by illumination of the polymer layer with photons having an energy larger than the bandgap.^[26] Without trapped electrons, the rate of the self-healing reaction Eq. (2.1) is expected to be negligible. To verify this hypothesis, the post breakdown conduction was measured with and without illumination. First, dielectric breakdown was induced, followed by illumination for 1000 s. Subsequently, the post breakdown conduction was measured as a function of time up to 25 hours. Fig. 2.7 shows that the current remains high, and constant.^[26] By optically emptying the electron traps, the self-healing is completely suppressed. Next, the capacitor was subjected to a voltage ramp up to 5 V. This restored the trapped electrons density and, hence, triggered the self-healing reaction.^[26] Indeed, Fig. 2.7 shows that after the voltage ramp, the current decays with a power law of time, *cf.* Fig. 2.5. After reaching the pristine state, the capacitor was electroformed again under identical conditions but not submitted to illumination. The current decay shown in Fig. 2.7b follows the same power-law kinetics. The practically complete inhibition of the decay of the conduction (self-healing) after illumination indicates that electrons trapped at the oxide/polymer interface are crucial for the recovery and, at the same time, it confirms the suggested self-healing reaction Eq. (2.1).

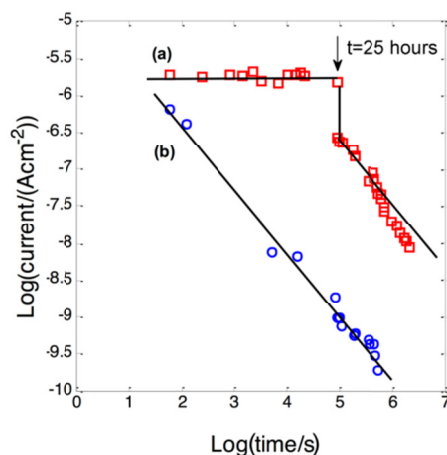


Figure 2.7: Inhibition of self-healing. Current-time plots for a capacitor electroformed with constant low current stress of 1 μA . (a) After emptying electron traps with 1000 s illumination with a blue LED ($350 \leq \lambda \leq 650 \text{ nm}$, $\lambda_{\text{max}}=440 \text{ nm}$) the current remains constant. The voltage ramp (0 ~ 5 V) at $t = 25$ hours triggers the decay of the current. (b) The same capacitor again electroformed, kept in the dark and short-circuited. The post breakdown current decays with a power-law dependence on time with the same exponent as in Fig. 2.5a. Reprinted from Ref. [26]. Copyright 2013, AIP Publishing LLC.

2.3.3 Memristor formation

The resistive state created after electroforming depends on the dissipated power used. During dielectric breakdown, oxygen vacancies are formed and the molecular oxygen produced diffuses to the polymer/oxide interface. The breakdown starts in one spot, leading to filamentary currents and local heat production. When the dissipated power is low, there is limited Joule heating and the molecular oxygen remains in the device. As explained above in section 3.2, the O_2 molecules can trap electrons and the formed superoxide ions, O_2^- , can react with a neutral and a charged oxygen vacancy to re-form a defect-free Al_2O_3 lattice. Hence in this case the breakdown is reversible; the pristine state of the capacitor is recovered with time.

At high dissipated power there is significant Joule heating, the molecular oxygen can completely escape from the device. This evolution of oxygen upon electroforming has been well documented in the past.^[44] The breakdown is irreversible. The J - V characteristics show a sudden sharp and noisy irreversible increase in current density, *cf.* Fig. 2.2, trace III. We argue that a memristor is formed when the defect density exceeds a certain threshold. This threshold must be related to the formation of a percolating path for electrons involving electron states associated with the oxygen vacancy sites. The conductance is now bistable and can be switched between a high and a low level^[23] as shown in Fig 2.1d. The high level on-state exhibits an NDR region that is due to a cascade of discrete switching events that turns-off conducting filaments. The current flow through filamentary channels is discussed in the next section below.

A direct relation between injection of positive charge carriers and expulsion of molecular oxygen has experimentally be demonstrated for nanostructured ZnO. The electroforming induced by injected holes could be reversed upon exposure to O_2 gas.^[45] The oxygen provided by the gas phase can cause refilling of oxygen sites (Fig. 2.8). Solid state gas sensors based on metal oxides such as ZnO and SnO_2 operate via changes in conductivity upon creation/annihilation of oxygen vacancies.^[46]

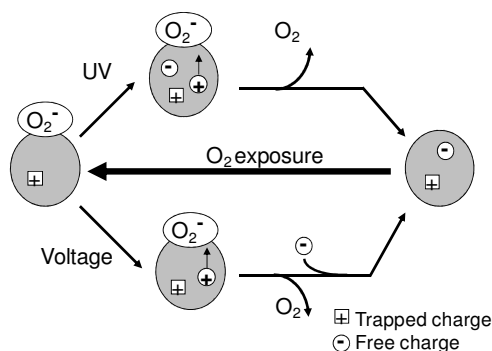


Figure 2.8: Schematic representation of the UV light and bias voltage induced changes in ZnO nanoparticles. An injected or photogenerated hole, induces desorption of molecular oxygen from the surface of the nanoparticles. The desorption liberates the electrons trapped on a surface bound O_2 and results in a rise in the density of mobile electrons in the particles which enhances the density of mobile electrons and raises the macroscopic conductivity. Reprinted from Ref. [45]. Copyright 2007, AIP Publishing LLC.

2.4 Filamentary conduction

The homogeneity of the conduction in the memristors was investigated by Cölle *et al.* with an IR enhanced CCD camera.^[47] The spatially resolved thermal images show, in the on-state, hot spots due to highly conductive paths. In the off-state, the spots disappear. However, the spots are not created and destroyed upon switching. Upon repeated switching between the on- and off-states, the same original hot spots were detected in the thermal image. From these observations it has been concluded that upon switching, filaments are neither generated nor destroyed, but that individual filaments are turned on and off, like switches. This conclusion has been corroborated by the anomalous temperature dependence of the on-state and by electrical noise measurements. We note that scanning probe measurement confirm the existence of conducting filaments in Al_2O_3 .^[48,49] The apparent nanometer scale lateral dimensions of the filaments indicate potential for high density data storage.

At low bias, in the Ohmic regime, the transport is almost activation-less. In the off-state at high bias the conduction is thermally activated. In a temperature range of 200 K to 300 K, an activation energy of about 66 meV has been reported by Gomes *et al.*^[50] Interestingly, the on-state behaves completely differently. Memristors were programmed in the on-state and the current was measured upon lowering the temperature. The current doubles in a temperature range of 150 K. This corresponds to a positive temperature coefficient of the electrical resistivity of about 0.01 K^{-1} , an anomalously large value when compared to typical values of metals, such as 0.0039 K^{-1} for Cu. Furthermore, in contrast to the smooth decrease in the resistivity of metals, that of the memristors decreases in a step-like fashion, which strongly suggests that additional conducting filaments become

active upon lowering the temperature. This behavior contradicts the widely held view that switching is due to filaments that are formed reversibly by the diffusion of metal atoms. Instead, the anomalous temperature dependence together with small-signal impedance measurements have indicated that creation and annihilation of filaments is controlled by filling of shallow traps localized at the oxide/polymer interface.^[50]

Filamentary conduction and trap assisted switching unambiguously follows from electrical noise measurements.^[51] The current noise, S_I (A^2/Hz), is presented in Fig. 2.9 as a function of frequency on a double logarithmic scale. The memristor is programmed in the on-state. At low bias, where the current is Ohmic, the noise follows the omnipresent $1/f$ dependence. A comprehensive theoretical analysis of $1/f$ noise in phase change memories has been presented by Nardone *et al.*^[52] Here the $1/f$ noise is analyzed using the empirical Hooge relation.^[53] The figure of merit extracted of 10^{-21} cm^2/Ω is typical for conducting materials such as metals and doped semiconductors. However in the memristor the current density is low, which indicates that the regions responsible for current transport and noise are narrow filaments between the contacts. Comparable noise measurements were obtained for the off-state. The extracted figure of merit scales with the conductivity.

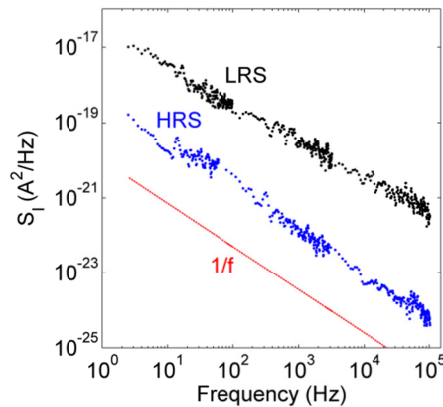


Figure 2.9: Electrical noise at low bias.^[54] Current noise spectra of a memristor programmed in the low resistance on-state (LRS) and in the high resistance off-state (HRS). At low bias, in the Ohmic region, the omnipresent $1/f$ noise is observed. The magnitude of the noise scales with the conductivity.

At high bias, close to the NDR region, the average noise level increases was measured by Rocha. Typical time records of 250 ms from a continuous measurement that took 6 hours are presented in Fig. 2.10. The time records show random telegraph noise (RTN); large discrete current fluctuations of about 45 nA, corresponding to $\Delta R/R \sim 5\%$. RTN has been observed in a variety of systems such as $p-n$ junctions,^[55] MIM junctions,^[56,57] MOS transistors^[58] and has been used to characterize resistance fluctuations in chalcogenide RRAMs.^[59] RTN shows up as discrete fluctuations in current-voltage or current-time characteristics when the charge transport is controlled by

the statistical capture / emission of electrons at electron trap sites. Especially when transport occurs through current-carrying filaments, large current fluctuations can occur. Because the noise is due to individual carrier trapping events which cause localized and discrete modulations of the current, RTN is an effective tool for probing the dynamic behavior of an electrically inhomogeneous system such as a memristor.

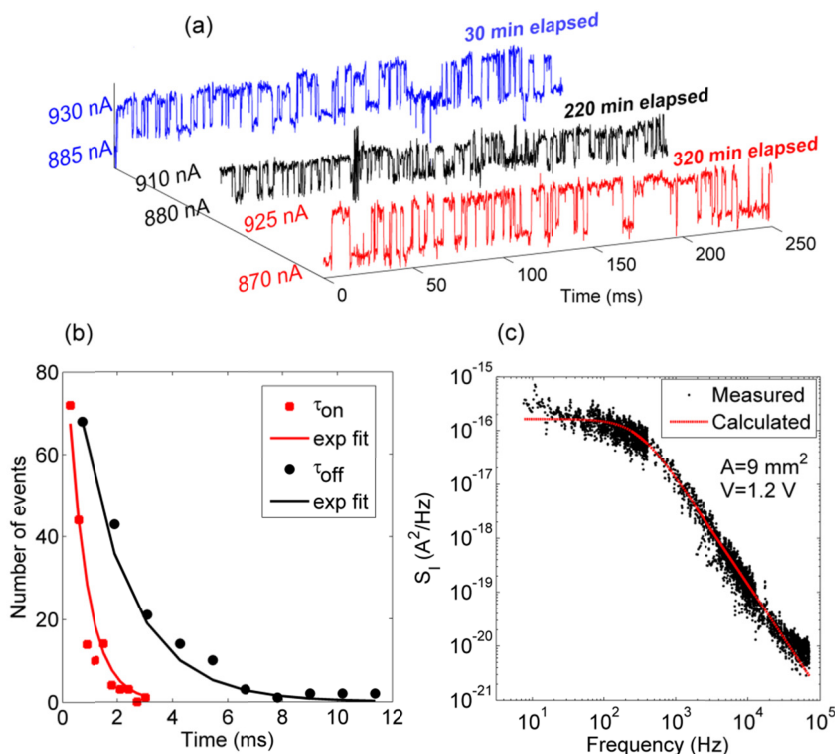


Figure 2.10: RTN noise at high bias.^[54] (a) Electrical noise of a memristor programmed in the on-state. The time records show the current RTN fluctuations under an applied bias of 1.2 V at different intervals during 6 hours of measurement. The discrete current levels are presented on the left side. (b) Histograms of the up and down times for the RTN fluctuations. Both times follow an exponential time distribution. (c) Measured (black dots) and calculated (dotted red line) current noise spectral power density $S_I(f)$.

The large discrete current fluctuations allow us to quantify the time that a filament is turned-on, τ_{on} , and is turned-off, τ_{off} . The first and second trace in Fig. 2.10a exhibit a filamentary path that is most of the time active, and only once in a while it is switched off with $\tau_{\text{off}} \sim 0.7$ ms. The third trace shows the filament being turned on and off at similar time scales of about 1.7 ms. The current fluctuations change their frequency in a random way. We derived the lifetime of a filament from a statistical analysis of the time traces by taking the probabilities P_{on} and P_{off} as exponentially distributed in time as:^[59]

$$P_{on,off}(t) \propto \exp(-t/\tau_{on,off}). \quad (2.2)$$

Fig. 2.10b shows the extracted time distribution for the up and down states. The fit of the experimental data for this particular case gives values for τ_{on} of 1.7 ms and for τ_{off} of 0.7 ms. A good agreement is obtained. Assuming a two level random signal, the voltage noise spectral power density has been calculated as:^[60]

$$S_I(\omega) = 4\delta I^2 (\tau_{eff} / (\tau_{up} + \tau_{down})) (\tau_{eff} / (1 + \omega^2 \tau_{eff}^2 p)) \quad (2.3)$$

with

$$1/\tau_{eff} = 1/\tau_{up} + 1/\tau_{down} \quad (2.4)$$

Fig. 2.10c shows that quantitative agreement is obtained using the previously derived time constants for τ_{on} and τ_{off} . Of course the time constants depend on device structure, history and applied bias. It only confirms that in the on-state the current flows through filaments. The switching is due to opening and closing of those filaments.

2.5 Switching dynamics

Reported memristor write and erase times vary by orders of magnitude, from nanoseconds to milliseconds. The discrepancies might be due to different types of semiconductor or device geometries. Here we will discuss the switching dynamics and show that the huge variation in reported switching times can also be explained by the different electroforming procedures and measuring protocols used to characterize the switching in the diodes. We first discuss the influence of the electroforming and then focus on the influence of the measuring protocol.

As discussed in section 2.3, the power dissipated in the electroforming step, is crucial in determining the switching characteristics of the diodes. At lower power, diodes do not show bistability but self-healing behavior after electroforming. In diodes containing 20 nm of oxide, electrical bistability can be induced by sweeping repeatedly up to 12 V. For diodes electroformed in this gentle way, Rocha *et al.* investigated the time needed to switch from off- to the on-state as function of the applied bias.^[61] For each measurement the memristor was first programmed in the off-state. Subsequently, the current was measured as a function of time following the application of a step voltage. Fig. 2.11a shows that the switching does not occur immediately upon applying the voltage.^[61] A so-called delay time, t_d , must elapse after voltage application before switching occurs. Furthermore, the lower the applied voltage, the longer the delay time

before switching occurs to be; a phenomenon also reported by Wang *et al.*^[62] In Fig. 2.11b, Rocha *et al.* show that the delay time follows an exponential dependence on applied voltage according to:

$$t_d = t_0 \exp(-\gamma V_a) \quad (2.5)$$

where t_0 is a constant and γ a voltage acceleration factor. A good fit to the data is obtained for $t_0 = 4.77 \times 10^9$ s and $\gamma = 3.37$ /V. We note that the functional dependence of t_d on applied voltage is similar to that observed for the time-to-dielectric-breakdown observed in thin films such as SiO₂ since the late 1970's.^[63] The dielectric breakdown is then driven by the total accumulated charge. Here however, as will be discussed in section 2.6, we assume that the origin is different. A filament is switched from the off-state to the on-state by injection of a trapped hole. Holes are minority carriers and are injected above the flat-band voltage, which set the threshold voltage for switching. Their density however is injection limited. Assuming that a certain critical hole density is needed for switching, the delay time for switching the off-state to the on-state depends exponentially on applied bias.

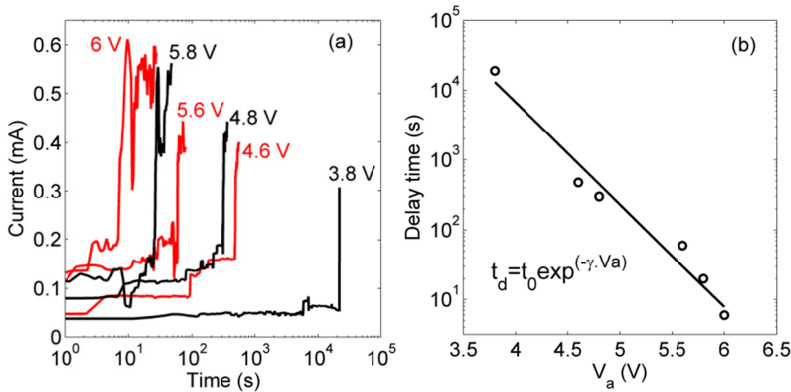


Figure 2.11: Switching dynamics. (a) Temporal evolution of current from the off- to the on-state after applying voltage steps of different magnitudes. The experimental sequence was from high to low bias. (b) Voltage dependence of the delay time for switching from the off-state to the on-state. Reprinted from Ref. [61]. Copyright 2013, AIP Publishing LLC.

Curiously, switching times are on the ms timescale, which is orders of magnitude more slowly than the fastest switching times reported in literature for aluminum oxide (~ 10 ns^[64]). Experimentally, investigation of the bias dependence from switching on- to off is challenging because the memory is not stable, once switched off, it will switch on again. Therefore no attempt was made to investigate the kinetics for switching from off- to on-state as function of bias voltage.

To explore the ultimate speed for switching in aluminum oxide / polymer diodes,

it is of interest to consider diodes with thinner oxide layer (10 nm) that were electroformed at higher power dissipation. Electroforming was now performed by applying a constant voltage (15 V) that was terminated immediately upon reaching a current compliance limit of 10 mA. Verbakel *et al.* first measured single switching events by implementing a waiting time of 10 s before the application of the bias voltage pulse.^[65] Fixed bias voltage amplitudes were used, corresponding to the top and bottom of the NDR.^[65] The current density was measured before and after switching using a low reading bias of 1 V. The current density as a function of pulse length for switching from the high resistance off-state to the low resistance on-state is shown in Fig. 2.12a, and from the on- to the off-state in Fig. 2.12b. Fig. 2.12a shows that a minimum pulse length of 200 ns is needed to induce a change in resistance from the off- to the on-state. Fig. 2.12b shows that the switching time from the on- to the off-state is 400 ns. These times are comparable to the fastest switching times reported in the literature.

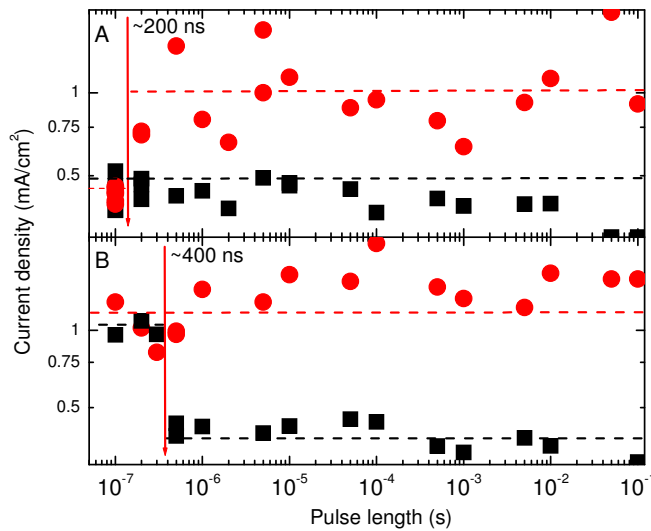


Figure 2.12: Discrete switching events. The current density measured using a low reading bias of 1 V before and after switching after an ON or OFF voltage pulse with varying length. (A) OFF (■) to ON (●) switching with a +4 V pulse; (B) ON (●) to OFF (■) switching with a +8 V pulse. The initial states were prepared ~ 10 s before the programming pulse. Reprinted from Ref. [65], copyright (2008), with permission from Elsevier.

After switching, the system is not immediately in thermodynamic equilibrium. It takes time to readjust the distribution of free electrons and trapped holes. This time is revealed by repeated pulse sequence measurements.^[65] An example of the voltage sequence is given in Fig. 2.13a,b. The programming pulse length is fixed to 0.5 ms. Using a high bias of 8 V the memory is switched off. After 1 ms the memory is switched back to

the on-state. This pulse sequence is repeated with a varying delay time. The current density is measured after each pulse using a low reading voltage of 1 V. Fig. 2.13 shows the current density in the first cycle (open symbols) and the second cycle (closed symbols) as a function of delay time between the cycles. Repeated off-on switching is presented in Fig 2.13c. For times longer than 3 ms the current densities in the first and second cycle are identical; the closed symbols overlap the open symbols. For shorter delay times the memory can be switched in the first cycle (open symbols) but not anymore in the second programming cycle (closed symbol). This demonstrates the presence of an adjustment, or “dead” time of about 3 ms for off-on switching. Similarly, Fig. 2.13d shows a dead time of about 1.5 ms for repeated on-off switching. The readjustment times depend on bias and device layout such as layer thicknesses. We note that the times derived are several orders of magnitude longer than the RC time constant. The huge variation in reported switching times might therefore be due to different measuring protocols. Measurements of single switching events yield nanosecond or microsecond switching times. The use of repeated switching cycles invariably leads to significant larger switching times (milliseconds) dominated by the dead time.

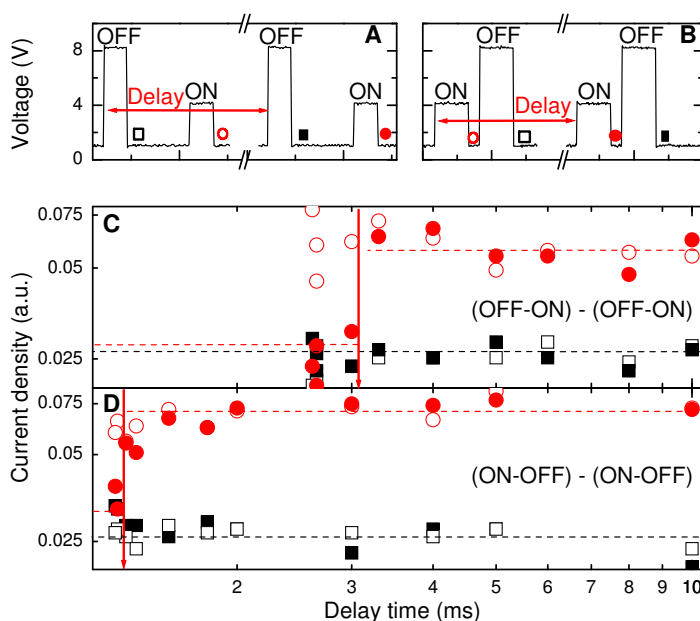


Figure 2.13: Repetitive switching. (A,B) Pulse sequence for (off-on)-(off-on) and (on-off)-(on-off) switching, and (C,D) current density under application of +1 V bias voltage monitoring the conductivity state after: □ first +8 V off pulse ; ○ first +4 V ON pulse ; ■ second +8 V OFF ; ● second +4 V, ON pulse. Reprinted from Ref. [65], copyright (2008), with permission from Elsevier.

The adjustment time can only be due to an intrinsic, slow process within the active layer(s) of the memristor and it puts a limitation on the access time of the memory. The dead time can be interpreted in terms of a time needed for the redistribution of charge density at the oxide/polymer interface, in such a way that a next switching event can occur. This time will be controlled by the charge transport properties of the insulator materials in the MIM diodes.

We note that the occurrence of a dead time is a key ingredient to observe unipolar switching. Take a memristor programmed in the high resistance off-state at high bias. After programming, the bias applied to the memristor needs to be restored to zero to store the information in a nonvolatile way. Lowering the bias applied to the diode, will necessarily bring it to a voltage range where switching to the on-state normally occurs. However, if a dead time for on-switching exists and if the bias voltage is ramped down on a time scale smaller than the dead time, the memory cannot switch back to the on-state. The off-state is preserved. Thus, a dead time is a prerequisite for unipolar memory operation.

2.6 Operation mechanism

In this section we will present a phenomenological interpretation of the memristor operation. The tentative interpretation is used to qualitatively explain the switching characteristics of unipolar memristors.

As explained in section 2.3.2, application of bias voltage can lead to the formation of defects in the oxide, including most likely oxygen vacancies. At sufficiently high defect densities, percolating paths for electrons are established leading to filamentary current distributions. This rudimentary understanding of the operation of a memristor may now be compared to that of a conventional NAND flash floating gate transistor (see Fig. 2.14a). In the flash memory, the floating gate acts as a charge trap. Upon injecting holes into the floating gate, electrons will accumulate in the channel of the transistor and form a conducting bridge between the source and drain. In analogy to the floating gate transistor, the operation of a unipolar memristor can qualitatively be understood in terms of defects in the oxide acting as a hole trap. At low voltage the trapped holes on the defects will be compensated by mobile electrons in the semiconductor (Fig. 2.14d). At a sufficiently high density of trapped positive charge, a percolating path for electrons will be established that may be observed experimentally as a current filament. Switching the filament to the on-state requires hole injection into the defects. Switching the filament to the off-state is due to recombination of the holes trapped at the defects with electrons from the semiconductor.

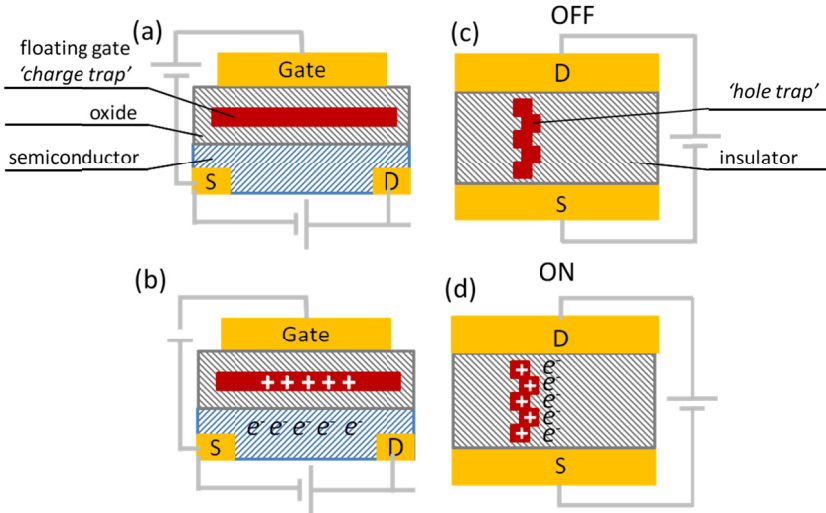


Figure 2.14: Schematic representation of (a,b) a floating-gate transistor, (c) a memristive diode after electroforming, with defects acting as floating gate. (d) Injection of holes into the defects allows for accumulation of electrons and formation of a current filament in the on-state of the memristor.

A crucial question in this qualitative picture of switching in a unipolar memristors is identifying the reason for the electrical bistability of the filament. Why is the filament stable in both the on- and off-state? Apparently, direct recombination of electrons and trapped holes in the on-state does not occur nor do the defects ionize spontaneously producing mobile carriers.

The high defect densities and the high (local) conductivities suggest a metal-insulator transition in the filament when it switches from the off- to on-state, as has been put forward by several authors.^[16,66,67]

A metal-insulator transition may be regarded as a phase transition. A convenient, yet simplified, way to describe phase transitions is by mean-field theories. The Debye-Hückel theory is such a mean-field theory that has been used to describe phase transitions and phase coexistence in ionic liquids.^[68-70] The Debye-Hückel theory accounts for screening of the Coulomb interaction between ions. This screening depends on the density of mobile charges (ions), which itself depends on the strength of the effective Coulombic interaction between the charges. The screening of charges by charges, provides a key ingredient in a possible mechanism for the switching of the filaments.

The Debye-Hückel expression for the screened potential between univalent charges is:

$$V_{DH}(r) \propto \frac{e^{-kr}}{r}, \tag{2.6}$$

where $1/\kappa$ is the Debye-Hückel screening length. The Debye-Hückel theory may be used to describe the ionization of a neutral defect (c) inside a dielectric into a positively charged (ionized) defect (p) and a mobile electron (n):



The Gibbs free energy for dissociation (ΔG) taking into account the dielectric screening can be expressed as:

$$-\frac{(\Delta G + \Delta G_0)}{k_B T} = \ln \left[\frac{\gamma_n \gamma_p n p}{c_0 - p} \right] = 2 \ln[\gamma] + \ln \left[\frac{n p}{c_0 - p} \right] \quad (2.8)$$

Here the γ_n (γ_p) represent activity coefficients for electrons (ionized defects); γ is an average activity coefficient and c_0 denotes the total defect concentration. ΔG_0 is a reference free energy corresponding to the ionization of fully isolated defects. The activity coefficient γ depends on the screening:

$$2 \ln[\gamma(n, p)] = -\frac{T_{ref}}{T} \frac{\kappa(n, p) a}{1 + \kappa(n, p) a} \quad (2.9)$$

We adopt the hard sphere model, which assumes a minimum distance a between the electron and the core of the defect. The minimum distance may be interpreted as the Bohr radius of the 1s state of the neutral defect. The expression for the activity coefficients in the hard sphere model is:

$$T_{ref} = \frac{q_e^2}{4\pi\epsilon_0\epsilon_r k_B a}, \quad (2.10)$$

with T_{ref} an intrinsic temperature for the system. Adopting $a = 0.35$ nm and $\epsilon_r = 9$, we obtain $T_{ref} = 5305$ K. The free energy for dissociation, assuming electroneutrality ($n = p = x$), can then be expressed as:

$$-\frac{(\Delta G + \Delta G_0)}{k_B T} = -\frac{1}{T_s} \frac{\sqrt{8\pi \frac{c_s}{T_s} x_s}}{1 + \sqrt{8\pi \frac{c_s}{T_s} x_s}} + \ln \left[\frac{x_s^2}{1 - x_s} \right] \quad (2.11)$$

with ΔG_0 the free energy, $T_s = T / T_{\text{ref}}$ a dimensionless temperature, $c_s = c / c_{\text{ref}} = c a^3$ a dimensionless defect concentration, and $x_s = x / c$ the degree of dissociation of the defects.

Importantly, for certain values of T_s and c_s , Eq. (2.11) predicts the coexistence of two phases, one with predominantly ionized defects, the other one with mainly neutral defects. Obviously, the phase coexistence also depends on ΔG_0 and its temperature dependence. Here we assume for simplicity $\Delta G_0 = \Delta S_0 = 0.3$ eV, independent of temperature. The region of coexistence predicted by Eq. (2.11) is illustrated in Fig. 2.15. Consistent with earlier results,^[68,71] we find a critical point (T_c, c_c) for the coexistence of neutral and ionized phases with a reduced temperature $T_c = 0.06$ (≈ 332 K for $T_{\text{ref}} = 5305$ K), above which the phase coexistence region vanishes. In addition, a critical reduced defect density c_c is predicted above which the insulator-metal transition vanishes. The critical density found amounts to $c_c = 0.012$ ($\approx 1 \times 10^{20}$ /cm³ for $c_{\text{ref}} = 1 / a^3 = 2.3 \times 10^{20}$ /cm³). Phase coexistence of an ionized (conducting) and a neutral (insulating) phase has been demonstrated experimentally for a variety of systems: ionic liquids,^[72] alkali metals dissolved in liquid ammonia^[73] and vanadium^[74] and manganese oxides.^[75-78]

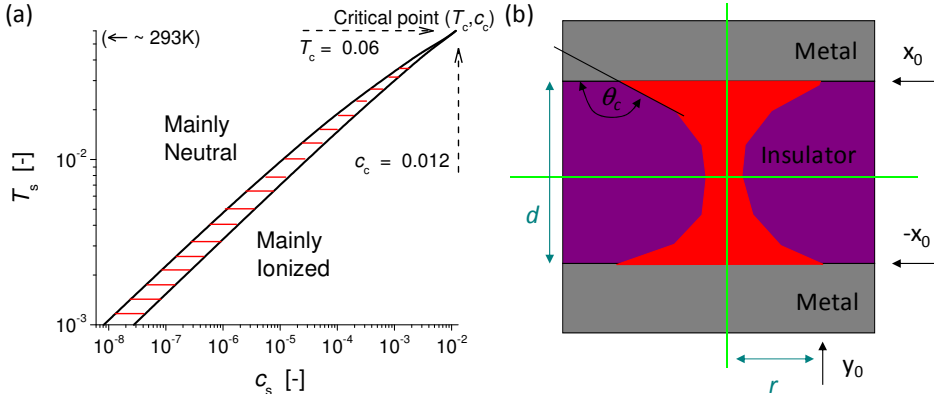


Figure 2.15: Coexistence of neutral (insulating) and ionized (conducting) phase in doped oxide. (a) Domain of phase coexistence (narrow red hatched area) in a reduced temperature (T_s), reduced defect concentration (c_s) diagram as predicted by Eq. (2.11). Above the critical temperature T_c and defect concentration c_c , the distinction between neutral and ionized phase vanishes. (b) Formation of a conducting bridge between metal electrodes of ionized phase embedded in insulating phase. The bridge has a minimal catenoid surface of revolution. By analogy with the water-air-glass system, differences in interface energy between ionized phase-metal electrode and ionized-neutral phases give rise to a contact angle θ_c that determines the exact radius r of the catenoid. In general, $r \propto d$, with d the thickness of the insulator.

Eq. (2.11) and the phase coexistence diagram in Fig. 2.15 offer the following scenario for electroforming and resistive switching in MIM diodes. Starting at zero defect concentration ($c_s = 0$), the diode is in the insulating state. During electroforming defects

are generated. Upon increasing the defect concentration at room temperature ($T < T_c$), the system will progressively pass from an insulating state, through the phase coexistence domain, and then finally into a conducting state. If the electroforming is performed carefully, the defect formation may be halted such that the system stays in the region of phase coexistence. In this region of phase coexistence, percolation paths for charge via the ionized conducting domains can constitute a current filament. This was shown experimentally for manganese oxides.^[77,78] Such a percolation type description of the insulator-to-metal transition has also been developed and tested for 2-D transport in inorganic semiconductor heterostructures.^[79-81]

Phase coexistence of insulating and conducting phases can thus explain the apparent electrical bistability of the memristor. The phase coexistence does not yet explain the reversible switching of the filaments between on- and off-states. This question is addressed in the following paragraphs.

Regarding coexistence of the ionized and neutral states, we argue that the interface between ionized and insulating phases will have a large positive interface energy, meaning that energy needs to be added to the system to enlarge the interface area between the phases. This is because the dielectric screening of defects at the interface will be only partial. The insulating phase does not contribute to the screening. In this respect, the interface between insulating and conducting phases resembles the air-water interface with its large surface tension due to unsatisfied hydrogen bonding interactions of the surface layer of water molecules.

Due to the large surface energy, nucleation of the ionized phase in the insulating phase is a rate limiting step in establishing the phase coexistence. Small regions or domains of ionized phase in the insulating phase will spontaneously dissipate, because of the high interface surface energy. To explain the formation of conducting regions in the coexistence domain, we argue that an applied electric field can assist in the nucleation of the ionized phase.

In analogy to a description of the insulator-to-metal transition for 2-D charge transport in semiconductor heterostructures,^[82] we now put forward the following qualitative picture for resistive switching in diodes. Application of a potential to a memristor with (T, c) below (T_c, c_c) on the insulator side of phase coexistence region can induce to injection of a hole into the oxide. That injected hole can give rise to defect formation similar as to the process during electroforming. The additional defect raises the local defect density allowing for establishment of a region of ionized phase. Electrical polarization of the ionized phase may result in further stabilization and the domains of ionized phase will also acquire an elongated cigar like shape.^[83] When the elongated region of ionized phase touches the metal electrodes, a conducting bridge will be formed. Experimental evidence supporting electrically driven insulator-to-metal transitions exists.^[84,85]

Because the metal can contribute to the dielectric screening of the ionized phase, we argue that the interface energy between ionized phase and metal will be much lower

than for the ionized phase and the insulating phase. As a result of the difference in interface energy, the ‘drop’ of ionized phase between the metal electrode will adopt a catenoid shape, just like a drop of water between two closely spaced (hydrophilic) glass plates (See Fig. 2.15b). The conducting phase will ‘wet’ the metal surface with a certain contact angle. The contact angle fixes the catenoid shape of the ionized domain. The region is now thermodynamically stable because it has a geometry with minimal interface area.^[86] We note that based on geometrical arguments, the minimal diameter of the conducting filament will be on the order of the thickness of the insulating layer.

Switching the filament to the off-state requires dissipation of the conducting domain. Within the phase coexistence model, the breaking of the conducting filament involves recombination of ionized defects with mobile electrons. The recombination of electrons and holes at defects is supported by electroluminescence measurements that show in the NDR region light emission from the Al_2O_3 . The dissolution of the conducting filament may be triggered by the removal of a single defect via processes similar as in the self-healing described above. An important experimental verification/falsification of the proposed mechanism would come from investigations on the (anti-)correlation of electrical switching and electroluminescence. If a considerable number of photons emitted as electroluminescence per switching event, experimental determination of such a correlation seems feasible.

We note that the phase coexistence diagram shown in Fig. 2.15a, predicts an anomalous temperature dependence of the conductivity in the MIM diode consistent with experimental observations as discussed in section 2.4.^[50]

The role of the contacts can now be understood as follows. Taking a pristine metal-insulator-semiconductor diode with two dissimilar electrodes, the different work functions will give rise to a built-in voltage. When the insulating oxide layer is thin, there will be a significant tunneling current. The presence of a built-in voltage will then yield rectifying I - V characteristics. However, when the insulator is thick, as the 20 nm in the present devices, the diode behaves as a capacitor. The current through the oxide is then negligible and rectifying properties do not originate from the built-in voltage but from transient trapping currents. Fig. 2.2 serves as an illustration. It shows that in the early stage of electroforming electrons are injected and trapped at the semiconductor / oxide interface when the capacitor is biased in the forward direction. However, in the reverse bias there is no current flowing because the current is injection limited. As a final result, a rectifying diode is obtained.

After electroforming however, the insulating properties of the oxide layer are severely altered. Since the defect density in the filaments is high, the depletion region associated with any barrier built-in-voltage is now extremely narrow and the interface region is transparent to the flow of electron. As a final result, the I - V characteristics are symmetric in applied bias for any combination of electrodes. To confirm the relative unimportance of the type of electrode on the current transport in unipolar memristors, nominally hole-only, electron-only and bipolar capacitors were fabricated. The contacts

were ITO/Pd, Al/Ba(Al) and ITO/Ba(Al) respectively. The I - V characteristics of the memristors after electroforming were symmetric and similar, independent of the applied electrodes.^[23]

In a large area memristor, several current filaments could exist side-by-side in the on- state. Because of statistical fluctuations of doping density and distribution, each filament will switch off under slightly different conditions. The different macroscopic current density in the on- and off-state of the memristor originates from the number of conducting filaments. The voltage controlled NDR exhibited by the unipolar memristor when going from the on- to the off-state can now be interpreted as the sequential switching off of a large number of individual current filaments. The current noise at biases where the switching occurs is random telegraph noise, as evidenced from discrete current fluctuations in the time domain (Fig. 2.10a) and the Lorentzian I/f^2 dependence of the noise in the frequency domain (Fig. 2.10c). The RTN noise indicates that the switching is due to opening and closing of discrete filaments. In the limit of small and narrow filaments, switching on and off of a single filament may be induced by trapping of a single charge carrier. This gives rise to discrete steps in the macroscopic conductivity of the memristor.

The occurrence of an insulator-to-metal phase transition and the presence of a critical point for the phase coexistence of ‘insulating’ and ‘conducting’ phase, as predicted above, may help to build a qualitative picture of the switching dynamics in the memristor. Near a critical point, fluctuations in the order parameter (in our case the degree of ionization of defects in the electroformed oxide) are predicted to show *critical slowing down*.^[87] Slow conversion between states with different electrical resistivity at zero bias is of course the defining characteristic of a resistive switching memory cell. The role of the voltage pulses applied to switch between different conduction seems to drive the system away from its critical point where dynamics is very slow and thus allow for switching in a finite time interval. As mentioned in section 2.5, any unipolar resistive memory operation requires a time delay or dead time for switching from the off-state to the on-state. The finite time interval needed for nucleation of the conducting phase in the phase coexistence model provides such an intrinsic dead-time required for any unipolar switching. The finite time for nucleation is related to the slow dynamics of the order parameter of a system near its critical point. It thus seems that unipolar switching requires operating conditions (T , c) close to the critical point (T_c , c_c).

Recent experiments have indicated that a transition from bipolar to unipolar switching is possible by increasing the maximum current density allowed in the electroforming.^[20,21] Assuming that the maximum forming current correlates with the defect density obtained, the observation of unipolar switching at high defect density may then indicate closer proximity of the operating conditions to the critical point.

We note that the quasi-random generation of defects in the electroforming procedure, should inevitably lead to spatial variation in the defect density. This spatial variation may be related to the highly heterogeneous dynamics of the switching process as

discussed in section 2.5. Holes injected during the switch-on voltage pulse into regions with subcritical defect density will not contribute to the formation of conducting filaments but could induce a built-in potential that prevents a second voltage induced switching event in the nearby regions with above-critical defect concentration. The slow recombination of injected holes in the subcritical regions that occur on the ms timescale (section 2.3.2) could then set a time limitation for fast repeated switching.

Critical slowing down of the dynamics near the critical point is often related to so-called ‘mode coupling’. Close to the critical point modes for transport of heat, propagation of sound and fluctuations of the order parameter become coupled via non-linear interactions. In view of the possibility of such mode coupling, it may not be possible to interpret the system dynamics in terms of a particular mechanism involving just one of these coupled modes. For instance, a switching mechanism based only on thermal effects may not be viable because of the strong coupling of heat transport to other modes near the critical point.^[87]

Near the critical point dynamic scaling relations may exist. For instance, for superconducting copper oxide,^[88] the relaxation time of the order parameter can be expressed as a function of magnetic field that is independent of $|T-T_c|$, provided that time and field scales are rescaled by appropriate powers of $|T-T_c|$.^[87] For resistive switching it is of great practical importance to understand the relation between time needed for switching events and the applied external electric field. This is discussed in more detail in the next section.

2.7 Practical consequences

In order to realize practical resistive switching memories, the so-called *voltage-time dilemma* has to be overcome.^[89] The switching between the two resistance states must be accomplished by a switching voltage pulse preferably less than 100 ns while it must withstand read voltages for up to 10 years using a reading voltage that is, for reasons of circuit design, no less than a tenth of the switching voltage. This puts certain requirements on the dynamics scaling relation between correlation time and electrical field. In the unipolar memories presented here, the dilemma is overcome by an exponential dependence of switching time on applied bias, and by a threshold voltage that originates from injection of trapped holes in the oxide.

The delay time for switching to an on-state increases exponentially with decreasing voltage. This imposes a limitation on the ability to switch. For a given scan rate, the internal device capacitances and resistances will determine which, and how many, local filaments switch-on at a particular value of the applied voltage. Current versus time histograms have shown that in a real device, a wide distribution of turn-on voltages and turn-on times exists. Some filaments, once switched-off in a previous scan, will not recover during the subsequent faster voltage ramp because the lower voltage over the oxide attained does not remain applied for a sufficiently long time to effectively turn-

on the memory.

The internal structure of the memristor has dramatic consequences for the switching as a function of scan rate. The memristor consists of a bilayer of an oxide and a semiconductor presented in the equivalent circuit of Fig. 2.1e as a double RC circuit. The switching, due to opening and closing of filaments, is represented by an additional parallel branch. It is connected to the formed off-state region by the distributed resistance of the polymer film which is represented by the dotted resistance connection. The switch S represents the mechanism giving rise to the NDR. When closed it connects the resistance R_F into the circuit to simulate a highly conducting path (or filament). When S is open, the normal oxide resistance is connected to the circuit and the micro-filament turns off. The bias over the oxide is a function of the scan speed. At low speed, the voltage over the oxide is about the same as the applied bias. However, as the scan rate increases the fraction of the voltage appearing over the oxide decreases.

Experimental I - V characteristics of the on-state as a function of voltage scan speed are presented in Fig. 2.16. For increasing speeds, both the device currents and the magnitude of the NDR gradually decrease: the latter disappears at a scan speed of 1000 V/s, in good agreement with literature reports.^[10,65,90] Furthermore, the NDR behavior shifts to lower voltages upon increasing the scan speed. The origin is that at very low voltage scan rates, the voltage over the oxide follows closely the applied voltage so that a large number of micro-switches will be triggered, composed of a wide distribution of current carrying capacity. As the scan rate increases, the maximum voltage attained over the oxide decreases so that fewer switches, characterized by decreasing current magnitudes, will be activated. At sufficiently high scan rates, only low-voltage, low current switches will be activated so that the overall device current becomes dominated by the displacement current corresponding to the device in the off-state. To recover the switching and the NDR, the voltage sweep should be performed to higher applied biases.

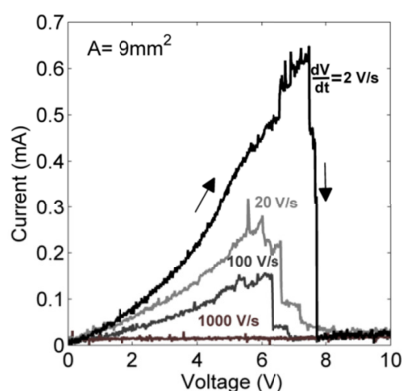


Figure 2.16: Transient response in the on-state. Experimental I - V characteristics of the on-state as a function of scan speed. Both the onset voltage and magnitude of the NDR gradually decrease with increasing scan speed. At 1000 V/s the NDR is lost. Reprinted from Ref. [61]. Copyright 2013, AIP Publishing LLC.

A fundamental limitation on the speed of operation of the memristor is not the switch-off process but the time- and voltage-dependence of the switch-on mechanism in the oxide. The switch-on time is further degraded by the internal capacitive structure of the device. The switch-on time can be reduced by decreasing the intrinsic relaxation time of the device. This in turn will reduce the rise time for the growth of the voltage across the oxide layer. The reduction might be achieved by minimizing both the oxide capacitance and the polymer resistance. However, careful optimization will be required.

2.8 Summary and conclusion

Unipolar switching in Al_2O_3 / polymer memristors involves defects that are created during the electroforming step. The density of defects is critical to the memory operation. Reproducible electroforming is possible by including in the device a well-defined thin layer of a semiconducting polymer. In their pristine state, the oxide / polymer diodes are insulating. The purpose of the polymer layer is threefold. Firstly, the polymer layer acts as a current limiting series resistance that prevents thermal runaway during electroforming. Secondly the presence of the polymer introduces an internal polymer/oxide interface, where electrons can accumulate. The trapped electrons stabilize positively charged defects that are generated during electroforming by electrostatic interactions. The trapped electrons promote injection of holes into the oxide, yielding a soft breakdown. Molecular oxygen is expelled and oxygen vacancies are formed. The third purpose of the polymer in the memristor is to buffer the molecular oxygen formed.

The experimental evidence indicates that the density of defects in the metal-insulator-metal diodes is of crucial importance to obtain a memristor with non-volatile memory properties. If the defect density is too high, the diode will short; if the density is too low, one is too far away from the phase coexistence region where both the insulating and conducting phase have thermodynamic stability. The coexistence seems crucial for electrical bistability. Noise measurements prove a unique tool to characterize the dynamics of the defect ionization and neutralization. The onset of discrete fluctuations and random telegraph signals may serve as a diagnostic to determine the difference between the actual defect density and the desired concentration for memory operation.

In summary, unipolar resistive switching poses a unique challenge to the materials scientist to design, deposit and characterize materials with appropriate electronic structure, defect ordering and internal charge carrier dynamics. This challenge seems parallel to development of e.g. materials for high temperature superconductivity. Fortunately, in the case of memristors, we have already the certainty from the present state-of-the-art involving the electroforming, that relatively simple materials exist with the right properties. The challenge is to gain control over the now largely random process of defect formation.

2.9 References

- [1] J. Hutchby and M. Garner, Assessment of the Potential & Maturity of Selected Emerging Research Memory Technologies Workshop & ERD/ERM Working Group Meeting (April 6-7, 2010) (ITRS Edition, 2010), pp. 1. http://www.itrs.net/Links/2010ITRS/2010Update/ToPost/ERD_ERM_2010FINALReportMemoryAssessment_ITRS.pdf
- [2] R. Waser, R. Dittman, G. Staikov, and K. Szot, *Adv. Mater.* **2009**, *21*, 2632.
- [3] Y. Yang, J. Ouyang, L. Ma, R. J. H. Tseng, and C. W. Chu, *Adv. Funct. Mat.* **2006**, *16*, 1001.
- [4] J. C. Scott and L. D. Bozano, *Adv. Mater.* **2007**, *19*, 1452.
- [5] B. Cho, T.-W. Kim, S. Song, Y. Ji, M. Jo, H. Hwang, G.-Y. Jung, and T. Lee, *Adv. Mater.* **2010**, *22*, 1228.
- [6] B. Cho, S. Song, Y. Ji, T. W. Kim, and T. Lee, *Adv. Funct. Mater.* **2011**, *21*, 2806.
- [7] Y. Ji, B. Cho, S. Song, T.-W. Kim, M. Choe, Y. H. Kahng, and T. Lee, *Adv. Mater.* **2010**, *22*, 3071.
- [8] S. Song, B. Cho, T.-W. Kim, Y. Ji, M. Jo, G. Wang, M. Choe, Y. H. Kahng, H. Hwang, and T. Lee, *Adv. Mater.* **2010**, *22*, 5048.
- [9] T. W. Hickmott, *J. Appl. Phys.* **1962**, *33*, 2669.
- [10] J. G. Simmons and R. R. Verderber, *Proc. R. Soc. London Ser. A* **1967**, *301*, 77.
- [11] J. F. Gibbons and W. E. Beadle, *Sol.-State Electron.* **1964**, *7*, 785.
- [12] G. Dearnaley, A. M. Stoneham, and D. V. Morgan, *Rep. Prog. Phys.* **1970**, *33*, 1129.
- [13] D. P. Oxley, *Electrocomp. Sci. Technol.* **1977**, *3*, 217.
- [14] H. Pagnia and N. Sotnik, *Phys. Status Solidi* **1988**, *108*, 11.
- [15] A. Asamitsu, Y. Tomioka, H. Kuwahara, and Y. Tokura, *Nature* **1997**, *388*, 50.
- [16] A. Sawa, *Materials Today* **2008**, *11*, 28.
- [17] R. Waser and M. Aono, *Nat. Mat.* **2007**, *6*, 833.
- [18] L. O. Chua, *IEEE T. Circuit Theory* **1971**, *18*, 507.
- [19] D. B. Strukov, G. S. Snider, D. R. Stewart, and R. S. Williams, *Nature* **2008**, *453*, 80.
- [20] T. Yanagida, K. Nagashima, K. Oka, M. Kanai, A. Klamchuen, B. H. Park, and T. Kawai *Sci. Reports* **2013**, *3*, 1657.
- [21] C. Schindler, S. C. P. Thermadam, R. Waser, and M. N. Kozicki, *IEEE T. Electron Dev.* **2007**, *54*, 2762.
- [22] J. H. Hur, M. Lee, C. B. Lee, and Y. Kim, *Phys. Rev. B* **2010**, *82*, 155321.
- [23] F. Verbakel, S. C. J. Meskers, R. A. J. Janssen, H. L. Gomes, M. Cölle, M. Büchel, and D. M. de Leeuw, *Appl. Phys. Lett.* **2007**, *91*, 192103.
- [24] S. L. M. van Mensfoort, J. Billen, S. I. E. Vulto, R. A. J. Janssen, and R. Coehoorn, *Phys. Rev. B* **2009**, *80*, 033202.
- [25] T. W. Hickmott, *J. Appl. Phys.* **2000**, *88*, 2805.
- [26] Q. Chen, H.L. Gomes, P. R. F. Rocha, D. M. de Leeuw, and S. C. J. Meskers, *Appl. Phys. Lett.* **2013**, *102*, 153509.
- [27] L. D. Bozano, B. W. Kean, V. R. Deline, J. R. Salem, and J. C. Scott, *Appl. Phys. Lett.* **2004**, *84*, 607.
- [28] International technology roadmap for semiconductors, 2011 Edition, Emerging research devices, <http://www.itrs.net/Links/2011itrs/2011Chapters/2011ERD.pdf>, accessed: December, 2013.

- [29] Q. Chen, B. F. Bory, A. Kiazadeh, P. R. F. Rocha, H. L. Gomes, F. Verbakel, D. M. de Leeuw, and S. C. J. Meskers, *Appl. Phys. Lett.* **2011**, *99*, 083305.
- [30] B. F. Bory, S. C. J. Meskers, R. A. J. Janssen, H. L. Gomes, and D. M. de Leeuw, *Appl. Phys. Lett.* **2010**, *97*, 222106.
- [31] Y. L. Chiou, J. P. Gambino, and M. Mohammad, *Solid-State Electron.* **2001**, *45*, 1787.
- [32] J. Maserjian and N. Zamani, *J. Appl. Phys.* **1982**, *53*, 559.
- [33] T. J. Mego, *Rev. Sci. Instrum.* **1986**, *57*, 2798.
- [34] K. Ziegler and E. Klausmann, *Appl. Phys. Lett.* **1975**, *26*, 400.
- [35] W. T. Li, D. R. McKenzie, W. D. McFall, Q.-C. Zhang, and W. Wiszniewski, *Solid-State Electron.* **2000**, *44*, 1557.
- [36] J. Lee, S. S. Kim, and S. Im, *J. Vac. Sci. Technol. B* **2003**, *21*, 953.
- [37] X. Wu, D. B. Migas, X. Li, M. Bosman, N. Raghavan, V. E. Borisenko, and K. L. Pey, *Appl. Phys. Lett.* **2010**, *96*, 172901.
- [38] A. Crespo-Yepes, J. Martin-Martinez, R. Rodriguez, M. Nafria, and X. Aymerich, *Microelectron. Reliab.* **2009**, *49*, 1024.
- [39] A. Crespo-Yepes, J. Martin-Martinez, A. Rothschild, R. Rodriguez, M. Nafria, and X. Aymerich, *IEEE Electron. Device Letters* **2010**, *31*, 543.
- [40] T. W. Hickmott, *J. Appl. Phys.* **2012**, *111*, 063708.
- [41] X. Wu, K. L. Pey, G. Zhang, P. Bai, X. Li, W. H. Liu, and N. Raghavan, *Appl. Phys. Lett.* **2010**, *96*, 202903.
- [42] H. D. Lee, B. Magyari-Köpe, and Y. Nishi, *Phys. Rev. B* **2010**, *81*, 193202.
- [43] B.D. Evans, *J. Nucl. Mater.* **1995**, *219*, 202.
- [44] M. D. Pickett and R. S. Williams, *Nanotechnology* **2012**, *23*, 215202.
- [45] F. Verbakel, S. C. J. Meskers, and R. A. J. Janssen, *J. Appl. Phys.* **2007**, *102*, 083701.
- [46] A. Gurlo and R. Riedel, *Angew. Chem.* **2007**, *119*, 3900.
- [47] M. Cölle, M. Büchel, and D. M. de Leeuw, *Org. Electron.* **2006**, *7*, 305.
- [48] O. Kurnosikov, F. C. de Nooij, P. LeClair, J. T. Kohlhepp, B. Koopmans, H. J. M. Swagten, and W. J. M. de Jonge, *Phys. Rev. B* **2001**, *64*, 153407.
- [49] Y. S. Kim, J.-S. Kim, J. S. Choi, I. R. Hwang, S. H. Hong, S.-O. Kang, and B. H. Park, *Appl. Phys. Lett.* **2011**, *98*, 192104.
- [50] H. L. Gomes, P. R. F. Rocha, A. Kiazadeh, D. M. De Leeuw, and S. C. J. Meskers, *J. Phys. D: Appl. Phys.* **2011**, *44*, 25103.
- [51] P. R. F. Rocha, H. L. Gomes, L. K. J. Vandamme, Q. Chen, A. Kiazadeh, D. M. de Leeuw, and S. C. J. Meskers, *IEEE T. Electron Dev.* **2012**, *59*, 2483.
- [52] M. Nardone, V. I. Kozub, I. V. Karpov, and V. G. Karpov, *Phys. Rev. B* **2009**, *79*, 165206.
- [53] F. N. Hooge, T. G. M. Kleinpenning, and L. K. J. Vandamme, *Rep. Prog. Phys.* **1981**, *44*, 479.
- [54] P. R. F. Rocha unpublished results.
- [55] D. Wolf and E. Holler, *J. Appl. Phys.* **1967**, *38*, 189.
- [56] X. G. Jiang, M. A. Dubson, and J. C. Garland, *Phys. Rev. B* **1990**, *42*, 5427.
- [57] H. Kohlstedt, K. H. Gundlach, and S. Kuriki, *J. Appl. Phys.* **1993**, *73*, 2564.
- [58] M. J. Kirton and I. I. Uren, *Adv. Phys.* **1989**, *38*, 367.
- [59] R. Soni, P. Meuffels, A. Petraru, M. Weides, C. Kügeler, R. Waser, and H. Kohlstedt, *J. Appl. Phys.* **2010**, *107*, 024517.

- [60] S. Machlup, *J. Appl. Phys.* **1954**, 25, 341.
- [61] P. R. F. Rocha, A. Kiazadeh, D. M. De Leeuw, S. C. J. Meskers, F. Verbakel, D. M. Taylor, and H. L. Gomes, *J. Appl. Phys.* **2013**, 113, 134504.
- [62] M. L. Wang, J. Zhou, X. D. Gao, B. F. Ding, Z. Shi, X. Y. Sun, X. M. Ding, and X. Y. Houa, *Appl. Phys. Lett.* **2007**, 91, 143511.
- [63] D. L. Crook, *Proc. Int. Rel. Phys. Symp.* **1979**, 1.
- [64] Y. Wu, S. Yu., B. Lee, and H.-S. P. Wong, *J. Appl. Phys.* **2011**, 110, 094104.
- [65] F. Verbakel, S. C. J. Meskers, R. A. J. Janssen, H. L. Gomes, A. J. M. van den Biggelaar, and D. M. de Leeuw, *Org. Electron.* **2008**, 9, 829.
- [66] H. S. Lee, S. G. Choi, H. H. Park, and M. J. Rozenberg, *Sci Rep.* **2013**, 3, 1704.
- [67] A. Odagawa, H. Sato, I. H. Inoue, H. Akoh, M. Kawasaki, Y. Tokura, T. Kanno, and H. Adachi, *Phys. Rev. B* **2004**, 70, 224403.
- [68] M. E. Fisher and Y. Levin, *Phys. Rev. Lett.* **1993**, 71, 3826.
- [69] M. E. Fisher, *J. Stat. Phys.* **1994**, 75, 1.
- [70] W. Schroerer, *Contrib. Plasm. Phys.* **2012**, 52, 78.
- [71] V. McGahay and M. Tomozawa, *J. Non-cryst. Solids* **1989**, 109, 27.
- [72] P. Chieux and M. J. Sienko, *J. Chem. Phys.* **1970**, 53, 566.
- [73] K. Gutkowski, M. A. Anisimov, and J. V. Sengers, *J. Chem. Phys.* **2001**, 114, 3133.
- [74] M. K. Liu, M. Wagner, E. Abreu, S. Kittiwatanakul, A. McLeod, Z. Fei, M. Goldflam, S. Dai, M. M. Fogler, J. Lu, S. A. Wolf, R. D. Averitt, and D. N. Basov, *Phys. Rev. Lett.* **2013**, 111, 096602.
- [75] A. Moreo, S. Yunoki, and E. Dagotto, *Science* **1999**, 283, 2034.
- [76] M. Fath, S. Freisem, A. A. Menovsky, Y. Tomioka, J. Aarts, and J. A. Mydosh, *Science* **1999**, 285, 1540.
- [77] M. Uehara, S. Mori, C. H. Chen, and S.-W. Cheong, *Nature* **1999**, 399, 560.
- [78] L. Zhang, C. Israel, A. Biswas, R. L. Greene, and A. de Lozanne, *Science* **2002**, 298, 805.
- [79] Y. Meir, *Phys. Rev. Lett.* **1999**, 83, 3506.
- [80] J. Shi, S. He, and X. C. Xie, *Phys. Rev. B* **1999**, 60, R13950.
- [81] S. Ilani, A. Yachoby, D. Mahalu, and H. Shtrikman, *Science* **2001**, 292, 1354.
- [82] S. Das Sarma, M. P. Lilly, E. H. Hwang, L. N. Pfeiffer, K. W. West, and J. L. Reno, *Phys. Rev. Lett.* **2005**, 94, 136401.
- [83] M. Cui, T. Emrick, and T. P. Russel, *Science* **2013**, 342, 460.
- [84] R. Könenkamp, *Phys. Rev. B* **1988**, 38, 3056.
- [85] H. Jeen and A. Biswas, *Phys. Rev. B* **2013**, 88, 024415.
- [86] J. Oprea, *The Mathematics of Soap Films: Explorations with Maple*, American Mathematical Soc., USA **2000**.
- [87] P. C. Hohenberg and B. I. Halperin, *Rev. Mod. Phys.* **2000**, 49, 435.
- [88] J. Kötzler, G. Nakielski, M. Baumann, R. Behr, F. Goerke, and E.H. Brandt, *Phys. Rev. B* **1994**, 50, 3384.
- [89] C. Schindler, G. Staikov, and R. Waser, *Appl. Phys. Lett.* **2009**, 94, 072109.
- [90] D. P. Oxley, in *Oxides and Oxide Films*, Vol. 6, p. 251 (Eds: A. K. Vijh), Marcel Dekker Inc., USA **1981**.

Chapter 3

Trapping of electrons in metal oxide-polymer memory diodes in the initial stage of electroforming

Abstract

Metal oxide-polymer diodes require electroforming before they act as non-volatile resistive switching memory diodes. Here we investigate the early stages of the electroforming process in Al/Al₂O₃/poly(spirofluorene)/Ba/Al diodes using quasi-static capacitance-voltage (QSCV) measurements. In the initial stage, electrons are injected into the polymer and then deeply trapped near the poly(spirofluorene)/Al₂O₃ interface. For bias voltages below 6 V, the number of trapped electrons is found to be $C_{\text{oxide}} V/q$ with C_{oxide} the geometrical capacitance of the oxide layer. This implies a density of traps for the electrons at the polymer/metal oxide interface larger than $3 \times 10^{17} /\text{m}^2$.

This Chapter has been published as:

B. F. Bory, S. C. J. Meskers, R. A. J. Janssen, H. L. Gomes, and D. M. de Leeuw, *Appl. Phys. Lett.* **2010**, *97*, 222106.

3.1 Introduction

Metal-insulator-semiconductor-metal diodes incorporating a metal oxide layer as an insulator show non-volatile resistive switching^[1-5] and can be used to store information.^[6-8] Switching is an intrinsic property of metal oxides,^[1,4,9] the semiconductor acts as a current limiting series resistance.^[10,11] Currently such bistable diodes are being considered as possible replacement for standard NAND-flash solid-state memories.^[12] For the memory functionality to become active, usually an electroforming step is required. In this step, the diode is subjected to a high bias voltage,^[13] leading to soft breakdown of the oxide.

The microscopic mechanism of this electroforming process is still unknown. In a previous study, Verbakel et al. have shown that the J - V characteristic shows hysteresis before forming, indicating deep trapping of charges.^[10] Here we investigate this trapping further using the voltage step quasi-static capacitance-voltage (QSCV) method.^[14,15] This method is ideally suited to investigate traps that fill quickly but empty slowly. We derive the location of traps and their density.

3.2 Experimental

The diodes consist of an aluminum bottom electrode on which a thin layer of aluminum oxide is sputtered. On top, a thin film of the organic semiconductor poly(spirofluorene)^[16] is spin coated. The top electrode is made by vacuum sublimation of barium followed by aluminum. The nominally electron-only diodes with an active area of 9 mm² are encapsulated with a getter in order to maintain an oxygen and water free atmosphere. Previously, we have shown that the diodes can be converted into bistable resistive switches in high yield after an electroforming process.^[10,17,18] Electrical characterization was performed using an Agilent 4155C semiconductor analyzer. Positive bias is defined as the Ba/Al top electrode being charged negative. J - V sweeps were recorded with 10 mV steps and 40 ms integration time. In QSCV measurements, an integration time of 4 s and a step of 100 mV were used.

3.3 Results

The electroforming process for a pristine Al/Al₂O₃/poly(spirofluorene)/Ba/Al diode is presented in Fig. 3.1a. Here we show cyclic J - V scans where the maximum bias is increased stepwise. The arrows indicate the direction of the voltage scans starting at 0 V, scanning forward and then backward to 0 V.^[10]

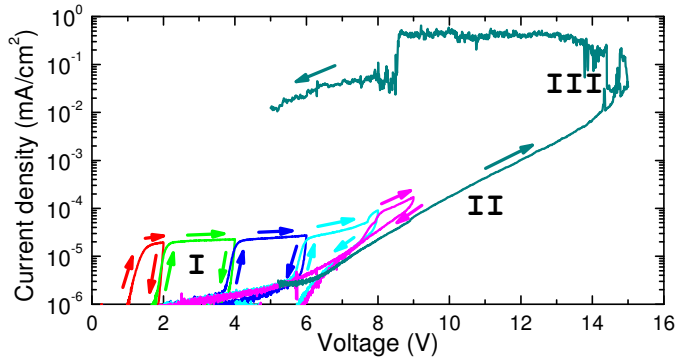


Figure 3.1: (a) Sequential J - V characteristics of a pristine Al/Al₂O₃ (20 nm) /polymer (50 nm) /Ba/Al diode. (b) Current density as function of time upon application of a voltage step from 0 to 6 V at time t equal to zero.

We discern three stages in the electroforming process. In the first stage, for voltages in the range between 0 and 8 V, we observe a pronounced hysteresis in the current-voltage characteristics. In the forward scan, the current increases with bias. However in the backward scan the current is negligible. Actually the current level on the return scan is approximately equal to the displacement current associated with the device geometrical capacitance C_0 , assuming that both oxide and polymer layer are insulators. If the subsequent J - V loop is recorded using the same bias conditions, the hysteresis is not present and the measured current equals the displacement current. Then, scanning forward to a higher bias voltage that has not been applied before, the current shows a large increase. Backward scans give the same low current value and are independent of the previous scans. The original hysteresis loops are only restored after resting for a few hours. The hysteresis strongly depends on the scanning speed and is only observed when charging the top Ba/Al electrode negatively. Figure 3.1b shows the electrical current as a function of time, applying a bias step from 0 to 6 V. In the first 10 s after the bias step, the current decreases sharply and approaches an asymptotic value, interpreted as residual leakage current. The leakage is more than an order of magnitude smaller than the initial charging current. This behavior suggests that the observed hysteresis results from traps that fill in a time scale of seconds but empty slowly, on a time scale of hours.

In the second stage of electroforming, for biases from 8 to 14 V, the amount of hysteresis decreases with increasing bias. The magnitude and voltage dependence of the

current can be tentatively modeled as being due to Fowler-Nordheim tunneling through the oxide^[19] using a barrier height of approximately 1 eV and assuming a potential drop over the oxide layer equal to the applied bias. In the third stage of electroforming, occurring at biases larger than 14 V, a sharp and irreversible increase of the current density is observed, indicative of soft breakdown. The resistance of the diode is now bistable and can be switched reversibly between a high and a low level.^[10]

The hysteresis observed in the first stage of forming can be studied in more detail using the QSCV method. Figure 3.2a shows cyclic C - V scans under the same bias conditions as for the J - V scans. Scanning in reverse bias ($V < 0$), a practically constant capacitance of 2.7 nF is recorded which we interpret as the geometrical capacitance C_0 . The hysteresis is due to a small leakage current.

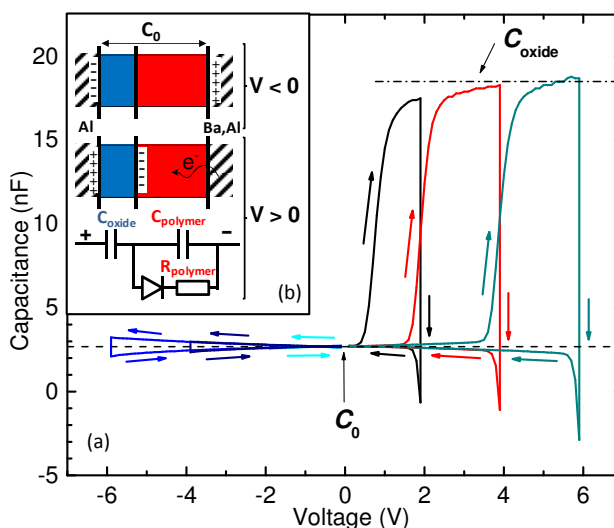


Figure 3.2: (a) QSCV characteristic of a pristine Al/Al₂O₃ (40 nm)/polymer (80 nm)/Ba/Al diode. (b) Schematic representation of the diode and equivalent circuit. For negative bias voltage V , no charge is injected into the polymer. Both oxide and polymer act as insulators. For positive bias, electrons are injected into the polymer and trapped near the metal-oxide/polymer interface.

In forward bias, we observe capacitances exceeding the geometrical capacitance by an order of magnitude when scanning over a bias voltage range to which the diode has not been subjected before. In the first cyclic scan ($0 \text{ V} \rightarrow 2 \text{ V} \rightarrow 0 \text{ V}$), scanning forward to 2 V, the capacitance reaches up to 17.5 nF. Scanning back from 2 to 0 V, we again find the geometrical capacitance C_0 . In the next scan to higher bias, we first observe C_0 up to 2 V, but at higher bias up to 4 V, the capacitance again rises sharply to 18 nF as before. The capacitance in the backward scan is again similar to C_0 . In the third cyclic scan up to 6 V, a maximum in the capacitance of 18.5 nF is recorded at 6 V. The reciprocal value of this

high capacitance, C_{high} , is plotted in Fig. 3.3b. For voltages exceeding 6 V, leakage currents significantly affect the capacitance measurement. Systematic variation of the oxide and polymer thickness yields a set of C_0 and C_{high} values whose reciprocal values are plotted in Fig. 3.3.

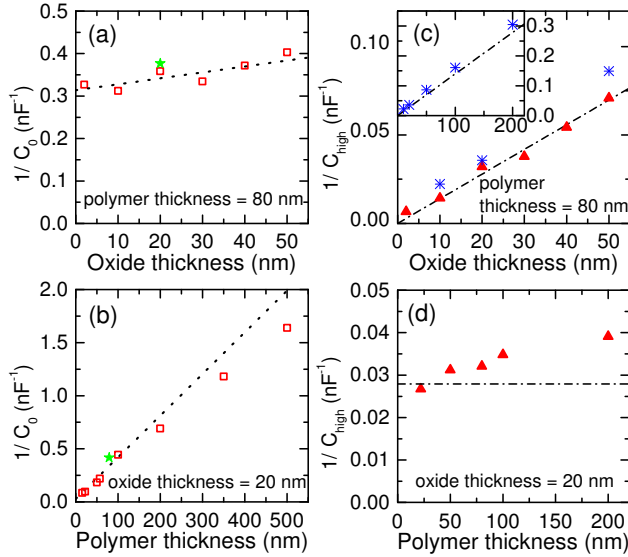


Figure 3.3: Capacitance for Al/Al₂O₃/ polymer/Ba/Al diodes. $1/C_0$ (\square) as function of (a) thickness of the oxide layer at constant thickness of polyfluorene layer (80 nm) and (b) thickness of the polyfluorene layer at constant oxide thickness (20 nm). $1/C_{\text{high}}$ (\blacktriangle) as function of (c) oxide thickness with 80 nm polymer and (d) polymer thickness with 20 nm oxide (20 nm). Star (\star) in (a, b) represents C_0 for a Al/Al₂O₃ (20 nm)/ poly(styrene) (79 nm)/Ba/Al. Stars (\star) in (c) show capacitance for Al/Al₂O₃/Ba/Al diodes without any polymer. The dashed lines in (a,b) represent the theoretical geometrical capacitance. Dash-dotted lines in (c,d) represent the oxide capacitance C_{oxide} .

3.4 Discussion

We consider the diode as a double-layer structure comprised of an oxide layer (with capacitance C_{oxide}) in series with a polymer layer (C_{polymer}). As expected, the experimental C_0 for diodes, as obtained from QSCV near zero bias (Fig. 3.3a,b), can be modeled accurately by the relation $1/C_0 = 1/C_{\text{oxide}} + 1/C_{\text{polymer}}$ using relative dielectric constants $\epsilon_{\text{Al}_2\text{O}_3} = 9$ and $\epsilon_{\text{polymer}} = 3.2$.^[20] $1/C_0$ is weakly dependent on the oxide thickness (Fig. 3.3a), but strongly varies with polymer thickness (Fig. 3.3b), because C_{oxide} is much higher than C_{polymer} . In contrast, the high capacitance from QSCV, C_{high} , varies strongly with oxide thickness (Fig. 3.3c) but is virtually independent of polymer thickness (Fig 3.3d).

Moreover C_{high} is essentially the same as the capacitance measured with QSCV on devices without polymer layer, and matches with the calculated C_{oxide} (Fig. 3.3c).

The equality of C_{high} and C_{oxide} can be explained as follows. Under sufficient forward bias, electrons are injected via the Ba/Al electrode,^[16] drift through the polymer and get trapped at the polymer/oxide interface. Representing the bilayer by the equivalent circuit in Fig. 3.2b, injection of mobile electrons lowers R_{polymer} sufficiently to shunt C_{polymer} , and raises the bilayer capacitance to C_{oxide} . Irreversible trapping of electrons at the interface, symbolized by the diode, explains why C_{oxide} is only observed using the QSCV method under forward bias that is applied for the first time. For instance, in the return path of the cyclic QSCV scan, there is no discharging current because of the trapping and the two layers behave again as pure insulators with overall device capacitance C_0 . In a second scan, new electrons can only be injected into the polymer when the bias voltage applied exceeds the built-in voltage resulting from the trapped electrons. Hence C_{oxide} is observed only if the applied bias voltage exceeds the maximum voltage of the previous scan. Under negative bias, a high injection barrier prevents injection of holes into the polymer and the capacitance equals C_0 .

From the observation that C_{high} matches with C_{oxide} for bias voltages up to 6 V (Fig. 3.3c), we conclude that the number of electrons stored at the oxide-polymer interface is determined by the capacitance of the oxide layer and the applied bias V_{appl} . This implies a density of trap states for electrons at the interface exceeding $C_{\text{oxide}}V_{\text{appl}} / (A q_e) = 3 \times 10^{17} / \text{m}^2$ with A the surface area of the capacitor, and q_e the electron charge using $C_{\text{oxide}} = 70 \text{ nF}$ as determined at 6 V for 10 nm oxide thickness. For very thick polymer layers, C_{high} is slightly smaller than C_{oxide} (Fig. 3.3d). A possible explanation is that the carrier trapping becomes slow with respect to the integration time because of the long transit time of electrons across the thick polymer layer with low electron mobility. In a diode with a layer of insulating polystyrene instead of semiconducting poly(spirofluorene), we do not observe any hysteresis loops in either J - V or C - V scans, indicating that electron injection into this insulating polymer is not possible.

3.5 Conclusion

We conclude that in Al/Al₂O₃/poly(spirofluorene)/Ba/Al diodes, electrons injected through the Ba/Al electrode are trapped at the internal oxide/polymer interface in the first stage of forming. The chemical nature of the traps is still unknown, yet, phenomenologically, they behave as border traps known from MOS devices.^[21] The trapping leads to a maximization of the potential drop over the oxide layer. This enhances tunneling currents through the oxide, stage two of the electroforming. Trapping of electrons also brings the electric field in the oxide closer to the threshold for dielectric breakdown at relatively low applied bias voltage, thus promoting the final stage of electroforming.

3.6 References

- [1] S. Karthäuser, B. Lüsse, M. Weides, M. Alba, A. Besmehn, R. Oligschlaeger, and R. Waser, *J. Appl. Phys.* **2006**, *100*, 094504.
- [2] R. Müller, J. Genoe, and P. Heremans, *Appl. Phys. Lett.* **2009**, *95*, 133509.
- [3] T. Chang, Y. Cheng, and P. Lee, *Appl. Phys. Lett.* **2010**, *96*, 043309.
- [4] T. Oyamada, H. Tanaka, K. Matsushige, H. Sasabe, and C. Adachi, *Appl. Phys. Lett.* **2003**, *83*, 1252.
- [5] B. Cho, S. Song, Y. Ji, and T. Lee, *Appl. Phys. Lett.* **2010**, *97*, 063305.
- [6] R. Waser, R. Dittmann, G. Staikov, and K. Szot, *Adv. Mater.* **2009**, *21*, 2632.
- [7] A. Sawa, *Materials Today* **11**, 28 (2008).
- [8] M. Lee, Y. Park, D. Suh, E. Lee, S. Seo, D. Kim, R. Jung, B. Kang, S. Ahn, C. Lee, D. Seo, Y. Cha, I. Yoo, J. Kim, and B. Park, *Adv. Mater.* **2007**, *19*, 3919.
- [9] J. G. Simmons and R. R. Verderber, *Proc. R. Soc. London, Ser. A* **1967**, *301*, 77.
- [10] F. Verbakel, S. C. J. Meskers, R. A. J. Janssen, H. L. Gomes, M. Cölle, M. Büchel, and D. M. de Leeuw, *Appl. Phys. Lett.* **2007**, *91*, 192103.
- [11] H. Gomes, A. Benvenho, D. de Leeuw, M. Cölle, P. Stallinga, F. Verbakel, and D. Taylor, *Org. Electron.* **119**, 9, 119.
- [12] J. Hutchby and M. Garner, *Assessment of the Potential & Maturity of Selected Emerging Research Memory Technologies Workshop & ERD/ERM Working Group Meeting (April 6-7, 2010)* (ITRS Edition, 2010), pp. 1.
- [13] T.W. Hickmott, *J. Appl. Phys.* **2000**, *88*, 2805.
- [14] T.J. Mego, *Rev. Sci. Instrum.* **1986**, *57*, 2798.
- [15] K. Ziegler and E. Klausmann, *Appl. Phys. Lett.* **1975**, *26*, 400.
- [16] S. L. M. van Mensfoort, J. Billen, S. I. E. Vulto, R. A. J. Janssen, and R. Coehoorn, *Phys. Rev. B* **2009**, *80*, 033202.
- [17] M. Cölle, M. Büchel, and D. M. de Leeuw, *Org. Electron.* **2006**, *7*, 305.
- [18] F. Verbakel, S. C. J. Meskers, R. A. J. Janssen, H. L. Gomes, A. J. van den Biggelaar, and D. M. de Leeuw, *Org. Electron.* **2008**, *9*, 829.
- [19] Y. L. Chiou, J. P. Gambino, and M. Mohammad, *Solid-State Electron.* **2001**, *45*, 1787.
- [20] S. L. M. van Mensfoort, S. I. E. Vulto, R. A. J. Janssen, and R. Coehoorn, *Phys. Rev. B* **2008**, *78*, 085208.
- [21] D. M. Fleetwood, M. R. Shaneyfelt, and J. R. Schwank, *Appl. Phys. Lett.* **1994**, *64*, 1965.

Chapter 4

Accumulation of charge at the LiF/organic semiconductor interface in the early stage of electroforming

Abstract

Application of forward bias voltage stress to metal/LiF/poly(spirofluorene)/Ba/Al diodes results in injection of electrons into the organic semiconductor via the Ba/Al contact and subsequent trapping of the electrons at the LiF/polymer interface. Increasing the bias voltage further, electrons can tunnel from the polymer into the LiF. The dc and ac conductivity of the diodes under forward dc bias in the range +2 to +5 V are found to be virtually independent of the thickness of the LiF layer (10-50 nm) and limited mainly by transport through the organic semiconductor. Tunnelling of electrons from the polymer into the LiF is assisted by positively charged defects in the LiF layer with a density of 10^{19} /cm³. The defects in LiF are induced by application of forward bias voltage and disappear spontaneously under short circuit. The results indicate that when the defect density in LiF exceeds a certain threshold, electroforming is completed by an irreversible change in conductivity, after which non-volatile memristive effects can be observed.

4.1 Introduction

Metal/ionic semiconductors/metal structures often show memristive effects, i. e. their electrical resistance depends on the previously applied bias voltage stress. The changes in resistance are often reversible and non-volatile, meaning that a particular resistance state is induced by a previously applied voltage, which persists, even under short-circuit conditions. Because of the reversibility and non-volatility, memristors are interesting for electronic data storage.^[1] However, memristors often need to be activated in order to function as electronic memories.^[2] The activation step usually involves putting the diodes under bias voltage stress and bringing it close to the threshold for dielectric breakdown.^[3] The processes induced by the electroforming procedure are presently not completely understood. Formation of defects in the ionic semiconductor during electroforming is by now well supported by experimental evidence. For instance, electroforming of Al_2O_3 results in Ohmic conduction and has been attributed to formation and ionization of defects.^[4] Electroforming of TiO_2 memristors has been shown to induce a phase transition to the Magnéli phases ($\text{Ti}_n\text{O}_{2n-1}$) at localized spots and is associated with formation of oxygen vacancies.^[5] Similarly, electroforming of niobium oxide (Nb_2O_5) results in formation of suboxide phases.^[6] Also for hafnium oxide (HfO_2), electroforming has been related to oxygen vacancies.^[7] Memristors made from intentionally highly oxygen deficient oxides, do not require electroforming.^[8] In Cr doped SrTiO_3 , oxygen vacancies have been imaged after electroforming and seem to determine the path for electrical conductivity.^[9]

Because electroforming occurs at bias voltages close to the threshold for breakdown, the process is difficult to control. By introducing a layer of a semiconducting polymer as current limiting element, the reproducibility and reliability of electroforming of Al_2O_3 /poly(spirofluorene) memristors is enhanced.^[3]

Many studies published so far have focussed on metal oxides as ionic semiconductors.^[10,11] Recently we showed that also alkali halides can be used as ionic semiconductors in memristors.^[12] Electroforming in alkali halides is known^[13] and also defect formation in alkali halides (“coloration”) has been studied in considerable detail.^[14,15] The ionic semiconductors in the alkali halide series form an interesting object of study because bandgap and electron energy levels vary over a wide range.

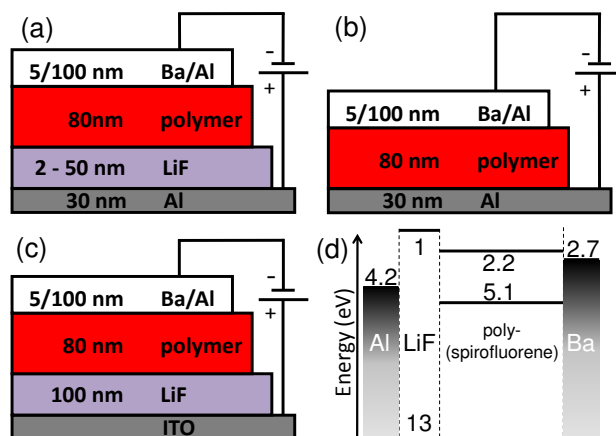


Figure 4.1: Diode structures of (a) Al/LiF/ poly(spirofluorene)/Ba/Al, (b) Al/native Al_2O_3 / poly(spirofluorene)/Ba/Al, (c) ITO/LiF/poly(spirofluorene)/Ba/Al. (d) Flat band diagram illustrating the valence and conduction bands of poly(spirofluorene) and LiF and the work functions of ITO and Ba with respect to the vacuum level.

Here we study the early stages of electroforming in LiF/polymer diodes in more detail. The diodes under study have as general structure metal/LiF/polymer/metal (Fig. 4.1). The thickness of the semiconducting poly(spirofluorene) polymer layer is kept constant, the thickness of the LiF layer is varied. To allow for optical access to the active layer, also diodes with transparent, indium tin oxide bottom contact are included in the studies. For the alkali halide/polymer memristors we find that initially, the course of the electroforming process is still reversible. Such reversibility has also been observed for some metal-oxide memristors and capacitors.^[16-20] Understanding of the reversible, early stages of electroforming is crucial for unravelling the critical, final stages of the process. We find that under application of moderate bias voltage stress that is not yet strong enough to induce complete electroforming, positively charged defects are introduced in the LiF layer that assist in tunnelling of electrons across the LiF/polymer interface. Our results indicate that the positively charged defects in the LiF are stabilized electrostatically by the presence of electrons trapped near the LiF/polymer interface. When the density of defects is kept below a certain limit estimated at 10^{19} to 10^{20} cm^{-3} , the defects in the LiF heal under short circuit conditions when illuminating the organic semiconductor with light to remove the trapped electrons and the alkali halide/polymer diode reverts to its pristine state. Formation of charged defects in the ionic semiconductor is therefore concluded to be an initial step in the electroforming of alkali halide/polymer memristors.

The organization of this chapter is as follows: after describing the experimental details, we first investigate the early stages of electroforming in the LiF/polymer diodes using dc and ac electrical methods. The thickness of the LiF layer is varied systematically. We then formulate a model for the electrical characteristics involving formation of

charged defects in the LiF. Finally, the presence of defects, induced during the early stages of electroforming, is confirmed by independent, electro-optical experiments on the LiF/polymer diodes.

4.2 Experimental

4.2.1 Materials and device fabrication

Three type of devices were fabricated and are described in Fig. 4.1.a-c. Devices with structure shown in Fig. 4.1a were fabricated under clean room conditions, on glass substrates. An Al bottom electrode was deposited by vacuum sublimation using a patterned mask. The LiF was deposited by thermal sublimation under high vacuum onto the entire substrate area. The layer of spirofluorene semiconducting polymer (CB01 from Covion) was spin cast in air from toluene. The top Ba/Al top electrode was thermally sublimated under vacuum. All the diodes were encapsulated with stainless steel caps glued onto the substrate. At the site where the glue is applied, the semiconducting polymer was removed by laser ablation to avoid the diffusion of water through the polymer. A getter was placed into the stainless steel cap to exclude H₂O. The encapsulated diodes have active areas of 1 or 9 mm².

For electron-only devices shown in Fig 4.1b, the bottom Al electrode was oxidized in air before coating with the polymer layer.^[21] The layer of spirofluorene semiconducting polymer was spin cast in N₂ from toluene. The bottom Al and top Ba/Al contact were deposited by thermal sublimation under vacuum, using masks to define the overlap of top contact with the bottom electrode.

ITO/LiF/poly(spirofluorene)/Ba/Al diode with structure represented in Fig. 4.1c were fabricated by thermal sublimation of LiF under 10⁻⁶ mbar directly onto glass substrates with patterned ITO. ITO substrates were cleaned, using in order, acetone, soap scrubbing, and isopropanol. The poly(spirofluorene) was bought from Merck under the reference SPB-02T, dissolved in toluene at a concentration of 5 mg/mL and spin-coated at a speed of 630 rpm. Subsequently, Ba and Al were deposited by thermal sublimation under vacuum. Diodes on ITO substrates were kept under inert atmosphere (N₂; O₂, H₂O < 1 ppm) at all times during fabrication and characterization. Throughout this study, positive bias is defined as the Ba/Al top electrode being charged negative.

4.2.2 Thickness characterization

The thickness of the polymer layer was estimated by surface profilometry and determined to be 80 nm. The thickness of the LiF layer was monitored by surface profilometry and checked by small-signal impedance spectroscopy using a reverse dc bias. Impedance spectroscopy gives parallel capacitance (C_p) and loss characteristics that do not vary with

frequency. The loss is found to be negligible and the C_p is compared in Table 4.1 to the calculated geometrical capacitance of the LiF and polymer layers in series. C_p was determined at -5 V dc bias, 50 mV perturbation signal and 10 kHz for diodes with different LiF thickness (Table 4.1). Measured C_p values confirm the estimated thickness of the active layer.

Table 4.1: Capacitance of the pristine diodes inserting a poly(spirofluorene) layer of 80 nm and a LiF layer varying from 2 to 50 nm. The C_p values measured for various thickness of LiF at -5 V dc bias, 50 mV perturbation signal and 10 kHz are shown in.

LiF thickness (nm)	2	10	20	30	40	50
Meas. Capacitance C_p (nF)	2.87	2.83	2.74	2.66	2.58	2.36
Calc. Capacitance (nF) ^a	2.97	2.87	2.76	2.66	2.56	2.47

^a) ϵ_r polyspirofluorene^[22] = 3.2 ; ϵ_r LiF^[23] = 9.

4.2.3 Opto-electrical measurements

J-V characteristics were obtained using an Agilent semiconductor parameter analyzer 4155C. Photoluminescence was recorded using a Edinburgh Instruments FLS920 fluorescence spectrometer. Small-signal impedance spectroscopy was performed with a Solartron 1260 impedance analyzer. For illumination during electrical characterization a tungsten halogen source with 100 mW/cm² and UV filter was used. Reflection experiments were performed using a Perkin Elmer Lambda 900 UV-Vis-NIR absorbance spectrometer with a module for specular reflection measurements.

4.3 Results and discussion

To study the early stage of electroforming in metal/LiF/polyspirofluorene/metal diodes, we apply a step voltage to the diodes starting from zero bias at time $t < 0$. We investigate the evolution of the current density through the diode induced by the voltage step. Measured current densities are plotted in Fig. 4.2 for various heights of the voltages step (1-6 V) and for various thicknesses of the LiF layer in the diodes (50 to 2 nm). For comparison we also provide current densities for diodes with similar structure but with Al₂O₃ as ionic semiconductor.

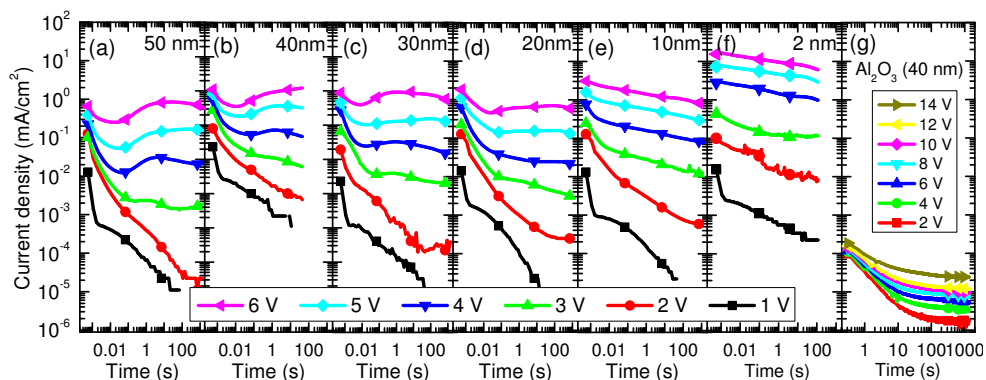


Figure 4.2: Current density as a function of time for metal/ionic semiconductor/polymer/metal diodes in pristine state with LiF and Al_2O_3 layers. The LiF thickness is varied (a) 50 nm, (b) 40 nm, (c) 30 nm, (d) 20 nm, (e) 10 nm, and (f) 2 nm under forward bias voltage stepped from 0 V for $t < 0$ to +1 V to +6 V for $t > 0$. (g) The diode incorporating 40 nm Al_2O_3 layer is characterized under forward bias from 2 to 14 V.

For small voltage steps (1-2 V) we observe a transient current that decays over time with very low current densities as asymptotic limit. This behavior is also observed for the Al_2O_3 /polymer diodes. We ascribe the transient current to *charging* of the diode. Because the polymer/Ba/Al top contact is quasi-Ohmic in nature, electrons can be injected into the polymer and will be transported towards the LiF/polymer interface when the applied bias is positive (forward). When the applied bias exceeds the built-in potential of the diode, drift transport of electrons towards the LiF/polymer interface becomes possible. The built-in potential may be estimated from the difference in workfunction of the two metal electrodes (4.2 eV (Al)- 2.7 eV (Ba) $/q_e = 1.5$ V). Experimentally we find that for bias voltages ≥ 3 V the current densities no longer tend towards zero but approach a finite current density at long times.

Interestingly, for diodes with LiF layer exceeding 10 nm in thickness, we notice that the initial decay of the current density due to charging is followed by an *increase* in current density over time for voltage steps exceeding 3 V and for times $t > 1$ s. This increase is not observed for the Al_2O_3 /polymer diodes. The increase in current density does not persist indefinitely: eventually the current density reaches a quasi-steady state level that increases with increasing applied bias. We note that the current transients are fully reversible, provided that in between measurements the diode is exposed to light from a fluorescent light tube for 10 min, in order to optically detrapp all accumulated charge carriers.^[16]

Further insight into the origin of the remarkable current transients for the metal/LiF/polymer/metal diodes can be obtained by plotting the saturation level of the current density as function of the applied stepped bias voltage (Fig. 4.3a). The saturation current is defined from Fig 4.2, as the current density reached at 100 s after the application of the bias voltage step to the diode. The saturation current densities J_{sat} for diodes with

LiF layer exceeding 10 nm in thickness are found to be very similar. Especially at high voltage, the current density is virtually *independent* of the thickness of the LiF layer. LiF is normally classified as a wide bandgap semiconductor, and the insensitivity of the current on thickness is counterintuitive. The independence of current on LiF thickness suggest doping of the LiF such that its effective resistance is small compared to that of the semiconducting polymer layer.

The dependence of the limiting current densities J_{sat} as function of applied bias V (Fig. 4.3a) follows a power law and can be approximated by $J_{\text{sat}} \propto V^{6.5}$. Such a power-law dependence of current on applied bias is characteristic for trap-limited transport of electrons through polymeric semiconductors.^[24] To confirm this we have measured the current density due to electrons in a metal/poly(spirofluorene)/Ba/Al diode (Fig 4.1c). The resulting current density in this electron-only diode is also shown in Fig. 4.3a (pink line) As can be seen, the magnitude of the electron-only current density in the diode without LiF layer also follows the $J_{\text{sat}} \propto V^{6.5}$ dependence on voltage. The similarity in the dependence of current density on applied bias for the diodes with and without LiF suggest that the saturation currents in the LiF/polymer diodes are limited by electron transport through the polymer layer. Experiments with decreased temperature indicate a time shift of the minimal current density reached. The current density at long time scale also tends to lower values than at room temperature, indicating that the current density is limited by the polymer layer.

In order to investigate the role of the LiF in the charge transport further we now make the simplification that the potential difference over the poly(spirofluorene) layer (ΔV_{pol}) required for transport of electrons with a specific current density J is the same in the LiF/polymer and the electron-only diodes. This assumption implies a similar charge carrier density near the exit contact. Using this assumption, the potential difference over the LiF layer (ΔV_{LiF}) required to sustain an electron current density J , can be obtained by simply subtracting the $\Delta V_{\text{pol}}(J)$ for the electron only diode from the total applied bias $V(J)$ for the LiF/polymer. In Fig. 4.3b we plot the current density J as function of the potential differences ΔV_{LiF} . We note that, approximately, the current density through the LiF depends exponentially on the potential difference. Qualitatively, this is consistent with tunneling of electrons across a barrier which we imagine at the LiF/polymer interface. The dependence of current on tunneling voltage is very similar for LiF layers with thickness ≥ 10 nm. For the 2 nm LiF layer the tunneling voltage required is considerably lower. The similarity of the tunneling voltages for the thicker layers suggests that the barrier for tunneling of electrons is essentially confined to the spatial region in the LiF layer within the first 10 nm from the LiF polymer interface.

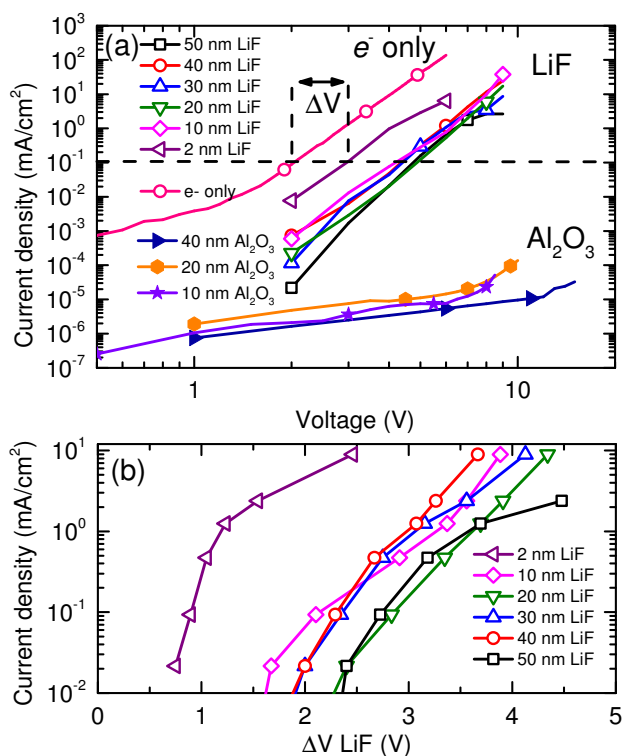


Figure 4.3:(a) J - V characteristic of an electron-only diode and saturation current of diodes incorporating LiF and Al₂O₃ with layer thicknesses from 2 to 50 nm. (b) Voltage shift induced by the LiF layer compared to the electron-only diodes. LiF layers from 2 to 50 nm are shown.

To confirm the surprising insensitivity of the electron transport to the thickness of the LiF layer we have turned to impedance spectroscopy. In Fig. 4.4a we show the parallel capacitance C_p and loss as function of modulation frequency and parametric in the applied dc bias voltage for a Al/LiF(30 nm)/poly(spirofluorene)/Ba/Al diode. At low dc bias (≤ 1 V) the loss is small. The capacitance at low dc bias is close to the geometrical capacitance expected for an insulating LiF/polymer stack (see Table 4.1) and independent of frequency up to 10⁵ Hz. Upon increasing the dc bias voltage, at low frequency, both the loss and C_p show a rise, indicating transport and storage of charge carriers. The rise in capacitance will be discussed in more detail in later parts of the chapter, we first focus on the loss. From the loss, the ac conductance of the diodes is calculated, and shown in Fig. 4.4b. The conductance at 10 Hz for various applied dc bias voltages is plotted as function of the thickness of the LiF layer. For thickness ≥ 10 nm the ac conductances are essentially independent of the thickness of the LiF layer. This confirms the results from the dc current measurements shown in Fig. 4.3.

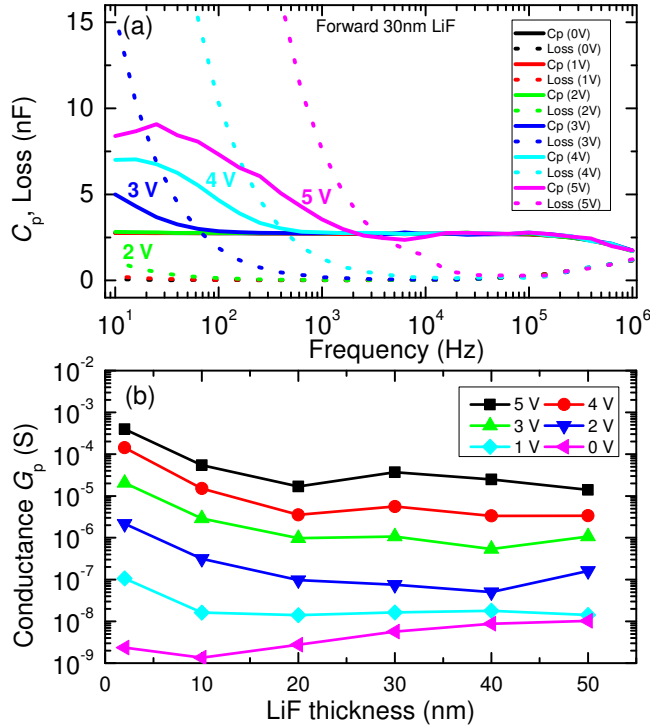


Figure 4.4: (a) Small-signal impedance spectroscopy of a Al/LiF (30 nm)/poly(spirofluorene)/Ba/Al diode. The parallel capacitance (C_p) and loss (dashed lines) are plotted as function of the frequency for different dc bias. (b) Conductance G_p measured at 10 Hz at voltages ranging from 0 to 5 V of devices with a LiF layer from 2 to 50 nm.

Summarizing, the results on the initial stages of electroforming in LiF/polymer diodes, so far, we have obtained evidence for charging of the diode at low voltage involving injection of electrons through the Ba/Al contact. At high bias voltage we have obtained indications for tunneling of electrons across a narrow barrier near the LiF/polymer interface. In order to understand the relation between the charging and tunneling phenomena and the time evolution of the current density under the stepped bias, we now analyze the electron transport quantitatively. Following our earlier analysis of charging of the Al_2O_3 /polymer,^[8] we assume that electrons injected into the polymer drift to the insulator-polymer interface under the influence of applied bias and get trapped there. Assuming electron-only current through the polymer layer with^[25] $J = V^{n+1}/r$, the electrons injected from the Ba/Al electrode drift through the polymer and accumulate at trapping sites located at the polymer/oxide interface. The current transient can be expressed as:^[16]

$$I_{\text{charg}}(t) = \frac{1}{r} \left[\frac{1}{\frac{nt}{rC_{\text{LiF}}} + \left(\frac{1}{V_{\text{pol}}}\right)^n} \right]^{1+\frac{1}{n}} \quad (4.1)$$

where V_{pol} is the initial voltage drop over the polymer, C is the capacitance associated with the LiF layer ($\epsilon_{\text{LiF}} = 9^{[23]}$). Parameters r and n depend on the energy distribution of the polymer traps and describe the electron transport and can be obtained from experiment on the electron-only current diode (Al/polymer/Ba/Al). The surface density $\sigma(t)$ of charge trapped at the LiF polymer interface follows from integrating the transient current given by Eq. (4.1) over time.

$$\sigma(t) = \int_0^t I_{\text{charg}}(t) dt. \quad (4.2)$$

In order to determine the electric field distribution over the polymer and LiF layers, we use the Poisson equation and restrict ourselves to one dimension.

$$\frac{\partial(\epsilon E)}{\partial x} = \sigma_f(x), \quad (4.3)$$

with ϵ the dielectric constant, E the electric field, and σ_f the free charge density i.e. charge density constituted by trapped carriers and not resulting from polarization of dielectrics. We define x_1 and x_2 as the borders of the interface containing the trapped carriers. Integration by parts of Eq (4.3) gives the spatial distribution of the electric field over each layer:

$$\int_{x_1}^{x_2} \sigma_f(x) dx = [\epsilon_0 \epsilon_r E]_{x_2} - [\epsilon_0 \epsilon_r E]_{x_1} = \epsilon_2 E_2 - \epsilon_1 E_1 = \sigma_f. \quad (4.4)$$

The free charge density is now assumed to be confined in space, essentially to a very narrow region around the LiF interface and equated with the charge density σ in Eq. 4.2, obtained from integrating the transient current. We furthermore assume the charge density in the bulk of the LiF and polymer layers to be negligible, implying that the electric fields over the LiF and polymer layers are constant. This then implies a fixed relation between the field strengths in the polymer and LiF layers (E_{pol} and E_{LiF}) and the combined potential difference over polymer and LiF layer (V_{appl}):

$$E_{\text{LiF}} = \frac{V_{\text{appl}} - d_{\text{pol}} E_{\text{pol}}}{d_{\text{LiF}}} . \quad (4.5)$$

Where, V_{appl} is the external applied voltage, d_{pol} and d_{LiF} are respectively the polymer and LiF thicknesses. Inserting (4.5) into (4.4), we can express the electric field in the LiF layer as a function of V_{appl} and t :

$$E_{\text{LiF}}(V_{\text{appl}}, t) = \frac{(1 - d_{\text{pol}} \epsilon_{\text{LiF}}) V_{\text{appl}} + \frac{\sigma_f(t) d_{\text{pol}}}{\epsilon_0}}{d_{\text{LiF}} (\epsilon_{\text{pol}} d_{\text{LiF}} + \epsilon_{\text{LiF}} d_{\text{pol}})} . \quad (4.6)$$

Knowing the electric field strength in the LiF layer, it now becomes possible to estimate the current due to tunneling of electrons across the LiF/polymer interface assuming a Fowler-Nordheim (F-N) tunneling process:^[26]

$$I_{\text{F-N}}(E) = A E^2 e^{-\frac{B}{E}} , \quad (4.7)$$

with

$$A = \frac{m_e q_e}{8\pi h \phi_B m_{\text{eff}}} \quad \text{and} \quad B = \frac{8\pi}{3} \left(2 \frac{m_{\text{eff}}}{h^2} \right)^{\frac{1}{2}} \left(\frac{\phi_B}{q_e} \right)^{\frac{3}{2}} , \quad (4.8)$$

and E the electric field over LiF, m_e the electron mass, m_{eff} the effective electron mass in LiF ($m_{\text{LiF}}^* = 1.2 m_e$ ^[27]), q_e the electron charge, and ϕ_B the tunnelling barrier from the LUMO of the polymer to the conduction band of LiF.

By equating the total current to the sum of the time dependent charging and tunnelling current we can now simulate the transient current in Fig. 4.2. In Fig. 4.5, we show the separate contributions of charging (Eq. 4.1) and tunnelling (Eq. 4.7) to the total current density and compare with experimental current transient for the LiF(50nm)/poly(spirofluorene) diode under +5 V stepped bias. Although the calculated and measured currents do not match quantitatively, the charging – tunnelling model for the current provides a qualitative explanation for the curious rise in current density of time following the initial decay of the current density.

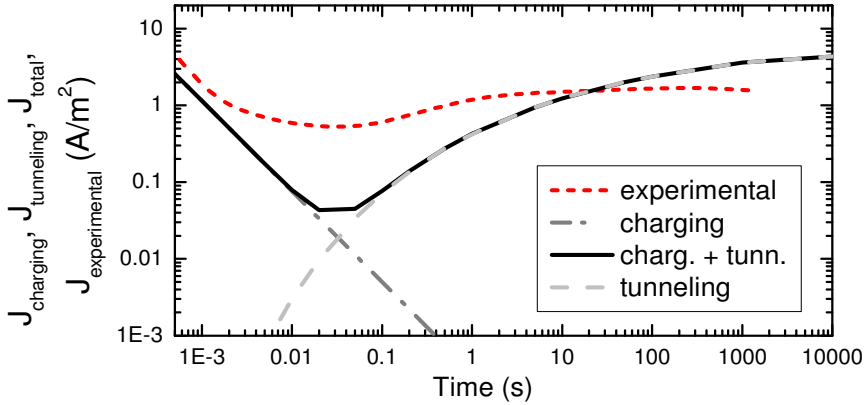


Figure 4.5: Calculated and experimental J - t characteristic of a Al/LiF (50 nm)/polymer (80 nm)/Ba/Al diode under a 5 V forward bias. The calculated $J(t)$ curve is the sum of the charging and tunneling currents. The estimated tunneling is estimated: $\phi_b = 0.8$ eV.

The predictive power of the charging tunnelling described above can be tested further by looking at the magnitude of the current densities directly after application of the stepped voltage bias as function of the LiF thickness. The initial current densities J_{ini} should be due to charging of the interface states at the LiF/polymer junction by electrons. Figure 4.6 shows J_{ini} at +5 V bias step for different LiF thicknesses. The data points are taken from Fig. 4.2a-f at time $t = 0.56$ ms after the voltage step. We observe an inverse relation between charging current density and thickness of the LiF. This inverse relationship is in agreement with charging of interface states at the polymer/LiF junction with electrons injected via the Ba/Al electrode and with the LiF layer acting, initially, as a current blocking dielectric. Fig. 4.6 also shows predictions from the charging tunneling models, using Eq. (4.1) to calculate the initial charging current density taking $r = 100$ $\text{m}^2\text{V}^{n+1}/\text{A}$ and $n = 5.5$ as determined for the electron-only diode. The model correctly predicts, without any adjustable parameters, the inverse dependence of J_{ini} on thickness and predicted current densities agree within a factor of 3 to 5 with the experiment.

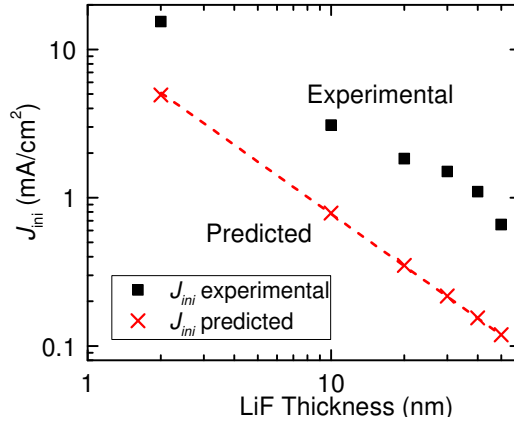


Figure 4.6: Initial current densities J_{ini} for Al/LiF/polyspirofluorene/Ba/Al diodes recorded at $t = 0.56$ ms after stepping the bias voltage from 0 to +5V. Black squares: experimental data from Figure 4.2, red crosses: theoretical predictions from Eq. (4.1), using r , n values determined for polyspirofluorene electron-only diodes.

The close agreement between experimental initial current densities and the predictions from the charging tunnelling model, provides support for trapping of electrons at the LiF/polymer interface. The trapping of electrons is further supported by the observation of hysteresis in the J - V characteristics similar to Al_2O_3 /polymer diodes.^[28] The electrons that get trapped at the LiF/polymer interface will modify the distribution of the electric field strength in such a way that the electric field in the LiF layer rises over time enhancing tunnelling of electrons. The charging-tunneling model correctly predicts the shift of the minimum in current density towards shorter times that is observed experimentally at +5 V bias step upon decreasing the thickness of the LiF layer from 50 to 30 nm (Fig. 4.2). The charging-tunneling model does however not account for the insensitivity of the final saturation current densities to LiF thickness. In the charging-tunneling model, the currents retain their main strong dependence on thickness of the LiF insulator layer.

To account for the insensitivity of the saturation currents and ac conductivity toward LiF thickness, we now propose that at long times after the turn-on of the bias voltage, positively charged defects accumulate in the LiF layer and limit the width of the tunneling barrier for electrons to around 10 nm. The density of positive charge in the LiF layer induces band bending causing a steeper drop in the potential across the LiF layer. For LiF thicknesses exceeding 10 nm we do not observe any significant modification of the current densities, therefore we infer that after induction of the positive charge density, the width of the tunneling barrier is confined to ~ 10 nm. To accommodate a potential difference of 0.8 V that we associate with the tunnel barrier for the LiF/polymer within a 10 nm distance from the interface, requires a density of positive charge of around 10^{19}

elementary charges $/\text{cm}^3$. This follows directly from the Poisson equation assuming continuous, uniform charge density. Defect densities of 10^{19} elementary charges $/\text{cm}^3$ have been found for ZnO in Ohmic ZnO/conducting polymer recombination contacts^[29] and are close to critical defect densities expected for a metal-insulator transition.^[30] To complete the explanation of the insensitivity of the currents towards LiF thickness we further assume that the transport of the electrons through the LiF, after passing the tunneling barrier at the LiF/polymer interface requires only a negligible potential difference. This assumption may be supported by the high mobilities reported for electrons in alkali halides.^[31,32] The charge distribution proposed for the LiF/polymer diodes is summarized graphically in Fig. 4.7.

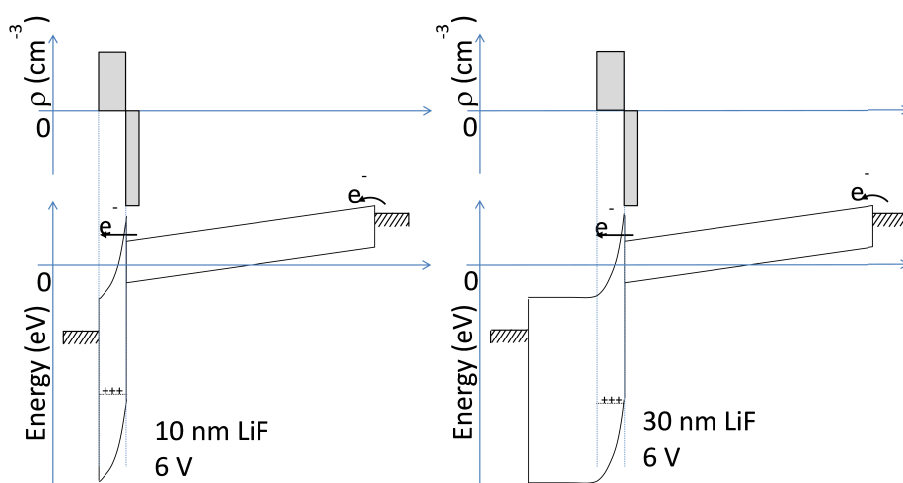


Figure 4.7: Schematic showing the net change density (top) and band diagram bottom Al/LiF/poly(spirofluorene)/Ba/Al diodes with 10 and 30 nm of LiF under a +6 V forward bias.

Direct experimental evidence for accumulation of charged defects in the LiF/poly(spirofluorene) layers can be obtained from optical experiments. In Fig. 4.8 we show the results of reflection measurements on ITO/ LiF(100nm)/ poly(spirofluorene)/ Ba/Al diodes. In these diodes the transparent bottom ITO contact is employed for optical access to the active layers. The Ba/Al top contact is highly reflective, allowing for measurements of the specular reflection on the complete diodes at small angles of incidence as function of wavelength. In the visible and NIR spectral ranges, the polymeric semiconductor is transparent so that one can probe for sub-gap optical transitions associated with defects induced by the application of bias voltage stress. Figure 4.8a shows the relative differential change in reflection of light ($-\Delta R/R$) induced by application of +15 V bias as function of photon energy. Positive bias voltages result in a reduction of the reflectivity; negative bias voltages give no significant change. We notice a broad band

centered around 1.75 eV in the differential reflectance $\Delta R/R$. We attribute this band to sub-gap absorption in the semiconducting materials in the diode induced by bias stress. The assignment of the differential reflectance to absorption (and not to an interference effect) can be supported by modeling of the reflection using the refractive index (n) and extinction coefficient (k) as function of wavelength of the materials in the layered stack. Upon application of a stepped bias voltage (Fig. 4.8b), the intensity of the band increases slowly over time. Importantly, upon removing the applied bias, the reflectivity reverts spontaneously and slowly approaches its original level before application of bias stress, (Fig. 4.9). The recovery can be accelerated by application of reverse bias. By measuring the current density through the diode simultaneously with the change in reflectivity at 800 nm during the bias stress and the subsequent recovery, we can correlate the changes in optical properties to charging of defects in the diodes (Fig. 4.8b-e). During recovery from the bias voltage stress under short circuit conditions, we observe a spontaneous discharging current with sign opposite to that of the current density during bias voltage stress. The decay of the short-circuit discharging current takes place on the same timescale as the decay of the differential reflectivity (Fig. 4.8c,e). The correlation between optical and electrical signal indicates that coloration and its recovery are related to charging and discharging of defects in the semiconducting materials in the diode. Application of reverse bias does not introduce the charged defect in the LiF. Diodes incorporating a 30 nm Al_2O_3 layer instead of LiF, do not show any appreciable change in reflection of light in the photon energy range from 3.5 to 0.6 eV. Therefore, we tentatively assign the sub-gap absorption in the LiF-polymer diodes induced by the bias voltage, to positively charged defects in the LiF layer. Charged defects in LiF with spectral characteristics matching those from the differential reflection spectra in Fig. 4.8a are known.^[33]

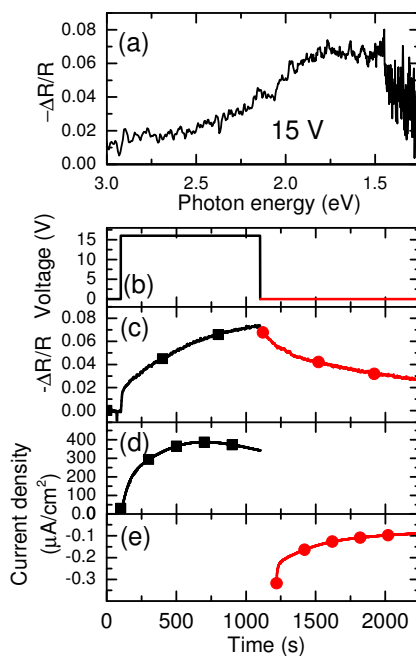


Figure 4.8: (a) Relative change in reflectivity ($-\Delta R/R$) for a ITO/ LiF(100 nm)/ poly(spirofluorene)/ Ba/Al diode as function of photon energy. (b-e) Time dependence of $-\Delta R/R$ probed at a photon energy of 1.55 eV induced a bias voltage step from 0 to +15 V as shown in (b). The current density transient (e,d) measured simultaneously with the change in reflectivity (c) indicate charging and discharging.

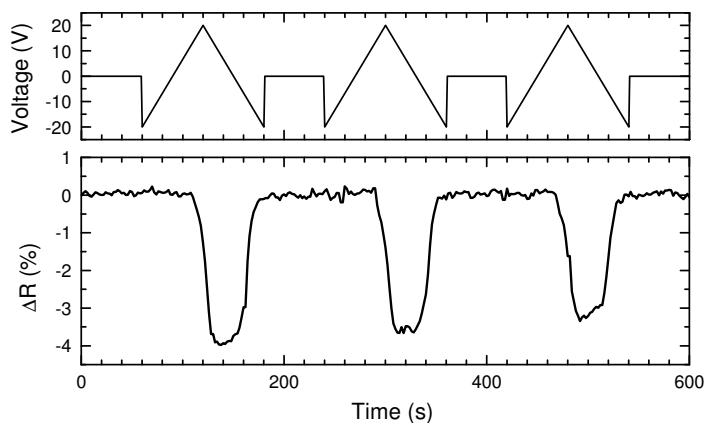


Figure 4.9: Differential reflectance ΔR probed at a photon energy of 1.55 eV, from a ITO/ LiF(100 nm) / poly(spirofluorene)/ Ba/ Al diode induced by time-dependent bias voltage stress as shown in the top panel.

The existence of trap sites at the LiF/polymer interface specific for electrons can be supported further by opto-electronic experiments relying on near-UV light to generate charge carriers in the polymer. The optical method for generating charge, rather than relying on electrical injection has the advantage that also the behavior of holes in the polymer can be studied without changing the nature of the electron injecting Ba/Al contact. In Fig. 4.10a,b, we show current transients for ITO/LiF(50 nm)/poly(spirofluorene)/Ba/Al diodes during broad band illumination and application of bias stress. The corresponding current transients during the recovery directly following the period of combined bias voltage as measured in dark are shown in Fig. 4.10c,d. Under forward bias (+2 V), we observe transient positive current densities, consistent with transport of electrons generated in the semiconducting polymer by light under influence of the bias towards the LiF/polymer interface. Short-circuiting the diode immediately after termination of illumination and bias voltage stress, results in a short-circuit current density that is opposite in sign to the charging current under illumination, but much smaller in magnitude (Fig. 4.10c). The low current densities during recovery indicate that the electrons are trapped at the LiF/polymer interface. The behavior of holes at the LiF/polymer interface can be studied by reversing the bias during illumination. Applying negative bias (-2 V) during illumination, we record a transient current (Fig. 4.10b) with sign opposite to the current under illumination and positive bias (+2 V, Fig. 4.10a), consistent with transport and accumulation of positive charge carriers at the LiF/polymer interface. In contrast to the case for accumulation of electrons at the LiF/polymer interface, for the hole accumulated at the LiF/polymer interface during -2 V bias stress and illumination, spontaneously leave the diode within a time frame of about 10 s, as evidenced by the short circuit current transient (Fig. 4.10d). Apparently, both electrons and holes can be accumulated at the LiF/polymer interface depending on the applied bias. However, the electrons are trapped more deeply than the holes and do not escape rapidly from the trap sites at the LiF/polymer interface in the dark under short circuit conditions.

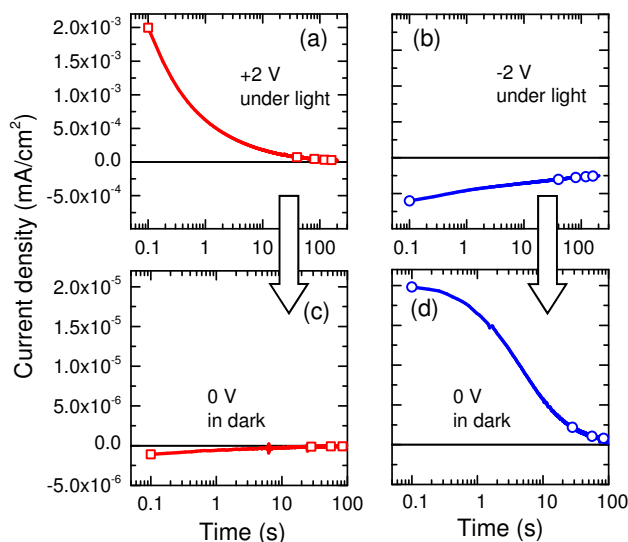


Figure 4.10: Current transient for ITO/LiF(50nm)/polyspirofluorene/Ba/Al diodes under bias voltage and white light illumination (a) +2 V and (b) -2 V. Subsequent current transient during spontaneous recovery in dark and short-circuit: (c) after +2 V bias stress and (d) after -2 V.

Finally, by monitoring the photoluminescence (PL) of the spirofluorene polymer during application of bias voltage stress to ITO/LiF/poly(spirofluorene)/Ba/Al diodes, we obtain further indications on accumulation of defects that quench the PL from the organic semiconductor. Measurement of the PL requires optical excitation of the semiconductor and during these experiment, the near-UV light used for excitation results in continuous generation of electron-hole pairs in the organic semiconductor. Illumination under short-circuit conditions prior to the application of bias voltage results in accumulation of holes at the LiF/polymer interface because of the built-in potential of the diode (Fig. 4.11a). The built-in potential results from the use of electrodes with different work function (ITO and Al). Upon slowly ramping the bias voltage from 0 to +4 V and simultaneously monitoring the PL intensity we find the intensity of PL rises by about 3 % upon approaching a bias voltage of +2.5 V. This is illustrated in Fig. 4.11d,e, showing the time traces for the PL intensity under low and high excitation intensity with UV light. Fig. 4.11c shows the corresponding voltage ramp applied. The rise in PL is ascribed to the removal of positive charge carriers at the LiF/polymer interface by application of the bias voltage. The holes have accumulated during illumination prior to application of the voltage ramp. Quenching of PL from conjugated polymers by polaronic charge carriers in the same material is well known.^[34,35] We argue that for bias V_{tr} near +2.5 V, charge neutrality at the LiF/polymer interface is reached. Upon further increase of the bias to +4 V, the PL intensity drops again, which we attribute to accumulation of electrons near the LiF/polymer interface. Upon subsequent lowering the bias voltage from +4 V back to +3 V, recombination of

trapped electrons with photogenerated holes restores the PL intensity. Lowering the bias voltage further below +3 V, the accumulation of holes at the LiF/polymer interface becomes favored and the PL intensity drops again to its initial level. Because holes cannot be injected via the Ba/Al contact but have to be generated optically, the rate of accumulation of holes depends on the intensity of the UV illumination. This is supported by the time traces for the PL at low and high intensity, compare Fig. 4.11d,e. Under low excitation intensity, the PL intensity only drops very slowly for $t > 200$ s while for more intense UV illumination, the reduction of the PL intensity to the initial level at $t = 0$ is complete within 10 s.

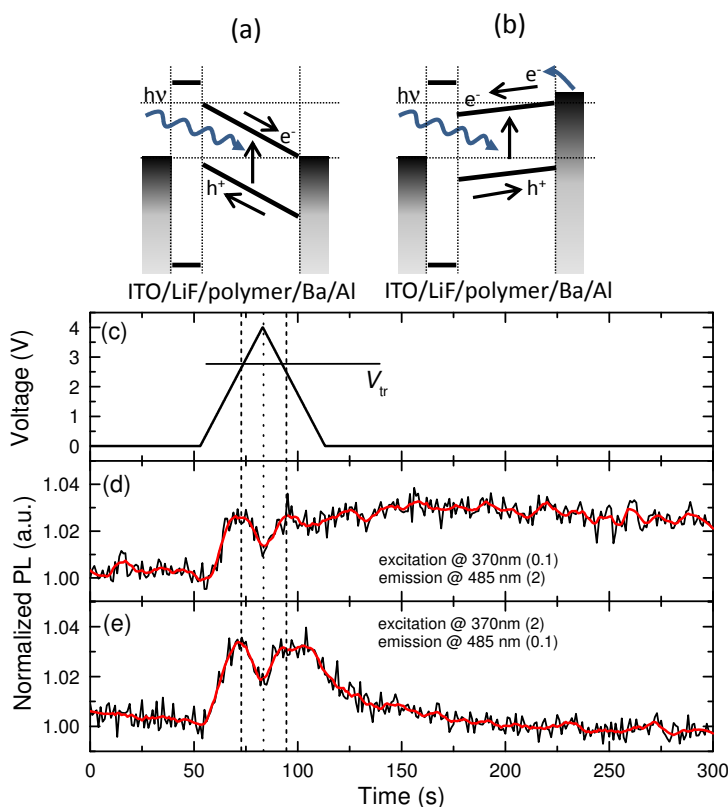


Figure 4.11: (a, b) Schematic band diagram representing the ITO/LiF (100 nm)/poly(spirofluorene)/Ba/Al diode under illumination excitation light. (a) In short circuit conditions. (b) At forward bias voltage exceeding the built-in potential. (c) Triangular voltage ramp from 0 up to +4 V and back to 0 V applied during photoluminescence measurements (d, e). (d, e) Photoluminescence transients of the polymer upon excitation at 3.35 eV and application of the voltage sweep shown in (c) under (d): low excitation intensity and (e): high excitation intensity. The ratio of high and low intensity is estimated at 4×10^2 . The thick solid red line in (d, e) shows an time-averaged intensity.

In summary, the various opto-electronic experiments discussed above, provide experimental evidence for the accumulation of electrons on the polymer side of the LiF/poly(spirofluorene) junction and positive charges on the LiF side of the junction. Additional evidence for trapping of charge carriers comes from the impedance measurements shown in Fig. 4.4. Because of the quasi-Ohmic Ba/Al contact for electron injection into the semiconducting polymer, one expects a contribution of electron transport to the parallel capacitance C_p of the Al/LiF/poly(spirofluorene)/Ba/Al diodes (Fig. 4.2a). At high frequencies ($> 10^4$ Hz) the poor mobility of the electrons in the polymeric semiconductor prevents a significant contribution of the electron transport to the capacitance and a value for C_p corresponding to the geometrical capacitance expected for combined polymer and LiF dielectric layers is obtained for all dc bias voltages studied (0 to +5 V). As mentioned above, application of positive bias results in charging of the polymer layer with electrons. At +5 V bias voltage and frequencies around 10^3 Hz, C_p rises above the geometrical capacitance estimated for the LiF polymer stack, indicating reversible storage of electrons in the polymer near the LiF/polymer interface layer. The rise in C_p at low frequency, depends on the magnitude of the applied dc bias voltage. This can be interpreted in terms of filling of trap states at the LiF/polymer interface. At high forward bias (+5 V) there is a significant population of *shallow* trap states by electrons. The electrons occupying these shallow states can contribute to the capacitance at low frequency.^[36] At lower bias voltages the injected electrons exclusively occupy deep trap states at the LiF/polymer interface and do not contribute to the capacitance at intermediate frequency. The electrons occupying deep trap states can only contribute to the capacitance at very low frequency, below to the very slow rate for release of trapped electrons from their deep trap states.

4.4 Conclusion

We have explored the early stage of electroforming in LiF/polymer MIS diodes. We find evidence for injection and transport of electrons in the polymer semiconductor and their subsequent trapping at the internal LiF/poly(spirofluorene) interface. The trapped electrons modify the internal field distribution in the diode, enhancing tunneling of electrons across the LiF/polymer barrier. The efficient electron transport across the semiconductor / insulator barrier is interpreted in terms of accumulation of positively charged defects in the insulator assisting the tunneling of electrons. The accumulation of these positive defects with densities estimated at 10^{19} /cm³, make the metal/LiF layer a good electron *collecting* contact for photovoltaic diodes containing semiconducting polymers.^[37] Interestingly, the observation of electroluminescence from the poly(spirofluorene), that coincides with the final stages of electroforming as reported earlier^[12] implies that in the final stages of electroforming, the charge transport property of the LiF layer switches from being electron collecting at moderate bias to hole injecting at high bias.

4.5 References

- [1] L. Chua, *Appl. Phys. A* **2011**, *102*, 765.
- [2] Y. V. Pershin, and M. Di Ventra, *Adv. Phys.* **2011**, *60*, 145–227.
- [3] F. Verbakel, S. C. J. Meskers, and R. A. J. Janssen, *Appl. Phys. Lett.* **2007**, *91*, 192103.
- [4] T. W. Hickmott, *J. Appl. Phys.* **2012**, *112*, 073717.
- [5] K. Deok-Hwang, K. Kyung Min, J. Jae Hyuck, J. Jong Myeong, L. Min Hwan, K. Gun Hwan, L. Xiang-Shu, P. Gyeong-Su, L. Bora, H. Seungwu, K. Miyoung, and H. Cheol Seong, *Nature Nanotechnology* **2010**, *5*, 148.
- [6] K. Jung, Y. Kim, Y. S. Park, W. Jung, J. Choi, B. Park, H. Kim, W. Kim, J. Hong, and H. Im, *J. Appl. Phys.* **2011**, *109*, 054511.
- [7] P. Lorenzi, R. Rao, and F. Irrera, *IEEE T. Electron. Dev.* **2013**, *60*, 438.
- [8] T.-M. Pan and C.-H. Lu, *Mater. Chem. Phys.* **2013**, *139*, 437.
- [9] M. Janousch, G. I. Meijer, U. Staub, B. Delley, S. F. Karg, and B. P. Andreasson, *Adv. Mater.* **2007**, *19*, 2232.
- [10] H. Hosono, *J. Non-Cryst. Solids* **2006**, *352*, 851.
- [11] J. Robertson, *Phys. Stat. Sol. (b)* **2008**, *245*, 1026.
- [12] B. F. Bory, H. L. Gomes, R. A. J. Janssen, D. M. de Leeuw, and S. C. J. Meskers, *J. Phys. Chem. C* **2012**, *116*, 12443.
- [13] H. Biederman, *Vacuum* **1976**, *26*, 513.
- [14] N. Itoh and K. Tanimura, *J. Phys. Chem. Solids* **1990**, *51*, 717.
- [15] K. Schwartz, *RAU Scientif Reports & Solid State Electronics and Technologies* **1996**, *1*, 3.
- [16] Q. Chen, H. L. Gomes, P. R. F. Rocha, D. M. de Leeuw, and S. C. J. Meskers, *Appl. Phys. Lett.* **2013**, *102*, 153509.
- [17] S. Lombardo, F. Crupi, C. Spinella, and B. Neri, *Mat. Sci. Semicon. Proc.* **1999**, *2*, 359.
- [18] A. Crespo-Yepes, J. Martin-Martinez, R. Rodriguez, M. Nafria, and X. Aymerich, *Microelectron. Reliab.* **2009**, *49*, 1024.
- [19] T. W. Hickmott, *J. Appl. Phys.* **2012**, *111*, 063708.
- [20] J. Sune, M. Nafria, and X. Aymerich, *Microelectron. Reliab.* **1993**, *33*, 1031.
- [21] H. T. Nicolai, A. Hof, J. L. M. Oosthoek, and P. W. M. Blom, *Adv. Funct. Mater.* **2011**, *21*, 1505.
- [22] S. L. M. van Mensfoort, S. I. E. Vulto, R. A. J. Janssen, and R. Coehoorn, *Phys. Rev. B* **2008**, *78*, 085208.
- [23] R. P. Lowndes and D. H. Martin, *Proc. R. Soc. Lond. A* **1969**, *308*, 473.
- [24] H. T. Nicolai, M. Kuik, G. A. H. Wetzelaer, B. de Boer, C. Campbell, C. Risko, J. L. Brédas, and P. W. M. Blom, *Nature Materials* **2012**, *11*, 882.
- [25] M. M. Mandoc, B. de Boer, G. Paasch, and P.W.M. Blom, *Phys. Rev. B* **2007**, *75*, 193202.
- [26] J. G. Simmons, *J. Appl. Phys.* **1963**, *34*, 2581.
- [27] L. J. Page and E. H. Hygh, *Phys. Rev. B* **1970**, *1*, 3472.
- [28] B. F. Bory, S. C. J. Meskers, R. A. J. Janssen, H. L. Gomes, and D. M. de Leeuw, *Appl. Phys. Lett.* **2010**, *97*, 222106.

- [29] G. Lakhwani, R. F. H. Roijmans, A. J. Kronemeijer, J. Gilot, R. A. J. Janssen, and S. C. J. Meskers, *J. Phys. Chem. C* **2010**, *114*, 14804.
- [30] N. F. Mott, *Metal Insulator transitions* 2nd Ed. Taylor and Francis London UK (1990).
- [31] R. K. Ahrenkiel and F. C Brown, *Phys. Rev.* **1964**, *136*, A223.
- [32] C. F. Seager, and D. Emin, *Phys. Rev. B* **1970**, *2*, 3421.
- [33] G. Baldacchini, S. Bollanti, F. Bonfigli, P. Di Lazzaro, A. Ya. Faenov, F. Flora, T. Marolo, R. M. Montereali, D. Murra, E. Nichelatti, T. Pikuz, A. Reale, L. Reale, A. Ritucci, and G. Tomassetti, *IEEE J. Quant. Electron.* **2004**, *10*, 1435.
- [34] V. Gulbinas, R. Karpicz, I. Muzikante, and L. Valkunas, *Thin Solid Films* **2010**, *518*, 3299.
- [35] R. Karpicz, M. Kirkus, J. V. Grazulevicius, and V. Gulbinas, *J. Lumin.* **2010**, *130*, 722.
- [36] J. G. Simmons, G. S. Nadkarni, and M. C. Lancaster, *J. Appl. Phys.* **1970**, *41*, 538.
- [37] C. J. Brabec, S. E. Shaheen, C. Winder, N. S. Sariciftci, and P. Denk, *Appl. Phys. Lett.* **2002**, *80*, 1288.

Chapter 5

Role of hole injection in electroforming of LiF/polymer memory diodes

Abstract

Al/LiF/poly(spirofluorene)/Ba/Al diodes submitted to bias voltages near 15 V undergo a change to a non-volatile memory known as electroforming. Prior to electroforming, electron trapping occurs followed by a tunneling current due to electrons from the polymer into LiF. At the onset voltage for electroforming, a sudden electroluminescence burst originating from electronic excitations in the polymer is detected. This confirms that hole injection into the polymer through LiF occurs leading to non-volatile resistive switching.

This Chapter has been published as:

B. F. Bory, H. L. Gomes, R. A. J. Janssen, D. M. de Leeuw, S. C. J. Meskers, *J. Phys. Chem. C* **2012**, 116, 12443.

5.1 Introduction

Non-volatile resistive switching in metal-insulator-semiconductor-metal diodes can be used to store information.^[1] Diodes incorporating a metal oxide as insulator, usually require an electroforming step in which a high voltage is applied to the oxide before electronic memory effects can be observed.^[2] The electroforming is presently not completely understood but it has been interpreted in terms of formation of defects in the oxide, e.g. oxygen vacancies resulting from expulsion of O₂.^[3-5] In SiO₂, resistive switching can be observed after voltage-induced, ‘soft’ electrical breakdown which has been related to hole generation or hole injection in the oxide.^[6-9] Electroforming results in percolating paths for transport of charge, also referred to as filaments. Resistive switching is often attributed to transitions between metastable electronic states of these filaments with different conductance.^[10]

Apart from metal oxides, also metal fluorides such as lithium fluoride (LiF) show electroforming.^[11,12] In contrast to oxides, LiF can also be electroformed in air.^[13] So far, electronic memory effects in metal fluorides have received very little attention. Here we investigate electroforming of a layer of LiF inserted in an Al/LiF/ poly(spirofluorene)/ Ba/Al diode (Fig. 5.1a). The blue-light emitting poly(spirofluorene) polymer layer serves two purposes. First it is intended as a current limiter, enhancing the reliability of electroforming and switching.^[14] Second, the electroluminescence from the polymer is used as a diagnostic for the type of carriers that are injected into the polymer. The high luminescence efficiency of the polymer enhances the sensitivity of this method as compared to inorganic insulators.^[15] We find that electroforming of LiF under high forward bias coincides with light emission from the polymer implying hole injection through LiF and electron injection from the Ba/Al electrode.

5.2 Experimental

The diodes studied (Fig. 5.1a) consist of an aluminum bottom electrode on which a thin layer of LiF is evaporated with adjustable thickness in the range from 2 to 50 nm. On top, an 80 nm thick layer of organic semiconductor, poly(spirofluorene) (CB01 from Covion), is spin coated. The top electrode is made by thermal evaporation of barium followed by aluminum in high vacuum. Approximate energy levels of the valence band and conduction bands are shown in Fig. 5.1b. The diodes are encapsulated with a steel cap, integrating a getter to maintain an oxygen and water free atmosphere. Electrical characterization was performed using an Agilent 4155C semiconductor analyzer and a Keithley 2601 for pulse measurements. Forward bias is defined as the Ba/Al top electrode being charged negative. Current voltage J - V sweeps were recorded with 50 mV step and 40 ms integration time.

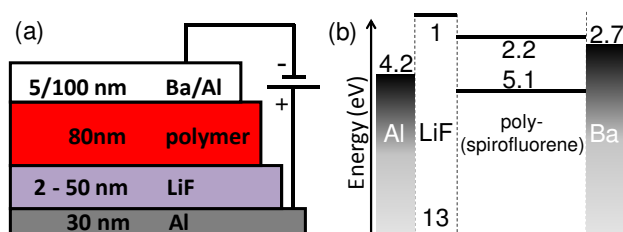


Figure 5.1: (a) Layout of the Al/LiF/poly(spirofluorene)/Ba/Al diode. (b) Flat band diagram illustrating the valence and conduction bands of poly(spirofluorene) and LiF and the work functions of Al and Ba with respect to the vacuum level.

5.3 Results and discussion

J-V characteristics of pristine Al/LiF/poly(spirofluorene)/Ba,Al diodes were recorded by sweeping the applied bias voltage in a cyclic manner as shown in Fig. 5.2. In each sweep, the bias is scanned starting at zero, going to a maximum and then back to zero bias. Sequential cyclic scans were applied in which the maximum voltage was raised in steps of 2 V. Under reverse bias, current densities are very low. In forward bias, currents are much higher resulting in a rectification ratio up to 10^6 . Diodes with inverted architecture, so glass/Ba/poly(spirofluorene)/LiF/Al, also show rectification. In the inverted diodes, the highest current densities are also obtained when charging the Ba electrode negative. Maximum current densities in inverted diodes are lower in magnitude in comparison to diodes with normal geometry. We attribute the lower current densities in the inverted diodes to degradation of the Ba contact during fabrication. The inverted diodes show that the rectification is not associated with a dipole layer arising during deposition of LiF.

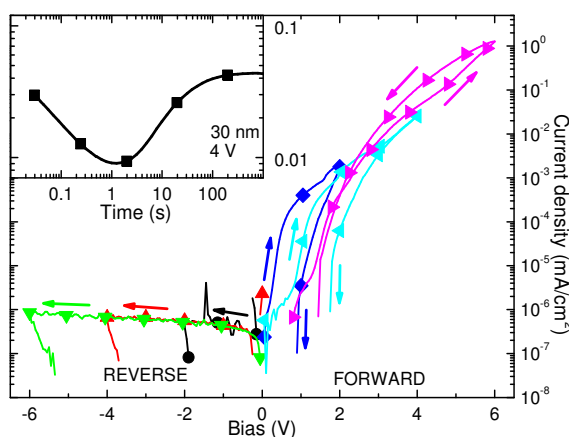


Figure 5.2: Current-voltage characteristics of a pristine diode with 30 nm LiF. The inset shows the current density as a function of time upon application of a voltage step from 0 to 4 V at time $t = 0$.

In the range from 0 - 4 V, the J - V traces recorded on Al/LiF/poly(spirofluorene)/Ba/Al diodes show pronounced hysteresis. Time domain measurements, applying a voltage step from zero to +4 V at time $t = 0$, provide further information on this hysteresis. The inset of Fig. 5.2 shows the current transient recorded upon the potential step. Initially the current decreases exponentially with time, while for $t > 1$ s the current begins to rise until it reaches a steady state value. The initial decaying current transient can be ascribed to filling of trap sites.^[16,17] The filling of the trap sites, which are most likely positioned near the LiF/polymer interface, results in a redistribution of the electric field strength within the diode such that the field strength in the LiF layer increases. When the electric field becomes high enough, tunneling of electrons from the polymer into the LiF becomes possible and a final steady-state current is reached. In comparison with Al/Al₂O₃/poly(spirofluorene)/Ba/Al diodes,^[17] the LiF diodes show much higher tunneling currents and higher rectification. This we attribute to a lower barrier for tunneling of electrons at the LiF/polymer interface in comparison to the Al₂O₃/polymer interface.

After the experiments shown in Fig. 5.2, the cyclic voltage scans were continued, raising the maximum forward voltage in steps of 2 V. When reaching ~ 15 V bias voltage, a sudden drop in the current density occurred (Fig. 5.3a). Returning to low bias voltages, the resistance of the diode had been reduced in an irreversible manner. In this experiment, electroluminescence (EL) from the diode was recorded simultaneously with the current (Fig. 5.3a). Coincident with the sudden decrease of the current density at 15 V, a sudden burst of blue light from the diode was observed. The spectral characteristics of the light resemble those of the fluorescence of the poly(spirofluorene) associated with the S₁ to S₀ electronic transition. A subsequent scan over the same voltage range yields blue EL with a reduced intensity as shown in Fig. 5.3b. Scanning to higher bias voltages in a third subsequent scan, an additional weak EL burst is seen, followed by a steep further drop in the EL intensity. The large drop in current near 15 V and the associated EL are irreversible events, which we attribute to electroforming of the diode. Because also bulk LiF shows electroforming,^[11,12] we argue that the forming originates primarily in the LiF layer. The process will certainly also affect and involve the LiF/polymer interface region and the polymer layer. Note that in the second and third scans, the hysteresis in the J - V characteristic has disappeared, indicating that electroforming has been completed.

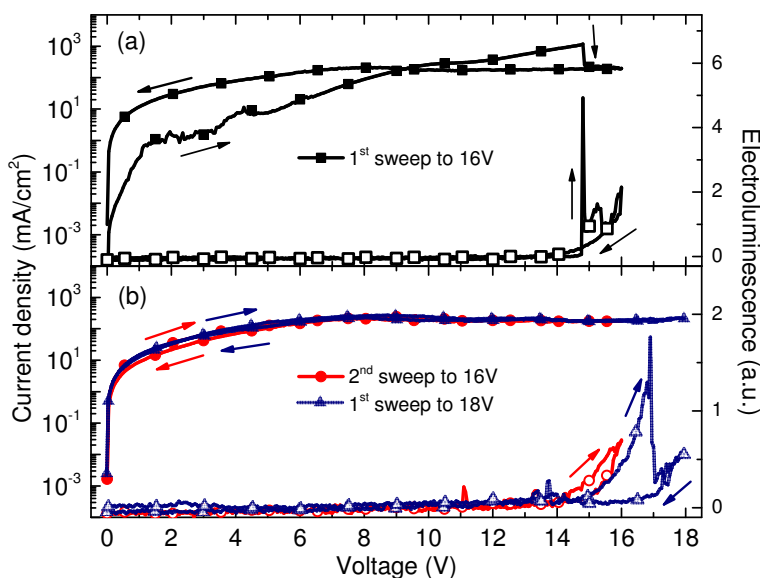


Figure 5.3: Current density-voltage (closed symbols) and electroluminescence intensity-voltage characteristics (open symbols) for a Al/LiF (10 nm)/poly(spirofluorene) (80 nm)/Ba/Al diode. (a) First voltage sweep to 16 V. (b) Subsequent voltage sweep to 16 V, followed by a voltage sweep to 18 V.

After electroforming, the current density through Al/LiF/ poly(spirofluorene)/Ba/Al diodes as function of bias clearly shows two different regimes (Fig. 5.3b). From 0 to about 7 V, the current density rises approximately linear with voltage. In the range 7 to 18 V, the current density slightly decreases with increasing voltage, which corresponds to a negative differential resistance. Negative differential resistance is a characteristic which is commonly found in electroformed metal-oxide/polymer diodes showing resistive switching.^[18] Also for the LiF/polymer diodes the resistance of the diode can be changed in a non-volatile manner by applying voltage pulses (Fig. 5.4) in a manner similar to the Al₂O₃/polymer diodes.^[14]

The LiF/polymer diode can be programmed in either a high resistance OFF state or a low resistance ON state by applying 100 ms long voltage pulses of respectively 8 V and 4 V. The resistance of a particular state can be determined using 1 V pulses. Fig. 5.4a shows current density values under +1 V reading pulses during repeated resistive switching in a Al/LiF(20nm)/ poly(spirofluorene)/ Ba/Al diode upon application of +4 V write and +8 V erase pulses. The diode can be switched repeatedly between different resistance states. With these pulse heights and widths, the ratio of the resistances of the ON and OFF states exceeds one order of magnitude. In these large area devices, the ON/OFF ratio may be limited by tunneling currents through parts of the LiF that have not yet been electroformed. The ON/OFF ratio may rise when a larger part of the surface area of the diode is converted to conducting filaments. By repeatedly probing the resistance of

the ON and OFF states, the retention of the memory can be evaluated (Fig. 5.4b). Application of +1 V pulses to measure the resistance, we find long retention times (> 1000 s). Importantly, in between the read pulses of 100 ms temporal width, the diode is held at zero bias. We conclude that the electronic memory effect is non-volatile. Electroforming and resistive switching is also observed in diodes with a gold bottom contact instead of aluminum. This shows that the switching is not associated with the possible native oxide of the aluminum bottom contact.

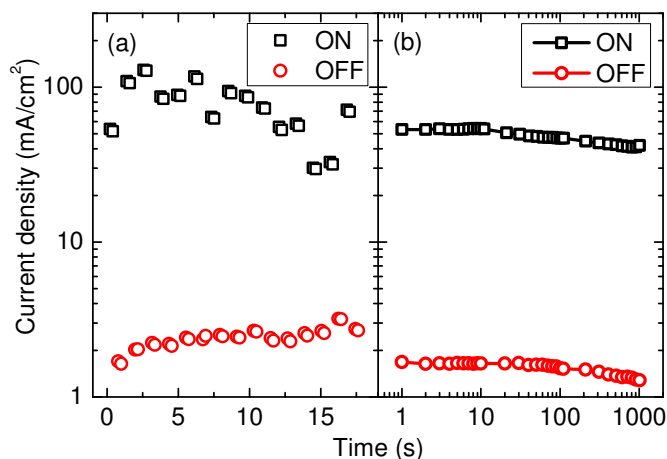


Figure 5.4: Current density of an electroformed Al/LiF (20 nm)/poly(spirofluorene) (80 nm)/Ba/Al diode in high resistance OFF state (circles) and low resistance ON state (squares) upon application of +1 V, 100 ms reading pulses. (a) Cycle endurance upon application of +4 V, 100 ms pulses to induce the ON state and +8 V, 100 ms pulses for the OFF state. Two sequential +1 V pulses are used to read the resistance and to test for non-destructive readout. (b) Stability of the high and low resistance state induced by a pulse of resp. +8 V and +4 V and probed by 100 ms, +1 V read pulses. In between the read pulses, the diode is held at zero bias.

To study electroforming in more detail, we have investigated Al/LiF/poly(spirofluorene)/Ba/Al diodes with different thickness of the LiF layer ranging from 2 to 50 nm. The voltage needed to induce electroforming in forward bias is plotted in Fig. 5.5a as a function of LiF thickness. The forming voltage shows only a modest increase with increasing LiF thickness. This contrast with the behavior of electroforming in Al/Al₂O₃/poly(spirofluorene)/Ba/Al diodes.^[14] An interpolation of experimentally determined electroforming voltages for diodes with different Al₂O₃ thickness^[14,17] is plotted alongside the data for LiF as dashed line in Fig. 5.5a. For Al₂O₃, the dependence of forming voltage on thickness is much more pronounced and directly indicates a field driven soft-breakdown process.

For the diodes with different LiF thickness, we estimate an upper limit for the electrical field strength needed to induce electroforming by assuming that the electrical

potential difference over the LiF layer equals the total applied voltage (Fig. 5.5b). Upon increasing the thickness of the LiF layer, the estimated upper limit for the breakdown field strength converges asymptotically to the field strength reported for breakdown in bulk LiF^[19] (3.1 MV/cm).

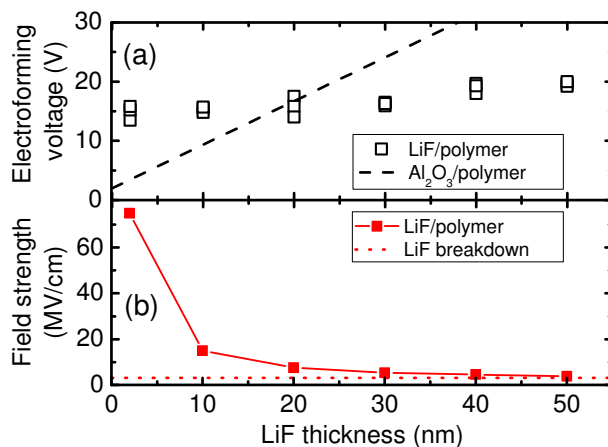


Figure 5.5: (a) Voltages needed to induce electroforming in Al/LiF /poly(spirofluorene) (80 nm)/ Ba/Al diodes under forward bias as a function of the thickness of the LiF layer (open symbols). The dashed line shows an interpolation of electroforming voltages reported for Al/Al₂O₃/poly(spirofluorene) (80 nm)/ Ba/Al diodes.^[14] (b) Estimated upper limit for electroforming field strength (closed symbols). Horizontal dotted line: breakdown field strength for bulk LiF (3.1 MV/cm).^[19]

The relatively high electroforming voltage and high current density under forward bias for diodes with thin LiF layer can now be explained as follows. Under forward bias, electrons are injected into the polymer layer through the quasi-ohmic Ba/Al contact.^[17] The injected electrons are trapped near the LiF/polymer interface, causing hysteresis in the J - V characteristics. Due to the trapped electrons, the electrical potential over the LiF layer is maximized and above a certain threshold voltage, electron tunneling from the polymer into the LiF occurs. Fig. 5.1b shows a flat band diagram, illustrating the energetic position of the valence and conduction band edges of poly(spirofluorene)^[14] and LiF^[20] together with the work functions of Ba and Al. The high injection barrier for injection of holes from the Ba/Al electrode precludes a similar mechanism for electrical conduction under reverse bias, which explains the high rectification of the diode (Fig. 5.2b).

At low applied voltages, the total device current is comprised of a transient electron trapping current and a small dc tunneling current across the LiF layer. After filling the electron traps near the polymer/LiF interface, the potential difference across the insulating LiF layer will be almost equal to the externally applied bias. The potential difference over the polymer layer is expected to be very small. As the applied voltage is

increased further, the dc tunneling current through the LiF layer rises dramatically. LiF becomes a leaky dielectric and the voltage drop across the LiF layer does not increase proportionally to the external applied voltage. Because of the non-zero current density, there must also be a significant potential difference over the polymer layer, resulting in an apparent modest thickness dependence of the electroforming voltages on LiF thickness.

We note that the tunnel barrier for electrons from the polymer into the LiF may be lowered by migration of ions, in a way similar as observed for light emitting electrochemical cells.^[21] For Al_2O_3 , electron tunneling is far less efficient presumably because of a band edge offset at the polymer/oxide interface.^[17] Furthermore, lowering of the injection barrier due to ion migration is less likely for Al_2O_3 because of the more covalent nature of Al_2O_3 in comparison to LiF. For the Al_2O_3 /polymer diodes, the applied voltage mostly drops across the oxide and the forming voltage becomes proportional to the layer thickness.^[14]

Application of a high bias voltage induces tunneling of electrons from the polymer into LiF. In addition, at high bias, also injection of holes into LiF becomes energetically allowed. Holes injected into LiF may transfer to the polymer where they can recombine with electrons, which are present in high density near the interface. The recombination can result in the formation of an electronic excitation in the polymer, which causes blue EL when it decays radiatively to the ground state. However, holes injected into LiF may also induce defect formation in the inorganic insulator.

Electroforming can also be observed in polymer diodes with alkali halide insulator layers other than LiF. The electroforming in CsI/poly(spirofluorene) diodes is illustrated in Fig. 5.6. Fig. 5.6a shows the current density in subsequent cyclic voltage sweeps with increasing maximum voltage, analogous to Fig. 5.2. For the diode incorporating CsI, electroforming already occurs at about 6 V, while for LiF electroforming starts at a much higher voltage (~ 15 V see Fig. 5.2). When applying a bias voltage inducing electroforming to a pristine diode incorporating the CsI insulator layer, transient EL is observed (Fig. 5.6b). The EL vanishes upon completion of the electroforming by prolonged application of bias voltages exceeding 6 V. This is evidenced by the hysteresis in the intensity-voltage characteristic (Fig. 5.6b) for the EL from the diode.

For CsI, the valence band maximum is at 6 eV, below the vacuum level,^[22] while for LiF it is at 13 eV. The barrier for injection of a hole from the Al electrode into CsI is therefore expected to be much lower compared to the barrier for Al/LiF. The lower electroforming voltage observed for CsI compared to LiF (~ 6 V vs ~ 15 V, Fig. 5.6a and 5.3a) supports the view that electroforming in alkali halides is related to hole injection.

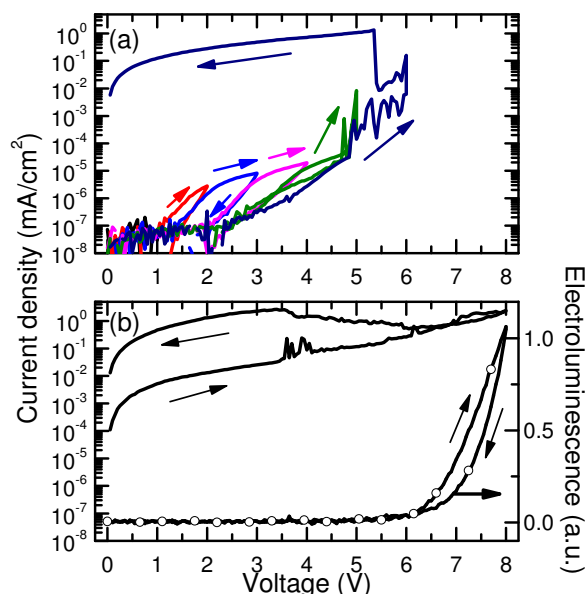


Figure 5.6: (a) Current-voltage characteristic upon application of sequential voltage sweeps on a Al/CsI (30 nm)/poly(spirofluorene) (80 nm)/Ba/Al diode. (b) Dependence of current density and electroluminescence intensity on voltage for a ITO/CsI (30 nm)/poly(spirofluorene) (80 nm)/Ba/Al diode. Prior to the measurement shown, a voltage sweep up to 6 V was applied, inducing already some electroforming.

The valence band in alkali halides primarily involves p orbitals on the halide^[23,24] Therefore injection of a hole into the conduction band of an alkali halide can be regarded as essentially oxidation of the halide ion. The higher energetic position of the valence band maximum in CsI compared to LiF is related to the lower oxidation potential of I^- compared to F^- (half-wave potential $E_{1/2}$ for the $\text{I}_2/2\text{I}^-$ redox couple: $E_{1/2} = 0.54$ V vs. SHE, while for $\text{F}_2/2\text{F}^-$: $E_{1/2} = 2.87$ V).

It is well known that in bulk alkali halides, the formation of defects can be induced by relatively low excitation energy. Excitation of the alkali halide often results in the formation of self-trapped excitons.^[25] Self-trapped excitons can split up into Frenkel defects pairs consisting of an anion vacancy and a halide atom at an interstitial position of the alkali halide lattice. For e.g. LiF, the anion vacancy can be seen as a trap site for holes. To explain the electroforming, we propose the formation of Frenkel defects with trapping of holes. The displaced halogen atom (F) can be stabilized by dimerization forming interstitial molecular anion.^[26,27] This process effectively leads to F vacancy formation. Vacancies may form percolating pathways for electrons through the insulator, resulting in filamentary currents. The filaments could give rise to resistive switching through a mechanism similar^[28] to that operative in Al_2O_3 /polymer diodes.^[14]

5.4 Conclusion

We have studied electroforming and non-volatile resistive switching in LiF/polymer diodes. Electroforming is associated with hole injection into the leaky LiF insulator, as evidenced by transient EL from the polymer. This indicates that in our diodes, electroforming is essentially a minority carrier effect resulting from hole injection into a dielectric filled with trapped electrons. EL turns out to be a sensitive method to detect minority carrier injection.

5.5 References

- [1] C. Kuegeler, R. Rosezin, E. Linn, R. Bruchhaus, and R. Waser, *Appl. Phys. A* **2011**, *102*, 791.
- [2] Y. V. Pershin and M. Di Ventra, *Adv. Phys.* **2011**, *60*, 145.
- [3] L. Goux, P. Czarnecki, Y.Y. Chen, L. Pantisano, X.P. Wang, R. Degraeve, B. Govoreanu, M. Jurczak, D. J. Wouters, and L. Altimime, *Appl. Phys. Lett.*, **2010**, *97*, 243509.
- [4] D. S. Jeong, H. Schroeder, U. Breuer, and R. Waser, *J. Appl. Phys.* **2008**, *104*, 123716.
- [5] J. J. Yang, F. Miao, M. D. Pickett, D. A. A. Ohlberg, D. R. Stewart, C. N. Lau, and R. S. Williams, *Nanotechnology* **2009**, *20*, 215201.
- [6] I. C. Chen, S. Holland, K. K. Young, C. Chang, and C. Hu, *Appl. Phys. Lett.* **1986**, *49*, 669.
- [7] R. Degraeve, G. Groeseneken, R. Bellens, M. Depas, and H. E. Maes, *IEDM* **1995**, 863.
- [8] D. J. DiMaria, and J. H. Stathis, *J. Appl. Phys.* **2001**, *89*, 5015.
- [9] K. F. Schuegraf, and C. Hu, *IEEE Trans. Electron. Devices* **1994**, *41*, 761.
- [10] R. Waser and M. Aono, *Nat. Mater.* **2007**, *6*, 833.
- [11] G. Dearnaley, A. M. Stoneham, and D. V. Morgan, *Rep. Prog. Phys.* **1970**, *33*, 1129.
- [12] H. Biederman, *Vacuum* **1976**, *26*, 513.
- [13] R. A. Collins, G. Bowman, and R. R. Sutherland, *J. Phys. D: Appl. Phys.* **1971**, *4*, L49.
- [14] F. Verbakel, S. C. J. Meskers, R. A. J. Janssen, H. L. Gomes, M. Cölle, M. Büchel, and D. M. de Leeuw, *Appl. Phys. Lett.* **2007**, *91*, 192103.
- [15] T. W. Hickmott, *J. Appl. Phys.* **2006**, *100*, 083712.
- [16] Q. Chen, B. F. Bory, A. Kiazadeh, P. R. F. Rocha, H. L. Gomes, F. Verbakel, D. M. de Leeuw, and S. C. J. Meskers, *Appl. Phys. Lett.* **2011**, *99*, 083305.
- [17] B. F. Bory, S. C. J. Meskers, R. A. J. Janssen, H. L. Gomes, and D. M. de Leeuw, *Appl. Phys. Lett.* **2010**, *97*, 222106.
- [18] F. Verbakel, S. C. J. Meskers, D. M. de Leeuw, R. A. J. Janssen, and H. L. Gomes, *J. Phys. Chem. C* **2008**, *112*, 5254.
- [19] H. B. Callen, *Phys. Rev.* **1946**, *76*, 1394.
- [20] S. Samarin, O. M. Artamonov, A. A. Suvorova, A. D. Sergeant, and J. F. Williams, *Solid State Commun.* **2004**, *129*, 389.
- [21] D. A. Bernardis, S. Flores-Torres, H. D. Abruña, and G. G. Malliaras, *Science* **2006**, *313*, 1416.
- [22] R. T. Poole, J. G. Jenkin, J. Liesegang, and R. C. G. Leckey, *Phys. Rev. B* **1975**, *11*, 5179-5189 (1975).
- [23] J.M. Adams, S. Evans, and J.M. Thomas, *J. Phys. C: Solid State Phys* **1973**, *6*, L382.
- [24] S. Satpathy, N.E. Christensen, and O. Jepsen *Phys. Rev. B* **1985**, *32*, 6793.
- [25] R. T. Williams, and K. S. Song, *J. Phys. Chem. Solids* **1990**, *51*, 679.
- [26] R. T. Casper, S. C. Jones, P. Braunlich, and P. Kelly, *Nucl. Instr. Meth. Phys. Res. B* **1990**, *46*, 231.
- [27] K. Tanimura and W. P. Hess, *Phys. Rev. B* **2004**, *69*, 155102.
- [28] M. Cölle, M. Büchel, and D. M. de Leeuw, *Org. Electron.* **2006**, *7*, 305.

Chapter 6

Electroforming in MIM diodes containing alkali halide-poly(spirofluorene) bilayer as insulator involves hole injection

Abstract

Electroforming of ITO/alkali halide/semiconducting polymer/metal diodes is investigated for 7 different alkali halides. The voltage needed to induce electroforming varies for different alkali halides and correlates with the energy of their valence band edge. Optical reflection measurements on the diodes with a reflecting back electrode during electroforming, indicate the formation of defects in the alkali halide. Within the series of alkali halides, the voltages corresponding to the onset of defect formation correlate with the energy of the valence band edge. Electroluminescence from the semiconducting polymer, observed during the electroforming process, confirms that the defect formation is related to injection of holes into the alkali halide.

6.1 Introduction

Memristors can be used as electronic memory cells to store information. A commonly used method to make memristors, is to first fabricate metal-insulator-metal (MIM) diodes and then to induce electroforming in the insulator of the MIM stack by applying a high bias voltage to its metal electrodes. Electroforming lowers the electrical resistance of the MIM diode and, importantly, makes the resistance ‘switchable’. By applying voltage pulses to the electroformed diode, the resistance at low voltage can often be changed reversibly and, depending on the material, changes can be non-volatile, i.e. the resistance states persist even under short-circuit conditions.

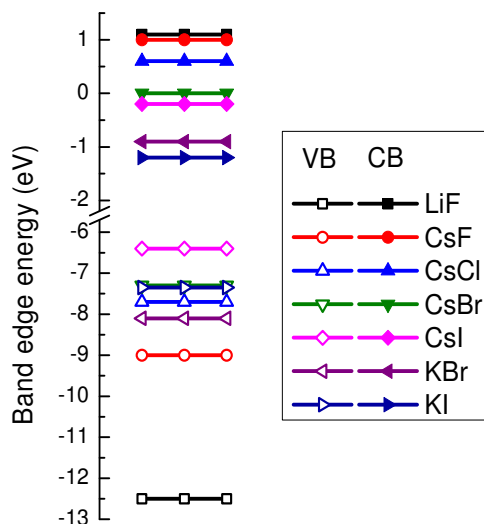


Figure 6.1: Band edge energy of LiF, CsF, CsCl, CsBr, CsI, KBr, and KI.^[1,2] Filled symbols represent the conduction band energy levels. The open symbols represent the valence band energy levels.

Memristors incorporating metal oxides^[3] and alkali halide^[4,5] as insulators have been reported. Electroforming of MIM stacks with oxide and halide layers with highly insulating electrical properties, can usually be induced by applying a bias voltage close to the threshold for dielectric breakdown. The close proximity of field strengths required for electroforming to the critical limit for dielectric breakdown, make that the electroforming is difficult to control.^[6]

Previous research has shown that the use of composite insulating layers in the MIM stack, can improve the reliability of the electroforming. Metal oxide or metal halide layers in combination with wide bandgap polymeric semiconductors can be electroformed with high reliability.^[7] Electroforming of the metal oxide is believed to be related to the formation of defects such as e.g. oxygen vacancies.^[8] Also for alkali halides, the formation of defects has been implicated (see Chapters 4 and 7).

Formation of defects in alkali halides can be induced by applying perturbations of various kinds. Even UV irradiation can induce defects in alkali halides. An optical photon of sufficient energy can excite an electron from the valence band to the conduction band. The resulting electronic excitation in the alkali halide is unstable. Optical studies have shown that the excitation undergoes self-trapping as the result of translation of a halogen atom (X) away from its equilibrium position in the lattice.^[9] The displaced halogen atom is stabilized by dimerization leading to formation of molecular anion X_2^- . The self-trapped exciton can subsequently dissociate into a Frenkel defect pair consisting of an anion vacancy (F -center) and a halide atom at an interstitial position of the crystal lattice (H -center). A self-trapped exciton can be seen as a precursor for lattice defects and have been shown to be involved in optically induced breakdown of alkali halide crystals induced by high intensity optical radiation.^[10,11]

Here we investigate electroforming of MIM diodes with a metal/alkali halide/organic semiconductor/metal device structure. The chemical nature of the alkali halide is varied, and the influence of the energetic position of conduction and valence band edge in the various alkali halides (Fig. 6.1) on the electroforming process is investigated. Apart from the electrical characteristics of the MIM diodes, the optical properties of the MIM diode will be monitored. By using a transparent conducting oxide electrode (indium tin oxide (ITO)) as bottom contact, and a highly reflecting metal top contact, optical properties of the insulator layers can be probed.

The combined results from optical and electrical investigations point to a connection between defect formation, electroluminescence, and electroforming. Correlation of voltages corresponding to the onset of electroforming and defect accumulation, with the energy of the valence band edge, suggests a crucial role for hole injection and accumulation in the alkali halide in the electroforming.

6.2 Materials and device fabrication

ITO/ alkali halide/ poly(spirofluorene)/ Ba/Al diodes were fabricated by thermal sublimation of alkali halide under 10^{-6} mbar directly onto glass substrates with patterned ITO. ITO substrates were cleaned, using in order, acetone, soap scrubbing, and isopropanol. The poly(spirofluorene) was bought from Merck under the reference SPB-02T, dissolved in toluene at a concentration of 10 mg/mL and spin coated at a speed of 3500 rpm. Subsequently, Ba and Al were deposited by thermal sublimation under vacuum. Diodes on ITO substrates were kept under inert atmosphere (N_2 ; O_2 , $H_2O < 1$ ppm) at all times during fabrication and characterization. Throughout this study, positive bias is defined as the Ba/Al top electrode being charged negative.

Table 6.1: Materials supplier, purity and type of boat or crucible.

Material	Supplier, purity	Type of Boat or crucible
Lithium Fluoride (LiF)	Sigma Aldrich, 99.9%	Alumina crucible or W
Potassium Bromide (KBr)	Sigma Aldrich p.a.	Mo baffled
Potassium Iodide (KI)	Sigma Aldrich, 99.99%	Ta
Cesium Fluoride (CsF)	Sigma Aldrich, 99.99%	Ta baffled or W
Cesium Chloride (CsCl)	Merck p.a.	Ta baffled
Cesium Bromide (CsBr)	Alfa Aesar, 99.999%	Ta baffled
Cesium Iodide (CsI)	Sigma Aldrich, 99.999%	Ta baffled or W

Current, electroluminescence intensity, voltage (J - EL - V) characteristics were recorded with an Agilent 4155C semiconductor parameter analyzer using a Si-photodiode to record light intensity. Current voltage J - V sweeps were recorded with 50 mV step and 40 ms integration time. Reflection experiments were performed using a Perkin Elmer Lambda 900 UV-Vis-NIR absorbance spectrometer with a module for specular reflection measurements.

Electroluminescence spectra were recorded using an intensified CCD camera. Spectra were corrected for the wavelength dependent sensitivity of this detection system. Correction factors were determined using a tungsten-halogen calibration standard lamp. Photoluminescence was recorded using a Edinburgh instruments FLS920 Fluorescence spectrometer. The PL spectra of CsI and poly(spirofluorene) were recorded on quartz substrates and were corrected for the wavelength dependent sensitivity of the detection channel.

6.3 Results and Discussion

6.3.1 Electrical characterization

Pristine ITO/alkali halide/poly(spirofluorene)/Ba/Al diodes were submitted to sequential cyclic current-voltage (J - V) scans in which the maximum voltage was raised in steps. The poly(spirofluorene)/Ba/Al contact is known to inject electrons into the polymer when the bias voltage exceeds the built-in potential and has quasi-Ohmic characteristics. At the other contact, the low energetic position of the valence band edge of the (pristine) alkali halides relative to the workfunction of the ITO electrode results in a large barrier for injection of holes into the insulator stack.

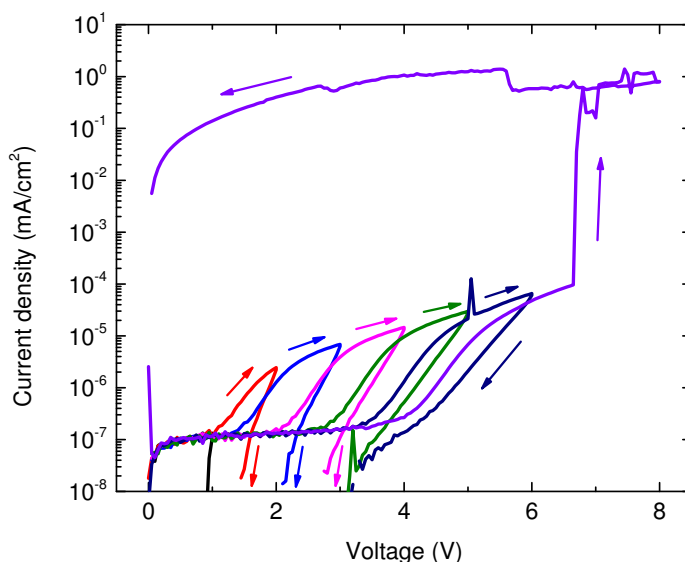


Figure 6.2: J - V characteristics of a pristine ITO/CsF (35 nm)/poly(spirofluorene)(80 nm)/Ba/Al diode after subsequent cyclic voltage sweeps showing electroforming at ~ 7 V.

As an example, Fig. 6.2 shows the J - V characteristics of a pristine diode incorporating CsF. The applied voltage is swept in a cyclic manner, starting at 0, going to a maximum and then back to zero bias. Diodes fabricated with the other alkali halides selected, show qualitatively similar J - V characteristics: all show hysteresis in the J - V characteristics below 4 V. In following sweeps, low current densities corresponding to the displacement current expected for the complete MIM stack are recorded, except when the voltage is sweep outward over a range to which the diode has not yet been subjected. This peculiar, history dependent hysteresis in the J - V characteristics can also be observed for metal/ Al_2O_3 /poly(spirofluorene)/metal diodes^[12] (see Chapter 3). The hysteresis can be attributed to trapping of electrons in deep trap sites at the alkali halide / semiconducting polymer internal interface. The high current densities during the outward sweep result from the flow of electrons from the metal electrodes towards the trap sites near the organic/inorganic interface. On the return sweeps, low current densities are recorded because the electrons remain trapped.

When the bias applied to the ITO/CsF/poly(spirofluorene)/Ba/Al exceeds 7 V, a sudden increase in current density occurs (Fig. 6.2). Upon the return sweep from +8 V to zero bias, the current density remains high. Near zero bias, the J - V characteristic is almost Ohmic. These changes mark the completion of the electroforming process.

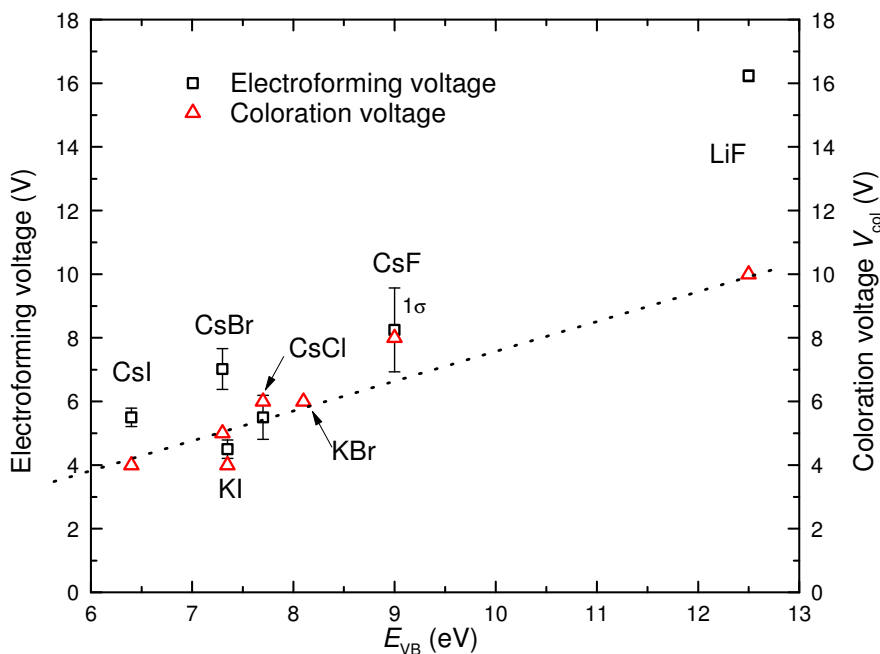


Figure 6.3: Minimal coloration voltage (black squares) and electroforming voltage as a function of the valence band energy level of the alkali halides under study. The line is a line to guide the eye.

For all of the 7 alkali halides used in construction of ITO/alkali halide/poly(spirofluorene)/Ba/Al MIM diodes, electroforming voltages have been determined. The electroforming voltage is defined as the voltage required to induce a current density exceeding 10^{-1} mA/cm² in a pristine, insulating diode and resulting an irreversible increase of the conductivity at low bias voltage.

Figure 6.3 shows electroforming voltages for different alkali halides in combination with the semiconducting polymer. Average values for the electroforming voltages are given together with standard deviation. We note that due to reasons related to fabrication, there is variation in the thickness of the alkali halide layers (30-100 nm). Previous detailed studies on LiF/poly(spirofluorene) diodes revealed that the electroforming does not strongly depend on the alkali halide thickness (Chapter 4).

Electroforming voltages correlate with energies of the valence band edge. If we adopt the generally held view that electroforming is due to defects formation, the correlation between forming voltage and E_{VB} suggests that defect formation in the alkali halide depends on injection of holes into the material.

6.3.2 Optical characterization

Direct experimental evidence for accumulation of defects in alkali halide/poly(spirofluorene) layers during the electroforming can be obtained from optical experiments. The use of a transparent bottom electrode (ITO) in combination with a highly reflecting top contact Ba/Al allows for probing of the optical properties of the alkali halide/poly(spirofluorene) bilayer by means of spectrally resolved reflection measurements during application of bias voltage. We note that, in their pristine state, both the polymer and alkali halides have a wide bandgap (> 3.0 eV), and thus provide a large optical window to probe sub-gap optical transitions in the insulators of the MIM stack induced by application of bias voltage.

Figure 6.4 shows the relative change in reflectivity ($\Delta R/R$) induced by application of bias voltage. The voltage-dependent differential reflectivity ΔR is determined with zero bias as reference. For all alkali halides changes in reflectivity induced by forward bias voltage are observed featuring a broad band in the near infrared, in the photon energy range from 1.7 to 0.9 eV depending on the alkali halide used. The magnitude of $\Delta R/R$ at the maximum of this band is on the order of ten percent for bias voltages around 6 to 8 V. Spectra shown in Fig. 6.4 have been normalized to the maximum $\Delta R/R$ in the near infrared (NIR). The voltage-induced changes in reflectivity do not occur instantaneously but build up on the timescale of several minutes after the start of the application of bias voltage. Voltage induced changes in reflectivity are quasi-reversible and revert spontaneously back to the level of the pristine device on the time scale of an hour. Application of reverse bias voltages does not induce significant changes in reflectivity.

Figure 6.4a illustrates $\Delta R/R$ for LiF, KBr and KI. Figure 6.4b shows results for the homologous cesium series CsF, CsCl, CsBr, and CsI. As can be seen, the spectral position of the reflection band in the NIR region depends on the nature of the alkali halide. We assign the voltage induced reflection bands to absorption of light by defects in the alkali halide induced by the application of bias voltage to the ITO/alkali halide/poly(spirofluorene)/Ba/Al diodes.

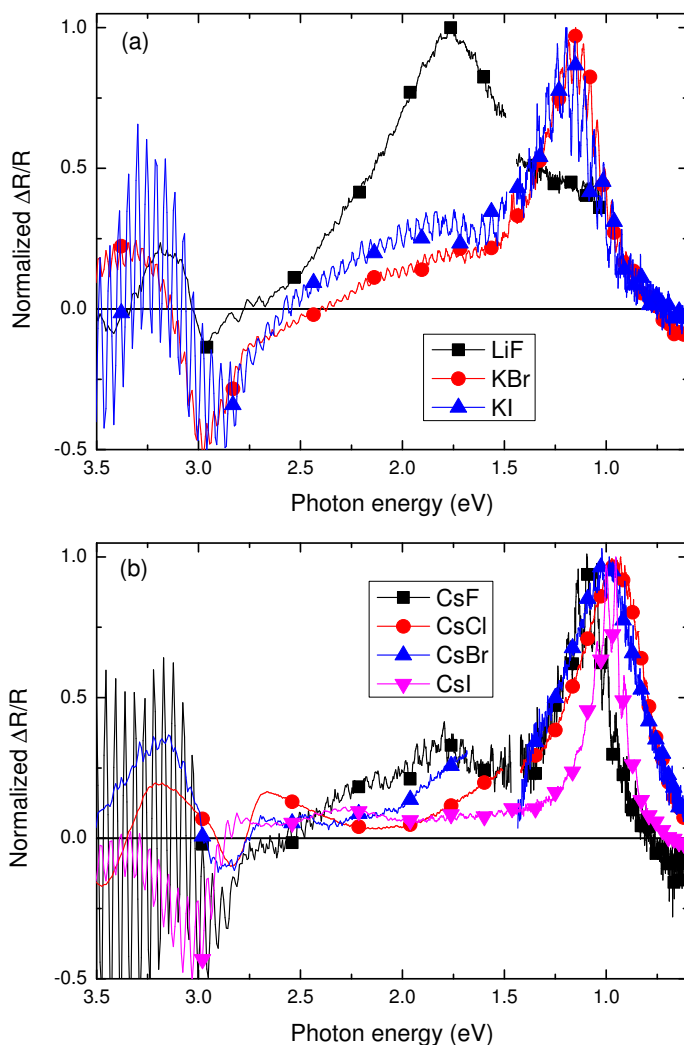


Figure 6.4: Normalized relative change in reflectivity ($-\Delta R/R$) for a ITO/ alkali halide (100 nm)/ poly(spirofluorene) (80 nm)/ Ba/ Al diode as function of photon energy. The applied bias were for (a) LiF 10 V, KBr 8 V, KI 8 V and (b) CsF 8 V, CsCl 8 V, CsBr 8 V, CsI 6 V.

As mentioned above, the changes in reflectivity depend on the magnitude of the applied bias voltage. We find that for alkali halides with a very deep valence band edge (LiF), high voltages are needed to induce coloration by voltage-induced defects. For alkali halides with higher valence band edge energies (CsI, KI), lower bias voltages can already induce significant changes in reflectivity. To bring out the correlation between coloration and band edge energy more clearly, we first define an onset voltage for coloration (V_{col})

corresponding to a change in reflectivity near the maximum of the near infrared band exceeding 2.5%. In Fig. 6.3 we plot values for V_{col} for all halides investigated versus the energetic position of the valance band edge of the alkali halide E_{VB} . The plotted data indicate a correlation between V_{col} and E_{VB} . We interpret this correlation as an indication for a causal relation between defect formation in the alkali halide and the injection of positive charge carriers into the alkali halide because the barrier for injection of a hole from ITO into the alkali halide will be lower for higher E_{VB} .

The values for V_{col} obtained provide a clue on the mechanism for defect generation. As mentioned in the introduction, previous studies on optically induced defect formation suggest that the self-trapped exciton in the alkali halide is a crucial intermediate in defect formation at low energies. The energies of the self-trapped excitons have been determined from luminescence measurements. In Table 6.2 we list energies of the singlet state of the self trapped exciton in the alkali halides studied as obtained from literature. The energy of the self-trapped exciton (E_{STE}^*) is considerably lower than for the primary 1s exciton (E_{1s}), due to geometrical relaxation of the lattice. We find that the coloration voltages determined experimentally for the MIM diodes, matches within 2 eV with the energies of the self-trapped exciton from bulk alkali halide crystals (Table 6.2). The close correspondence between V_{col} and E_{STE}^* suggests that for bias voltages close to the $V = E_{STE}^* / q_e$, electrons and holes can tunnel into the alkali halide and recombine, forming a self-trapped exciton. The STE can subsequently dissociate into a Frenkel defect pair.

Table 6.2: Literature data on energies for the 1s primary exciton E_{1s} , the self-trapped exciton E_{STE} , coloration $E_{col} = V_{col} / q_e$, the optical transition of the F_2 , F_3^+ , F_2^+ , F_3^- aggregates of anion vacancy defects.

Alkali halide	E_{1s} ^[25,13,14] (eV)	E_{STE}^* (eV)	E_{col} (eV)	E_{F2} (eV)	E_{F3+} (eV)	E_{F2+} (eV)	E_{F3-} (eV)
LiF	12.9	9 ^[25]	10	2.8 ^[15]	2.8 ^[15]	1.94 ^[15]	1.6 ^[15]
CsF	10.7	6 ^[25,16]	8				
KBr	6.7	4.4 ^[25]	6	1.4		0.84 ^[17]	
KI	5.9	4.2 ^[25]	4			0.77 ^[17]	
CsCl	7.9	5.2 ^[18]	6	1.2			
CsBr	6.8	4.7 ^[19]	5	1.2			
CsI	5.3	4.3 ^[20]	4	1.0			

*determined from the maximum of σ -polarized luminescence assigned to the singlet spin state of the STE.

6.3.3 Metal/CsI/metal diodes

In the section above we have postulated the simultaneous injection of electrons and holes into the alkali halide, in order to explain defect formation via the self-trapped exciton. To

test the feasibility of such an injection process into the wide bandgap ionic semiconductors under study, we have investigated CsI in more detail. In Fig. 6.5a we show J - V characteristics for a ITO/CsI (200 nm)/Al diode. Large current densities are observed indicating transport of charge carriers through the ionic semiconductor. The J - V characteristics are almost symmetric around $V = 0$, indicating low barriers for charge injection for the majority carrier.

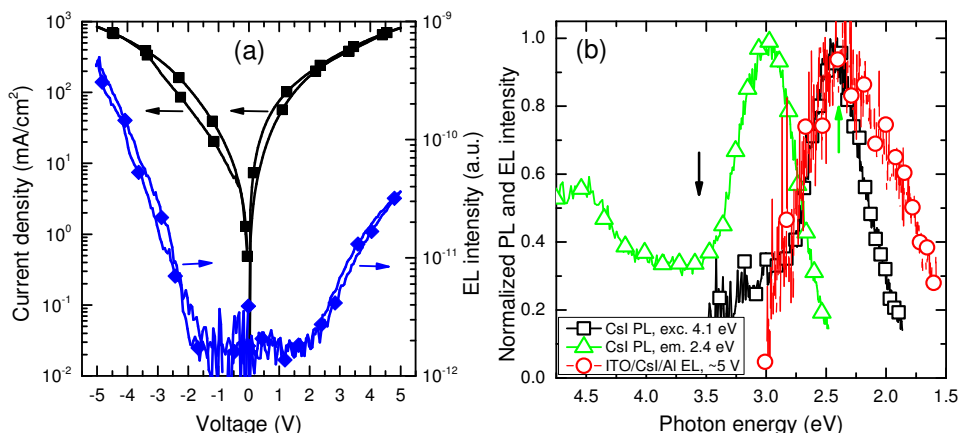


Figure 6.5: (a) J - V - EL characteristics of an ITO/CsI (200 nm)/Al diode from -5 V to +5 V. (b) PL spectra of a 200 nm CsI layer on quartz, the excitation is recorded at 2.4 eV, indicated by the green arrow. (green triangles), emission is recorded for an excitation of 4.1 eV indicated by the black arrow (black squares) and EL of a ITO/CsI/Al diode under a bias of -5 V (red circles).

Electroluminescence measured simultaneously with the current density provide further information on the charge carrier injection processes. We observe white electroluminescence from the metal/CsI/metal diode for both positive and negative bias voltage V when $|V|$ exceeds 2 V. Electroluminescence from CsI is known and has been attributed to radiative recombination of electrons with self-trapped holes.^[21] Also for KI and KBr, electroluminescence has been reported.^[22]

Spectrally resolved measurements of the electroluminescence are shown in Fig. 6.5b. A broad luminescence band centered around 2.2 eV is observed. Measurement of the photoluminescence (PL) of a film of CsI on quartz substrate yields a slightly narrower band centered around 2.3 eV. Measurement of the excitation spectrum of the photoluminescence shows that the emitting centers can be excited by photons of 3 eV. This indicates that the PL is originating from defects in the CsI. The close correspondence between electro- and photo- luminescence, points towards the electroluminescence originating from defects in CsI.^[23-25]

Electroluminescence provides direct evidence for simultaneous injection of electrons and holes into the alkali halide. The fact that electroluminescence can be

observed for both positive and negative applied voltages, points toward ‘plasticity’ of the contacts, and implies that upon changing the sign of the bias voltage, the electron injecting contact can change to a hole injecting contact and vice versa.

6.3.4 Correlation between defect formation and electroforming.

As shown in Fig. 6.3, both the voltage for electroforming and the onset voltage of coloration seem to correlate with the energy of the valence band edge. This brings up the question on the relation between defect formation as probed by coloration and electroforming. We try to answer this question by measuring simultaneously current density and coloration. In Fig. 6.6 we show the J - V characteristic of a pristine ITO/alkali halide(100 nm) /poly(spirofluorene) /Ba/Al diode together with differential reflectance ΔR at 1.55 eV. Reflection data show that significant changes in reflectivity set in for applied bias voltages above 12 V. Almost simultaneously with the onset of reduced reflectivity, there is a sharp increase in conductivity of the diode at about 13 V. Upon raising the bias further to +16 V and then lowering back to zero, conductivity remains high. The defect absorption slowly decays over time and reverts back to the original level for the pristine diode. A second voltage sweep shows that an irreversible change in conductivity has occurred, i. e. electroforming has taken place. We interpret these results as follows. Application of bias voltage induces defect formation. With increasing defect concentration, percolating pathways for charge transport can form. Electroforming reaches completion with the formation of a few of such percolation paths. Upon lowering the bias voltage, the majority of voltage-induced defects disappear again. The defects forming the percolating paths however, remain even at zero bias, as evidenced by the non-volatile change in conductivity. The number of defects involved in the paths is limited and stays below the detection limit of the reflection measurement.

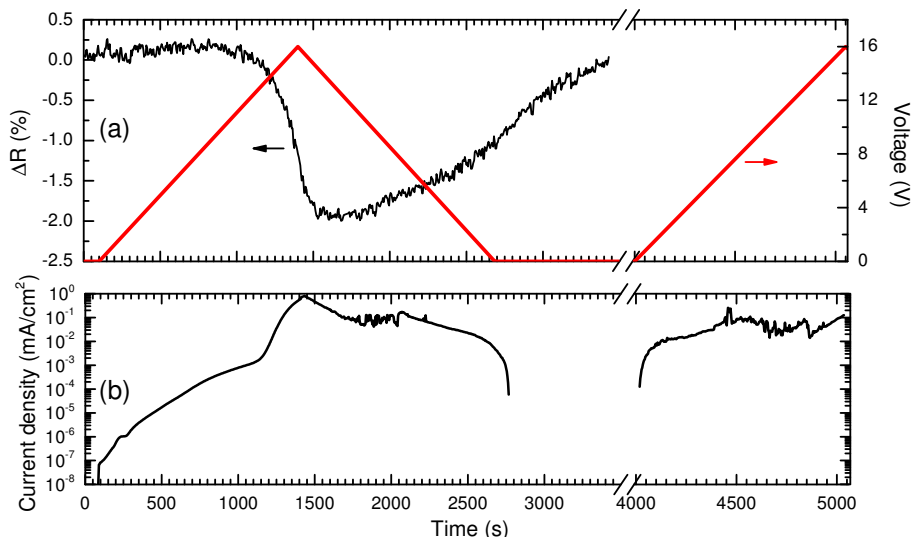


Figure 6.6: (a) $J-V$ characteristic of a ITO/LiF (100 nm)/poly(spirofluorene)/Ba/Al diode with a voltage sweep from 0 to 16 V and back to 0 with a voltage rate of 12.5 mV/s. (b) Voltage dependence of ΔR probed at a photon energy of 1.55 eV. The voltage and time scale are synchronized, with the voltage sweep starting at $t=100$ s.

After electroforming, the $J-V$ characteristics of the ITO/alkali halide/poly(spirofluorene)/Ba/Al diodes have one particular feature in common: all $J-V$ characteristics feature a voltage region in which current density decreases with increasing voltage, corresponding to a negative differential resistance (NDR). Figure 6.7 shows three examples. The NDR sets in for voltages exceeding 4 V and ends at roughly 6 V. Voltages corresponding to the local maximum in current density ($V_{J_{\max}}$) and the minimum in current density marking the end of the bias range of negative differential resistance ($V_{J_{\min}}$) are listed in Table 6.3 for various alkali halides.

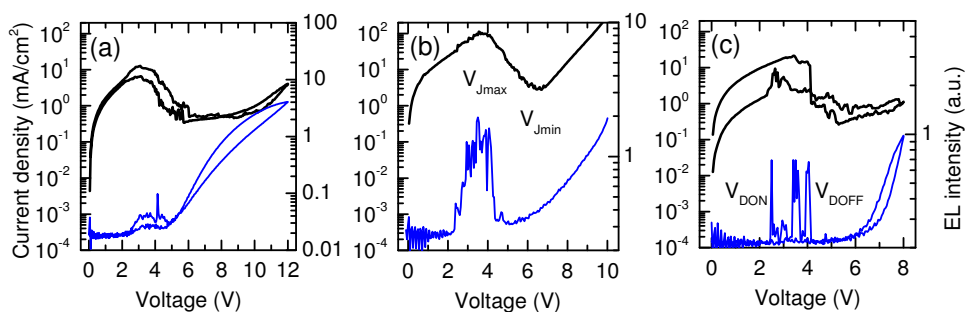


Figure 6.7: $J-V-EL$ characteristics of ITO/alkali halide/poly(spirofluorene)/Ba/Al diodes after electroforming and showing a NDR region for (a) LiF, (b) KBr, and (c) CsI.

Table 6.3: Voltages corresponding to the local maximum in current density (V_{Jmax}), the local minimum (V_{Jmin}), the onset of defect related EL (V_{DON}) and the voltage above which the defect EL is no longer observed (V_{DOFF}) for ITO/alkali halide/ poly(spirofluorene)/ Ba/Al diodes after electroforming.

Alkali halide	V_{Jmax}	V_{Jmin}	V_{DON}	V_{DOFF}
LiF	3	6	2	6
CsF	3	7.5	2	5.5
KBr	3.5	6.5	2	5
KI	3	6	2.5	4.5
CsCl	3.5	6	2.5	6
CsBr	3.5	7	3.5	6
CsI	3	6	2	5

6.3.5 Electroluminescence characterization

For all ITO/alkali halide/ poly(spirofluorene)/ Ba/Al diodes we observe electroluminescence under forward bias. Figure 6.7 shows the total electroluminescence (EL) intensity over the 1-3 eV photon energy for three different alkali halides. We find that for all alkali halide/poly(spirofluorene) MIM diodes investigated, the electroforming is accompanied by electroluminescence, consistent with earlier results for LiF/poly(spirofluorene) diodes^[5] (Chapter 5). For voltages above 6 V all alkali halides show EL that rises smoothly with increasing voltage. In the bias voltage range corresponding roughly to the NDR, we notice erratic EL with an intensity that fluctuates violently with increasing voltage. For some alkali halides this erratic EL is intense (KBr), for others it is faint (LiF). Spectrally resolved measurements of the electroluminescence provide further information on the nature of the excitations and recombination processes involved.

Figure 6.8. shows the electroluminescence spectrum at high bias voltages (8 V) for the 7 types of ITO/alkali halide/ poly(spirofluorene)/ Ba/Al diodes investigated. Prominent features in the spectra for all alkali halide at 2.75 eV and 2.55 eV can be readily assigned to electroluminescence from the polymer by comparison with the photoluminescence spectrum of just poly(spirofluorene) layer on quartz substrate. For CsI, we observe an additional band at 2.2 eV that may be attributed to luminescence emitted by defects in the CsI (see Figure 6.5).

Spectrally resolved measurements of the erratic electroluminescence in the voltage range corresponding to NDR yield spectral distributions very much different from those in Fig. 6.8. The erratic EL involves broad featureless bands with maxima in the near infrared. Because the bands of the erratic EL from the diodes do not match with known luminescent transitions in the polymer and because near infrared emission does not correspond with the bandgap of the alkali halides, we conclude that the luminescence originates from defects in the alkali halide.

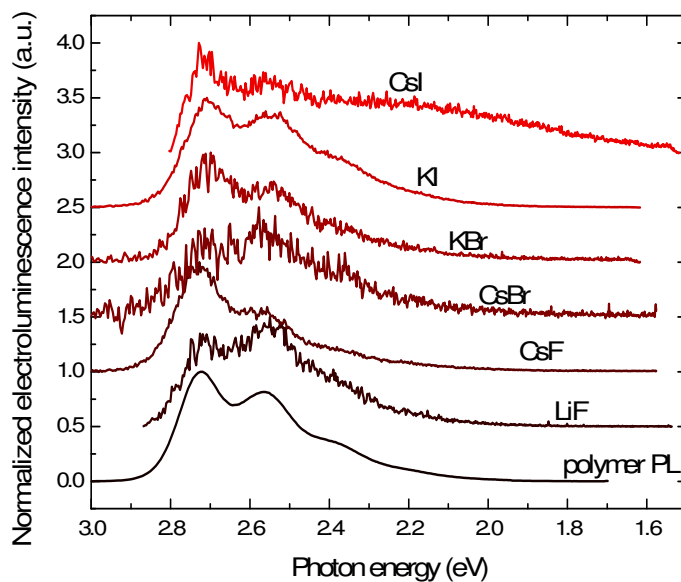


Figure 6.8: Normalized electroluminescence spectra at +8 V bias as a function of photon energy for ITO/alkali halide/polymer/Ba/Al. An offset of 0.5 is inserted in between each spectrum. From bottom to top: LiF, CsF, CsBr, KBr, KI, and CsI.

From the observation of electroluminescence from the polymer we conclude that holes must be injected into the polymer via the alkali halide layer. This further supports the hypothesis of hole injection into the alkali halide at high voltages. Electroluminescence from the polymer also implies injection of electron from the Ba/Al top contact at high voltage. The occurrence of negative differential resistance at voltages just below the onset of electroluminescence suggest a change in the charge injection properties of at least one of the two electrodes. The observation of luminescence from defects in the same voltage range as the region of NDR (Table 6.3) provides an experimental indication for recombination of trapped charges in the charge injection layer.

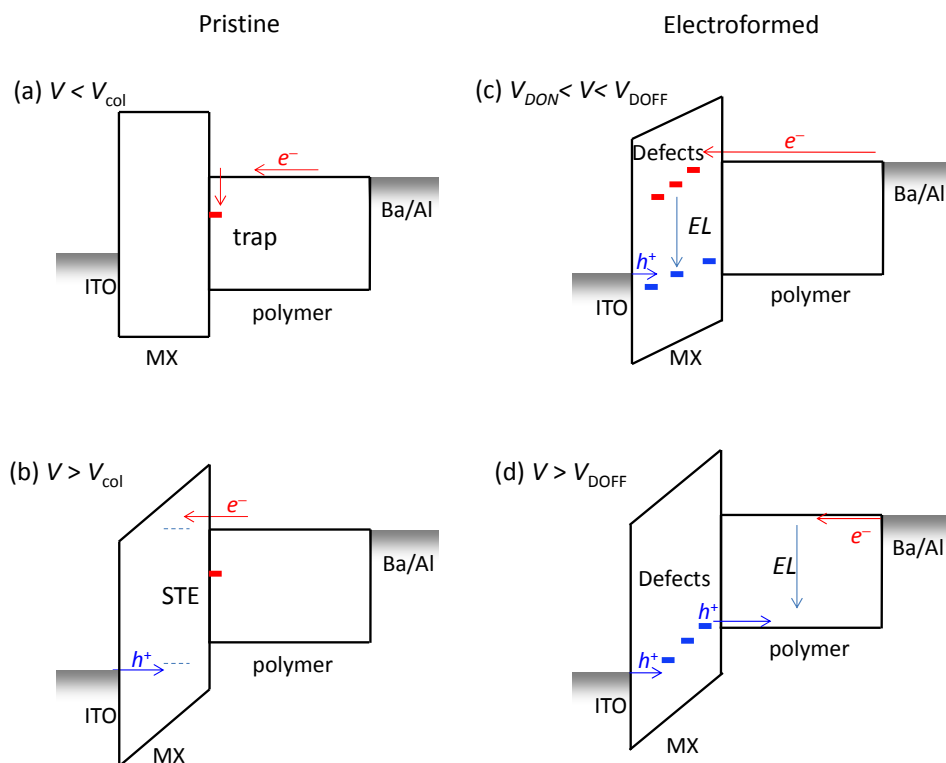


Figure 6.9: Schematic band diagram of the ITO/alkali halide (MX)/polymer/Ba/Al diode under different bias voltages. (a) Pristine diode at $V < V_{col}$ illustrating the electron trap at the MX/polymer interface. (b) Pristine diode at $V > V_{col}$ showing injection of electrons and holes resulting in the formation of STE. (c) Electroformed diode, with $V_{DON} < V < V_{DOFF}$, illustrate the electroluminescence from defects in the MX. (d) Electroformed diode with $V > V_{DOFF}$ shows MX as a hole injecting layer and electroluminescence from the polymer.

6.4 Conclusion

Metal-insulator-metal diodes incorporating a bilayer of alkali halide and organic semiconductor can be electroformed by application of bias voltage. The voltage needed for electroforming depends on the electronic structure of the alkali halide. Evidence for electroforming due to injection of charge carriers into the halide and subsequent defect formation in the ionic semiconductor leading have been presented. Electroforming, electroluminescence, and voltage-induced coloration are related to injection of holes into the alkali halide.

6.5 References

- [1] R. T. Poole, J. G. Jenkin, J. Liesegang, and R. C. G. Leckey, *Phys. Rev. B* **1975**, 11-12, 5179.
- [2] J. A. Smith and W. Pong, *Phys. Rev. B* **1975**, 12, 5931.
- [3] R. Waser and M. Aono, *Nat. Mater.* **2007**, 6, 833.
- [4] H. Biederman, *Vacuum* **1976**, 26, 513.
- [5] B. F. Bory, H. L. Gomes, R. A. J. Janssen, D. M. de Leeuw, and S. C. J. Meskers, *J. Phys. Chem. C* **2012**, 116, 12443.
- [6] J. C. Scott and L. D. Bozano, *Adv. Mater.* **2007**, 19, 1452.
- [7] F. Verbakel, S. C. J. Meskers, R. A. J. Janssen, H. L. Gomes, M. Cölle, M. Büchel, and D. M. de Leeuw, *Appl. Phys. Lett.* **2007**, 91, 192103.
- [8] M. D. Pickett and R. S. Williams, *Nanotechnology*, **2012**, 23, 215202.
- [9] R. T. Williams and K. S. Song, *J. Phys. Chem. Solids* **1990**, 51, 679.
- [10] R. T. Casper, S. C. Jones, P. Braunlich, and P. Kelly, *Nucl. Instr. Meth. Phys. Res. B* **1990**, 46, 231.
- [11] K. Tanimura and W. P. Hess, *Phys. Rev. B* **2004**, 69, 155102.
- [12] B. F. Bory, S. C. J. Meskers, R. A. J. Janssen, H. L. Gomes, and D. M. de Leeuw, *Appl. Phys. Lett.* **2010**, 97, 222106.
- [13] D. Pooley and W. A. Runciman, *J. Phys. C: Solid St. Phys.* **1970**, 3, 1815.
- [14] L. A. Lisitsyna *Russian Phys. J.* **1996**, 39, 1050.
- [15] G. Baldacchini, S. Bollanti, F. Bonfigli, P. Di Lazzaro, A. Y. Faenov, F. Flora, T. Marolo, R. M. Montekali, D. Murra, E. Nichelatti, T. Pikuz, A. Reale, L. Reale, A. Ritucci, and G. Tomassetti, *IEEE J. Sel. Top. Quant.* **2004**, 10, 1435.
- [16] W. Hayes and I. B. Owen, *J. Phys. C: Solid St. Phys.* **1977**, 10, L197.
- [17] I. Scheinder, *Optics Lett.* **1981**, 6, 157.
- [18] I. M. Blair, D. Pooley, and D. Smith, *J. Phys. C: Solid St. Phys.* **1972**, 5, 1537.
- [19] M. Itoh, K. Tanimura, and N Itoh, *J. Phys. Soc. Jpn.* **1993**, 62, 2904.
- [20] V. Nagirnyi, A. Stolovich, S. Zazubovich, V. Zepelin, E. Mihokova, E. Nikl, G. P. Pazzi, and L. Salvini, *J. Phys. Condens. Matter* **1995**, 7, 3637.
- [21] C. Paracchini, *Phys. Rev. B* **1973**, 8, 848.
- [22] C. Paracchini and G. Schianchi, *J. Lumin.* **1976**, 12-13, 903.
- [23] Z. Wu, B. Yang, and P.D. Townsend, *J. Lumin.* **2008**, 128, 1191.
- [24] F. Liu, X. Ouyang, M. Tang, Y. Xiao, B. Liu, X. Zhang, Y. Feng, J. Zhang, and J. Liu, *Appl. Phys. Lett.* **2013**, 102, 181107.
- [25] D. Totsuka, T. Yanagida, Y. Fujimoto, J. Pejchal, Y. Yokota, and A. Yoshikawad, *Opt. Mater.* **2012**, 34, 1087.

Chapter 7

Lithium fluoride injection layers can form quasi-Ohmic contacts for both holes and electrons

Abstract

Electroluminescence and current-voltage characteristics of metal/LiF/ poly(3-hexylthiophene)/ LiF/metal diodes are investigated. Electroluminescence is observed under both positive and negative bias voltages and with onset voltages close to the bandgap of the organic semiconductor. This indicates that LiF can form quasi-Ohmic contacts for injection of both electrons and holes. Diodes have to be conditioned at high bias voltages to induce efficient carrier injection. The formation of quasi-Ohmic contacts is attributed to accumulation of charged defects in the LiF layers. We argue that depending on the ionization state of the defects, either electrons or holes are injected into the organic semiconductor by the LiF. The diodes show non-volatile resistive switching under both unipolar forward and unipolar negative write and erase voltage pulses. The memristive effects are attributed to voltage induced changes in the ionization state of the defects in the LiF.

7.1 Introduction

Organic electronic devices such as light emitting diodes and solar cells require Ohmic contacts for their most efficient performance. Contacts of metals to organic semiconductors can often be improved by placing charge injection layers in between the semiconductor and the metal.^[1] Ionic semiconductor can be used as such interfacial layers, e.g. for hole injection MoO₃, V₂O₅,^[2] NiO,^[3] CuI and for electron injection: ZnO, CsCO₃ and LiF.^[4] Lithium fluoride (LiF) as injection layer has been studied in considerable detail. LiF interface layers lower the barrier for electron injection^[5] from Al into organic semiconductor due to a change in the effective workfunction of the LiF/Al contact. The mechanism by which the change in workfunction occurs is still under debate.^[6,7]

Here we report that the modification of the barrier for injection of charge carriers by LiF layers is not a static but a *dynamic* phenomenon. The effective workfunction of the LiF/metal contact can be either raised or lowered depending on the applied bias voltage (“electrical conditioning”).^[8] Metal/LiF/organic semiconductor contacts can switch from electron injecting to hole injecting and vice versa by electrical conditioning. This is demonstrated by electroluminescence (EL) for poly(3-hexylthiophene) (P3HT) in metal/LiF/P3HT/LiF/metal stacks under both positive and negative applied bias. The stacks are also memristive and show a non-volatile electronic memory effect associated with the switching. We argue that depending on the charge state of defects inside the LiF layer, LiF acts either as electron or hole injection contact. Alternation of the ionization state of the defects under influence of applied bias, results in a switch of the type of charge carrier that is injected/collected by a LiF/organic semiconductor contact.

This chapter is organized as follows. We first present experimental evidence from EL measurements for the injection of hole and electron by LiF layers. Next, spectroscopic measurements of absorption and EL provide support for the role of defect in the LiF in the charge injection process. Finally we provide a qualitative model for the dynamic doping profile in the LiF/P3HT/LiF diodes to account for the EL and memory effects.

7.2 Experimental

All diodes were fabricated onto glass substrates with patterned ITO. ITO substrates were cleaned, using in order, acetone, soap scrubbing, and isopropanol. LiF (Sigma Aldrich, 99.9%) was deposited by vacuum sublimation from an alumina crucible under 10⁻⁶ mbar. MoO₃ sublimed under vacuum from a baffled Mo boat under 10⁻⁶ mbar. ZnO layers were prepared from a sol-gel of zinc acetate dihydrate in methoxyethanol/ethanolamine by spin coating and subsequent thermal annealing at 150 °C.^[9] Poly(3,4-ethylenedioxythiophene) poly(styrenesulfonate) (PEDOT:PSS) was provided by Heraeus under the reference

Clevios PVP A14083, filtered and spin cast at 3000 rpm to form layers of 40 nm. P3HT (> 98% head to tail, $M_n = 54,000$ to $75,000$ g/mol, Plextronics, purchased from Aldrich), was dissolved in *o*-DCB with a concentration of 15 mg/mL and casted at 800 rpm. Poly(spirofluorene) was bought from Merck under the reference SPB-02T, dissolved in toluene at a concentration of 10 mg/mL and spin coated at a speed of 3500 rpm. Ba and Al top metal contacts were sublimed under 10^{-6} mbar. The diodes with LiF bottom layers were prepared under inert atmosphere. Diodes were kept and characterized in N_2 atmosphere ($O_2, H_2O < 1$ ppm).

Current, electroluminescence intensity, voltage (*J-EL-V*) characteristics were obtained using an Agilent 4155C semiconductor parameter analyzer together with a Si-photodiode. A Keithley 2601 source-measure unit was utilized for pulse measurements. Current voltage *J-V* sweeps were recorded with 50 mV step and 40 ms integration time. Throughout this chapter, positive bias is defined as the Ba/Al top electrode being charged negative. Reflection experiments were performed using a Perkin Elmer Lambda 900 UV-Vis-NIR absorbance spectrometer with a module for specular reflection measurements.

7.3 Results and discussion

Efficient EL from an organic semiconductor is achieved when the injection of electrons and holes into the semiconductor is balanced.^[10] Unlike the current density, which often mainly reflects the behavior of just the majority carriers, EL for organic semiconductors is highly sensitive to the probability for injection of the minority carrier in the semiconductor. This property, deriving from the strong recombination regime for electrons and holes in the low dielectric organic semiconductor, makes measurement of EL intensity a very useful research tool to investigate carrier injection processes.

Fig. 7.1a, b shows the EL intensity from a ITO/LiF (5 nm)/P3HT/LiF (5 nm)/Al diode plotted versus voltage. Both positive and negative bias voltages induce EL. Curves shown are obtained after electrical conditioning, as will be discussed in detail below. Scanning the bias voltage from -14 V to zero (Fig. 7.1a), we note an onset of EL at around -4 V; scanning from +10 V to 0 the EL onset is at +2 V. These voltages are close to the bandgap of the polymer (1.9 eV) implying low barriers for charge injection. The observation of EL under both positive and negative polarity implies that from either LiF contact both electrons and holes can be injected, depending on the bias and bias history of the device. The current densities under positive and negative bias voltage are almost similar, consistent with the symmetric structure of the LiF/polymer/LiF stack.

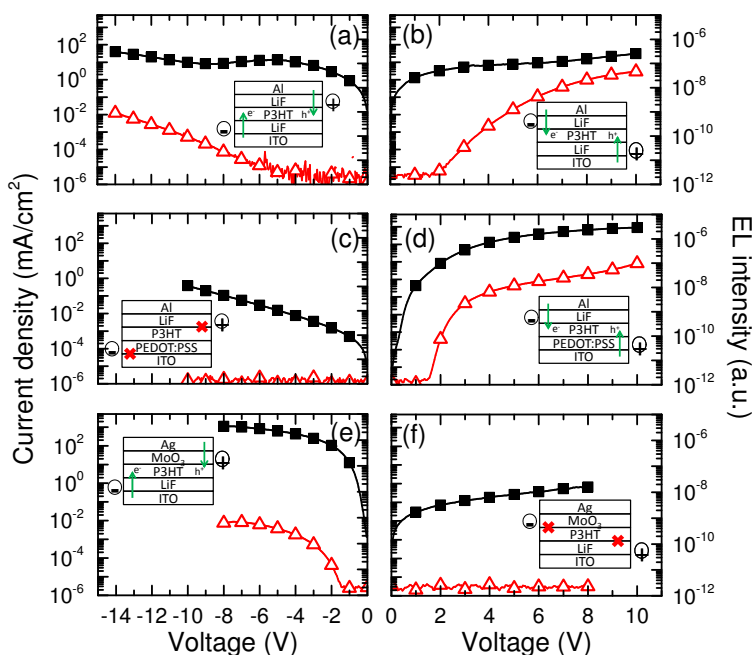


Figure 7.1: Current-Electroluminescence-Voltage (J - EL - V) characteristic of (a, b) ITO/LiF (5 nm)/P3HT (70 nm)/LiF (5 nm)/Al. after electrical conditioning, scan directions -14V \rightarrow 0 or +10 V \rightarrow 0 (c, d) ITO/LiF (5 nm)/P3HT (70 nm)/LiF (5 nm)/Al. (e, f) ITO/LiF (5 nm)/P3HT (70 nm)/MoO₃ (10 nm)/Ag. Filled black squares: J , Open red triangles: EL .

The electron injecting property of LiF (top) interface layers is well documented; only few reports on hole injection via LiF are available.^[11-13] Optimal LiF thickness for enhanced electron injection ranges around 1 nm. Thicker LiF layers seem to allow for hole injection. To gauge the efficiency of hole injection by the LiF interlayer, we compare the current densities and EL intensities of the LiF/P3HT/LiF stacks with the performance of diodes with known hole injecting contacts PEDOT:PSS (Fig. 7.1c,d) and MO₃ (Fig. 7.1e,f).

Under positive bias, the LiF/P3HT/LiF stack shows current densities and EL intensities comparable to a conventional PEDOT:PSS/P3HT/LiF/Al diode (Fig. 7.2a), indicating the formation of an efficient ITO/LiF hole injecting contact. Similarly, current densities and EL intensities of LiF/P3HT/LiF diodes under negative bias are comparable to those for inverted ITO/LiF/P3HT/MoO₃/Ag diodes (Fig. 7.2b). The EL intensities observed between the forward and reverse bias for the LiF/P3HT/LiF diodes (Fig. 7.1a,b) indicate lower intensities in reverse which are in turn comparable to those obtained with the inverted configuration. This indicates the relative limitation that suffers the ITO/LiF contact for electron injection. This shows that also the top LiF/Al electrode can act as

selective hole injection contact. We note that without the bottom LiF layer on ITO, no EL is observed for negative bias and current densities are much lower.

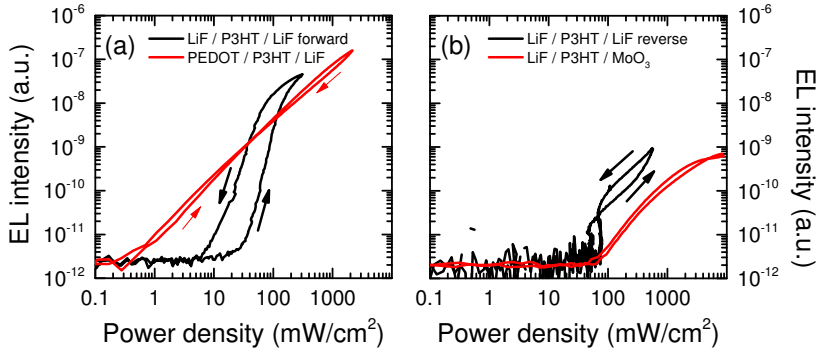


Figure 7.2: EL intensity versus electrical power density (a) in forward bias voltage for ITO/LiF (5 nm)/P3HT(70 nm)/LiF(5 nm) /Al after electric conditioning and ITO/PEDOT/P3HT/LiF(5nm)/Al. (b) in reverse bias voltage for ITO/LiF (5 nm)/P3HT(70 nm)/LiF(5 nm) /Al and for inverted ITO LiF(5 nm) /P3HT(70 nm)/MoO₃/Ag.

We note that at low bias ($|V| < 2\text{V}$), current densities through the symmetrical LiF/P3HT/LiF stack are more than six orders of magnitude larger than for a diode with contacts supporting only electron current (ITO/ZnO/P3HT/Ba/Al diode, (Fig. 7.3) but only two orders of magnitude lower than for a diode with contacts appropriate for only hole current (ITO/PEDOT:PSS/P3HT/MoO₃/Ag diodes (Fig. 7.3). This indicates that *at low bias* for diodes with the symmetrical LiF/P3HT/LiF layout, both LiF layers are selective for holes. This then in turn implies that one of the LiF layers in the LiF/P3HT/LiF stack switches from hole collecting to electron injecting contact when going from low to high bias. Considering the onset of EL in the LiF/P3HT/LiF stack, this switch occurs in the voltage range from 2 to 4 V.

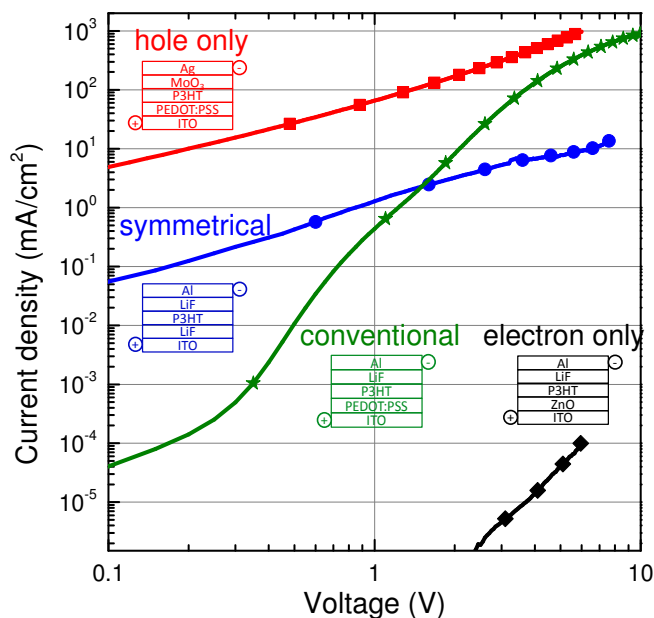


Figure 7.3: J - V characteristics for P3HT diodes with different electrode configurations supporting hole-only current (ITO/PEDOT:PSS/P3HT(70 nm)/MoO₃(10 nm)/Ag, red squares), bipolar current: (ITO/LiF(5 nm)/P3HT(70 nm)/LiF(5 nm)/Al, blue circles), bipolar current (ITO/PEDOT:PSS/P3HT(70 nm)/LiF(5 nm)/Al, green stars) and electron-only current (ITO/ZnO (30 nm)/P3HT(70 nm)/Ba/Al, black diamonds).

From the data in Fig. 7.1 we conclude that under appropriate conditions, LiF top and bottom interlayers can act as both electron and hole injecting contact. The selectivity of the LiF layer for either holes or electrons can be programmed by electrical conditioning. This is illustrated in Fig. 7.4. Here the LiF/P3HT/LiF stack that previously was emitting EL under positive bias (Fig. 7.1b) is subjected to several subsequent bias voltage sweeps of the negative bias voltage range. In the first sweeps, the EL at high negative bias (~ 8 V) gradually improves and saturates around the 10th sweep. Spectrally resolved measurements of the EL at high bias voltages confirm the singlet excited state in the polymer as the source of the electrically generated luminescence EL (Fig. 7.4b).

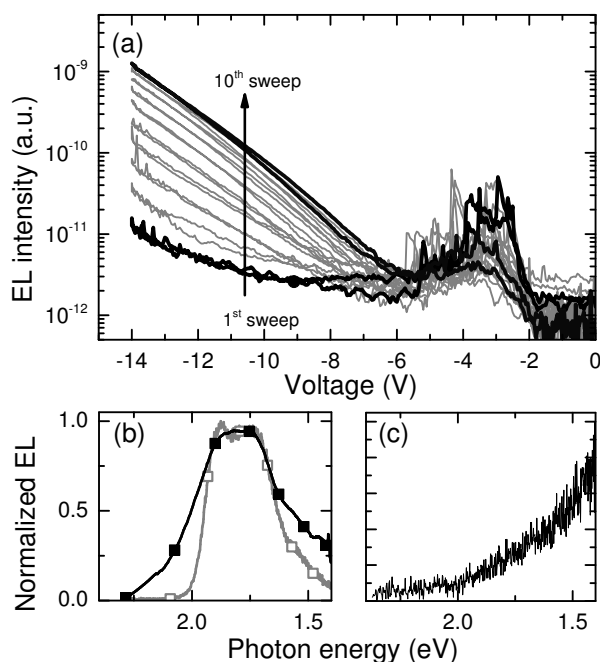


Figure 7.4: (a) *EL-V* characteristic of an ITO/ LiF (5 nm)/ P3HT/ LiF (5 nm)/ Al diode showing electrical conditioning during 10 consecutive voltage sweeps. (b) Normalized EL spectra of a ITO/ LiF (5 nm)/ P3HT/ LiF (5 nm)/ Al diode at -8 V (closed symbol) and of a ITO/ PEDOT:PSS/ P3HT/LiF (5 nm)/ Al at +4 V (open symbol). (c) Normalized EL spectra of a ITO/ LiF (5 nm)/ P3HT/ LiF (5 nm)/ Al diode at -3 V.

The *J-V* characteristics associated with the EL shown in Fig. 7.4, show comparatively little change during the electrical conditioning (data not shown); only a small increase of the current at high voltage is observed. *J-V* and *EL-V* characteristics during electrical conditioning as shown in Fig. 7.4a, thus imply an increase in EL efficiency due to enhancement of injection of minority carriers into the organic semiconductor and more balanced charge injection.

Interestingly, also in the low bias voltage range (-2 to -4 V) the LiF/P3HT/LiF stack shows EL. In this voltage range, the intensity of the EL shows a highly erratic ('spiky') behavior as function of applied voltage. The spectrum of this low-voltage EL, shown in Fig. 7.4c, is markedly different from the spectrum at high voltage assigned to P3HT. The spectrum at low voltage features the high energy shoulder of a broad band whose maximum must lie in the (near)-infrared region, outside the window of observation. Clearly, this emission must originate from a defect because the spectral position of the EL (< 1.5 eV) does not match with the bandgap for either LiF or P3HT. Interestingly, the defect EL at low voltage also shows a dependence on the history of the diode. This suggests a close relation between the memristive switching between hole and electron injecting states of the LiF and the defect luminescence.

Fig. 7.5 show $EL-V$ and $J-V$ characteristics of the LiF/P3HT/LiF diode after electrical conditioning as shown in Fig. 7.4 for two different bias voltage histories of the diode. The first set of traces (squares) shows current density and EL intensity recorded when sweeping the voltage from 0 to -14 V, directly following a slow voltage sweep from -14 V to 0 (not shown). The current density shows a local maximum near -2.7 V. As discussed above, high current densities for $|V| < 2.7$ are consistent with a hole-only current and two quasi-Ohmic LiF contacts, selective for holes. Following the maximum in current density at -2.7 V is a region of negative differential resistance (NDR) where the current density decreases with increasing voltage. The $EL-V$ trace recorded simultaneously with the current density, shows defect emission at low voltage and polymer EL at high voltage. Curiously, the voltage range in which the diode shows NDR, largely overlaps with the voltage range of erratic defect EL emission. At high bias ($|V| > 6$ V), current density rises again with increasing bias voltage, and stable EL from the polymer is observed. The onset of EL indicates the switch of the bottom LiF layer from hole collection to electron injection.

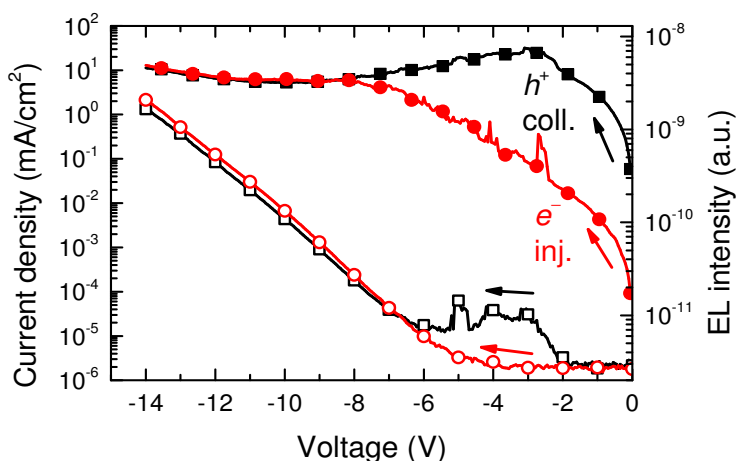


Figure 7.5: $J-EL-V$ characteristics of an ITO/ LiF(5 nm)/ P3HT/ LiF(5 nm)/ Al diode. The black squares pertain to the diode directly after a -14 V \rightarrow 0 V sweep, i.e. programmed in the high conduction state with the top LiF contact set to hole collection. The red circles show $J-EL-V$ for the same diode after a 0 V \rightarrow -14 V sweep followed by immediate lowering of the bias voltage to 0 V i.e. programmed in the low conduction state with the top LiF contact set to electron injection.

Fig. 7.5 also shows a second set of J and EL traces, indicated with circles, that was obtained for a different history of the bias voltage applied to the diode prior to the $J-EL-V$ measurement. Directly before the 0 \rightarrow -14 V sweep shown, the diode was subjected to a 0 \rightarrow -14 V voltage scan, after which the applied bias was immediately lowered from -14 V to 0 V in a $\sim\mu\text{s}$ time interval. With this history, the current densities at low bias ($|V|$

< 2 V) are much smaller. In the region -2 to -4 V, the current density does not show NDR and no defect emission is observed. Instead at high bias ($|V| > 8$ V), the J and EL traces for the different histories show a good overlap. We argue that upon lowering the bias rapidly from -14 V to zero, the bottom LiF contact in the LiF/P3HT/LiF stack retains its electron injecting and hole blocking properties. As a result, the diode will retain the built-in voltage associated with the electroluminescent state at high bias. The built-in voltage should be close to the bandgap of the polymer (1.9 eV). Consistently, diodes with the -14 V history, show low current densities at low voltage and no defect emission. For bias voltages going above the bandgap of the polymer, the diode starts entering again in the electroluminescent state.

The observation of memristive properties, *i.e.* optoelectronic properties that depend on the history of the diode, indicates an electrical bistability. The electrical bistability can be demonstrated directly in experiments using short voltage pulses to switch the resistance of the ITO/LiF/P3HT/LiF/Al diode; see Fig. 7.6. Voltage pulses with amplitude of $+8$ V and also pulses with -8 V amplitude, induce a state with high electrical resistance state, showing low current densities at probe voltages of 1 V. In contrast, voltage pulses with amplitude of $+4$ and -4 V induce a state with low electrical resistance near 1 V. The electronic memory effect associated with the LiF layers is non-volatile and can be read out non-destructively.^[14,15]

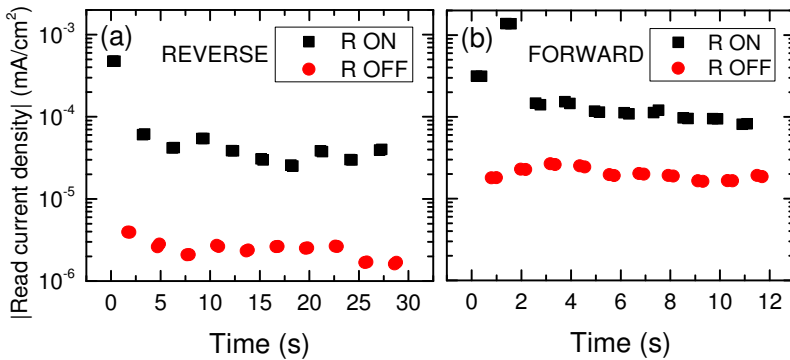


Figure 7.6: The electroluminescent device is characterized in term of a resistive switching memory. (a) the diode is turned into a HRS applying a -4 V pulse of 100 ms, the resistive state is read out applying -1 V of 100 ms (square symbols). Subsequently, the diode is turned in the LRS with a -8 V, 100 ms and read out with -1 V, 100 ms (circle symbols). (b) similar procedure than in (a) with positive voltages and 1 s pulse length. The pulse sequence is repeated 10 times, allowing for endurance properties of the memory diode. The HRS to LRS ratio is higher than 5.

Switching between hole collection and electron injection and associated memory effect were also observed for LiF/poly(phenylenevinylene) and LiF/poly(spirofluorene). We also detected defect EL accompanying the switching. This indicates that the defects

responsible for the EL do not reside in the polymer but in the alkali halide. Defect formation in alkali halides is well known and can already be induced by quanta of energy comparable to the bandgap of the alkali halide, e.g. UV photons.^[16]

A type of defect that has been shown to form in alkali halides at low energies is the Frenkel defect. Frenkel defects consist of an anion vacancy (F) and a halogen interstitial (H) and can be induced in alkali halides by e.g. absorption of an optical photon. The excited state resulting from photon absorption can undergo self-trapping, a process involving dimerization of two halogen atoms. The self-trapped exciton (STE) can subsequently dissociate into an F - H defect pair, with F an anion vacancy and H a halide interstitial, as depicted in Fig. 7.7a.^[17-20] Here we propose that recombination of an electron injected into the conduction band of LiF with a hole injected into the valence band can lead to the formation of an F - H pair with the STE as intermediate (Fig. 7.8). A lower limit for the onset of this electrically induced defect formation in LiF, is set by the energy of the STE. The energy of the STE in LiF estimated from its luminescence is above 6 eV, and so a bias voltages of 6 V is a lower limit for Frenkel defect formation. Interestingly, degradation of the insulating properties of LiF (electroforming) has been reported to set in at voltages around 5 V.^[21] The electronic bandgap of LiF (13 eV) serves a limit above which Frenkel defect formation via electronically injected charge carriers may be expected to become efficient.

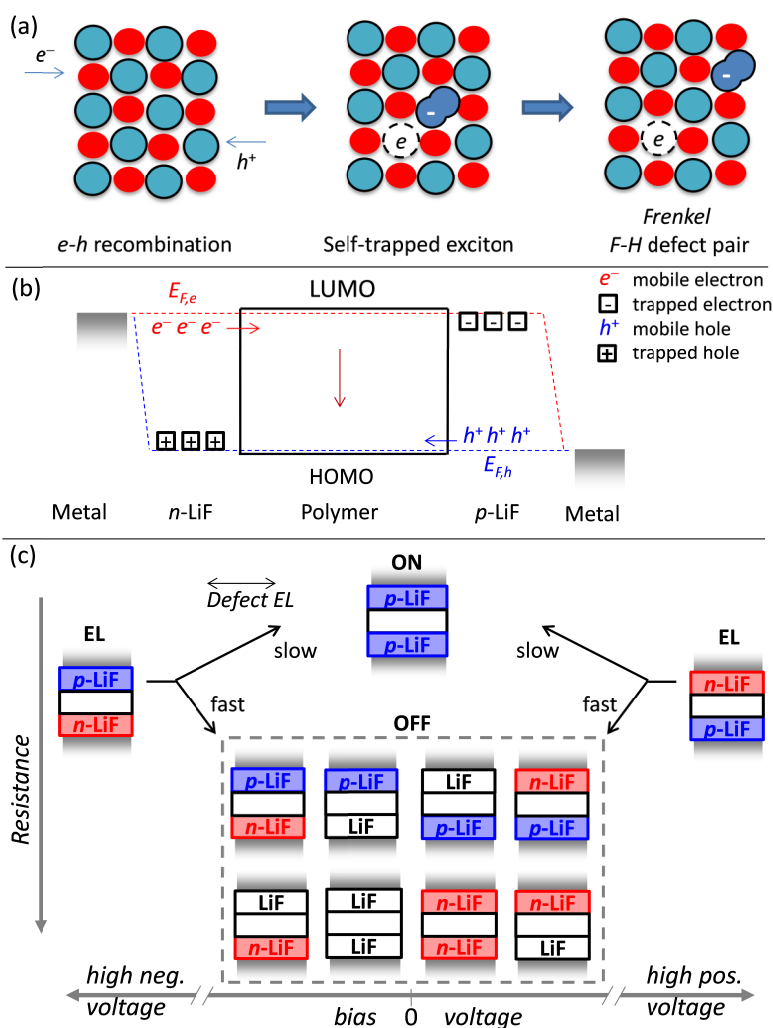


Figure 7.7: (a) Schematic illustration of defect formation in alkali halides. Injection of an electron into the conduction band and a hole in the valence band results in formation of an electronic excitation that subsequently undergoes self-trapping. Self-trapping involves migration of an anion to an interstitial position creating a vacancy (F) and halide interstitial (H) pair of point defects. F and H can dissociate further by diffusion and form aggregates. (b) Band diagram for an ITO/LiF/P3HT/LiF/Al diode at bias voltages corresponding to the onset of electroluminescence. The quasi-Fermi levels for electrons $E_{F,e}$ and holes $E_{F,h}$ are indicated. Trapped charge at ionized defects induces n - or p -type doping character of the LiF. (c) Doping configurations of the ITO/LiF/P3HT/LiF/Al diode for the electroluminescent (EL) states at high pos. and neg. bias voltage, the low resistance ON state near zero bias and various possible high resistance states (OFFs) near zero bias.

Optical absorption spectroscopy provides further evidence for electrically induced defect formation in LiF/polymer junctions. In optical experiments aimed at probing the alkali halide, diodes with P3HT polymer offer only a narrow spectral window because of the strong optical absorption of P3HT with an onset already at 1.9 eV. Poly(spirofluorene) (PF), with a bandgap around 3 eV, allows also the visible and UV ranges to be probed. We study specular reflection R of light of a pristine ITO/LiF (100 nm)/ PF/ Ba/Al diode as function of bias voltage. Application of forward bias to the ITO electrode results in reduction of the intensity of light reflected from the back Ba/Al metal electrode after entering the diode via the transparent front electrode. We ascribed the reduction in reflected intensity to absorption of light by defects induced in the LiF/polymer junction by the application of a bias voltage.

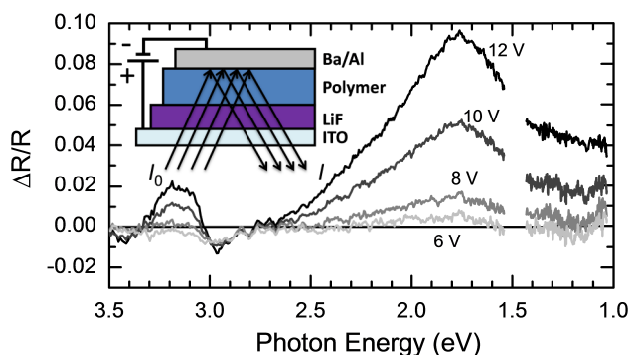


Figure 7.8: Relative change in reflectance $\Delta R/R$ of an ITO/ LiF (100 nm)/ poly(spirofluorene)/ Ba/Al diode induced by bias voltage V for 6 V to 12 V. The inset shows the diode structure with specular reflection traces onto the Ba/Al electrode. Specular reflection occurring at other interfaces are omitted for clarity.

Changes in reflection induced by bias are reversible, do not occur under reverse bias and are at maximum on the order of a 10 % change in reflected intensity. In Fig. 7.8 we show the relative change in reflection $\Delta R/R$. For small values of $\Delta R/R$ and for wavelengths $\lambda \gg d$ with d the total film thickness of LiF and PF, $\Delta R/R$ can (under certain conditions) be interpreted as the induced absorption ΔA by the LiF/polymer layers. Upon increasing the bias above 6 V to a maximum of 12 V, a broad absorption band appears, centered around 1.75 eV, with the amplitude of the absorption increasing with bias. A possible assignment of the induced absorption band is the F_2^+ defect. The F_2^+ defect center consists of two anion vacancies on adjacent lattice sites occupied by one electron. This defect is well known from studies of radiation damage in LiF.^[22,23] The isolated F center absorbs in the UV (at 5 eV^[24]) and may be masked by the strong polymer absorption.

Schlaf et al.^[7] have suggested that the change in effective work function of a metal is brought about by the LiF interface, and, could be due to charged Frenkel defects. Here we follow this suggestion and argue that the dynamic changes in effective work

function of the metal/LiF contact leading to the switching between electron and hole selective contacts is due to changes in the ionization state of the Frenkel defects. In the discussion below, we assume that defects in the LiF exist, and, that they can be switched reversibly between charge neutral and positively charged ionization states, and also, between charge neutral and negatively charged ionization state. The positively charged defects give rise to n -type conductivity in the insulator while the negatively charged defects give rise to p -type conduction. This assumption is supported by experiments on small, halogen-deficient LiF clusters that indicate an ionization potential for the F defect around 4.2 eV below vacuum, i.e. within the bandgap of the LiF.^[25] High levels of n - (p -) type doping in the LiF may give rise to formation of a quasi-Ohmic contact for electron (hole) injection from the electrode metal/LiF into the polymeric semiconductor.

The assumption of dynamic p - and n - type doping of the LiF allows one to explain the EL from the polymer at high bias voltage (See Fig. 7.7b). At the negative electrode, positive charges trapped at the defects in LiF give rise to n -type behavior and support electron injection into the polymer. Some of the electrons injected may get trapped in the LiF layer on the opposite site of the diode and induce p -type conduction in the LiF layer near the positively charged electrode. The p -type doping, may in turn lead to an Ohmic contact for holes, and trapping of some of the injected holes in the LiF near the negative electrode reinforces the n -type behavior of the other LiF layer. Recombination of electrons and holes injected into the polymer can lead to formation of excitons and result in EL from the polymer. The polymer semiconductor is considered as intrinsic (i). Explanation of the EL from the polymer via this p - i - n doping distribution requires slow recombination of the trapped carrier in the LiF with injected carriers of opposite sign. Additionally, the presence of defect states for electrons and holes in the LiF with appropriate energies are necessary, i.e. defects with energies close to the HOMO and LUMO levels of the polymer.

The experimental fact that EL can be observed for both positive and negative bias voltages indicates that the type of doping of the LiF layers can be switched from p to n - and from n - to p -. The switching of the type of doping in the LiF, also allows for a p - i - p doping configuration. In the p - i - p configuration, the diode would behave as a hole-only device. The experimental observation of current densities, at low bias in the ON state of ITO/LiF/P3HT/LiF/Al similar in magnitude to the hole only ITO/PEDOT/P3HT/MO₃/Ag diodes, and orders of magnitude higher than for the electron only ITO/ZnO/P3HT/LiF/Al ITO, lead us to the assignment of a p - i - p doping configuration for the low resistance ON state. (Fig. 7.7c). The proposed p - i - p configuration also explains the symmetric nature of the J - V characteristics around zero bias voltage and the apparent absence of a built-in potential.

The pulse measurements and the J - V sweeps (Figs. 7.5 and 7.6) show by rapidly lowering of the applied bias voltage that the diodes can be brought directly from the p - i - n (or n - i - p) electroluminescent state at high voltage to an OFF state at low bias voltage. This suggests a p - i - n (or n - i - p) doping configuration for the OFF states. In the p - i - n , the diodes

feature a built-in potential that prevents high current densities at bias voltages below the bandgap of the semiconductor. We note that in contrast to the uniquely defined ON state, diodes with several doping configurations can lead to high resistance (Fig. 7.7).

In contrast, upon *slowly* lowering the bias voltage applied to the diode in the *p-i-n* (or *n-i-p*) electroluminescent state, the diode switches to the *p-i-p*, the ON state. This switch will now be discussed in more detail. First we note that for bias voltages below the bandgap of the polymer $V < E_{\text{gap}}$, the steady state illustrated in Fig. 7.7b can no longer exist. Bipolar charge transport through the polymer is no longer possible for $V < E_{\text{gap}}$, and so the diode has to switch to unipolar charge transport. As discussed above, the majority carriers in the high conduction state are holes and thus, the electron injecting *n*-type contact has to switch to a hole collecting configuration with *p*-type doping of the LiF to enter into the high conduction state. The switching from *n*- to *p*-type within a LiF layer can be pictured as recombination for electron trapped at defects with holes injected into the LiF from the polymeric semiconductor. The occurrence of this recombination process is evidenced by the EL from the defects that can be observed during the switch at voltages around -4 V (Figs. 7.4 and 7.5).

Importantly, in order to be consistent with the observed stability of the resistance state at low bias, we are forced to assume that recombination of charges at defects changing their charge state does not occur at low bias. This requirement can be accommodated by adopting a Shockley-Read-Hall type of recombination mechanism where trapped charges only recombine with mobile charges. In disordered materials, the mobility of charge carriers depends strongly on its energy within the disorder broadened density of states (DOS). At low energy the carrier is confined to localized states deep within the DOS and may not be able to reach a trapped charge carrier of opposite sign and recombine. Hence, to induce recombination, the quasi-Fermi level for the charge carrier needs to be above a certain mobility edge. We note further that the trapped charges in the LiF may be stabilize electrostatically by a charge carrier of opposite sign residing in the polymeric semiconductor.

Now, crucially, in order to account for the high conduction at low bias voltage and at the same time also for the low recombination rate we have to assume the existence of highly localized percolation pathways for transport of low energy charge carriers. These pathways should reach across the LiF but not bring charge carrier in too close proximity to the defects of opposite charge. The existence of such percolation paths requires high defect densities and seem more likely for wide bandgap materials as in such material internal energy barriers between localized defects states can be high. We note that, in line with the argumentation given above, memristive effects are quite commonly found in wide gap oxide insulators (SiO_2 , Al_2O_3) after subjection to degradation by application of high bias voltages. The high conduction state usually involves localized paths also referred to as *current filaments*.

7.4 Conclusion

In summary, we have shown that junctions of LiF and organic semiconductor can show an electrical bistability and that the LiF can switch between electron and hole injecting configurations. The switching can be interpreted in terms of a modification of the effective work function of the metal/LiF contact to the semiconductor, due to a change in ionization state of the defects in the LiF layer. The bistability of the LiF/polymer contact allows LiF/polymer/LiF stacks to emit EL under both forward and reverse bias voltage. As a side effect, the bistability also gives rise to memristive properties: the electrical conductivity can be switched between different levels by applying voltage pulses of the same polarity. In our interpretation, the unipolar switching relies essentially on branching point in the kinetics occurring at a bias voltage near the band gap of the semiconductor. Starting from the electroluminescent state, slow passage through the branching point allows the device to reach a second steady state characterized by unipolar transport and high conductivity. Fast passage of the branching point does not allow enough time for the ionization state of the 'slow' defects to change.

7.5 References

- [1] H. Ma, H. L. Yip, and F. Huang, and A. K. Y. Jen, *Adv. Funct. Mater.* **2010**, *20*, 1371.
- [2] V. Shrotriya, G. Li, Y. Yao, C.-W. Chu, and Y. Yang, *Appl. Phys. Lett.* **2006**, *88*, 073508.
- [3] J. Bandara and H. Weerasinghe, *Sol. Energ. Mat. Sol. C.* **2005**, *85*, 385.
- [4] L. S. Hung, C. W. Tang, and M. G. Mason, *Appl. Phys. Lett.* **1997**, *70*, 152.
- [5] T. M. Brown, R. H. Friend, I. S. Millard, D. J. Lacey, J. H. Burroughes, and F. Cacialli, *J. Appl. Phys.* **2000**, *93*, 6159.
- [6] H. Heil, J. Steiger, S. Karg, M. Gastel, M. Stoessel, H. Ortner, and H. von Seggern, *J. Appl. Phys.* **2001**, *89*, 420.
- [7] R. Schlaf, B. A. Parkinson, P. A. Lee, K. W. Nebesny, G. Jabbour, B. Kippelen, N. Peyghambarian, and N. R. Armstrong, *J. Appl. Phys.* **1998**, *84*, 6729.
- [8] M. Lu, P. de Bruyn, H. T. Nicolai, G.-J. A. H. Wetzelaer, and P. W. M. Blom, *Organic Electronics* **2012**, *13*, 1693.
- [9] C.-H. Chou, W. L. Kwan, Z. Hong, L.-M. Chen, and Y. Yang, *Adv. Mater.* **2011**, *23*, 1282.
- [10] R. H. Friend, R. W. Gymer, A. B. Holmes, J. H. Burroughes, R. N. Marks, C. Taliani, D. D. C. Bradley, D. A. Dos Santos, J. L. Bredas, M. Logdlund, and W. R. Salaneck, *Nature* **1999**, 397, 121.
- [11] T. Xiao, W. P. Cui, M. Cai, R. Liu, and J. W. Andereg, J. Shinar, and R. Shinar, *J. Photon. Energy.* **2012**, *2*, 021006.
- [12] A. Turak, T. Aytun, and C. W. Ow-Yang, *Appl. Phys. Lett.* **2012**, *100*, 253303.
- [13] H. S. Kim, H. Lee, P. E. Jeon, K. Jeong, J. H. Lee, and Y. Yi, *J. Appl. Phys.* **2010**, *108*, 053701.
- [14] K. S. Yook and J. Y. Lee, *J. Ind. Eng. Chem.* **2010**, *16*, 230.
- [15] B. F. Bory, H. L. Gomes, R. A. J. Janssen, D. M. de Leeuw, and S. C. J. Meskers, *J. Phys. Chem. C* **2012**, *116*, 12443.
- [16] H. N. Hersh, *Phys. Rev.* **1966**, *148*, 928.
- [17] R. T. Williams and K. S. Song, *J. Phys. Chem. Solids.* **1990**, *51*, 679.
- [18] N. Itoh and K. Tanimura, *J. Phys. Chem. Solids* **1990**, *51*, 717.
- [19] J. J. Kolodziej, B. Such, P. Czuba, F. Krok, P. Piatkowski, P. Struski, M. Szymonski, R. Bennewitz, S. Schär, and E. Meyer, *Surf. Sci.* **2001**, *482-485*, 903.
- [20] N. Itoh, *Adv. Phys.* **1982**, *31*, 491.
- [21] S. G. Dearnaley, A. M. Stoneham, and D. V. Morgan, *J. Non Cryst. Solids* **1970**, *4*, 593.
- [22] G. Baldacchini, S. Bollanti, F. Bonfigli, P. Di Lazzaro, A. Y. Faenov, F. Flora, T. Marolo, R. M. Montoreali, D. Murra, E. Nichelatti, T. Pikuz, A. Reale, L. Reale, A. Ritucci, and G. Tomassetti, *IEEE J. Sel. Top. Quant.* **2004**, *10*, 1435.
- [23] L. A. Lisitsyna, *Rus. Phys. J.* **1996**, *39*, 1050.
- [24] D. B. Sirdeshmukh, L. Sirdeshmukh, and K.G. Subhadra, Springer Verlag Berlin, (2001).
- [25] S. Velickovic, V. Djordjevic, J. Cveticanin, J. Djustebek, and O. Neskovic, *Vacuum* **2009**, *83*, 378.

Summary

Electroforming and switching of organic-inorganic resistive memories

Resistive switching is a memristive effect which refers to a dependence of the electrical resistance of a diode on previously applied bias voltages, i. e. on the history of the diode. The changes in resistance are often reversible and metastable, allowing for application of memristive diodes in storage and processing of information. Resistive switching allows for programming the memristor into distinct resistive states by applying voltage pulses of selected amplitudes. Low voltages are then used for the reading out of the memory state.

A wide variety of materials can give rise to memristive effects when incorporated as active layer in a diode, e.g. metal oxides and alkali halides. The physical mechanism of reversible resistive switching is largely unknown.

Often, application of a high electric field, close to the breakdown voltage of the active material, is needed to induce the resistive switching. The initializing effect of a high electric field strength is also known as electroforming. Electroforming occurs in a large variety of electrical components, and affects the stability and operational lifetime of transistors, capacitors, and light-emitting diodes, including organic and polymer diodes.

The aim of the thesis is to investigate electroforming in organic-inorganic hybrid diodes with the ultimate aim to gain better control over resistive switching and failure of diodes.

Chapter 1 of the thesis provides an introduction into the electronic memory technology challenge. The limitations of current state-of-the-art NAND flash technology are discussed. Alternative memristor technology is introduced and compared to NAND flash. Memristor structure and materials are then presented. Memristors need to be activated by electroforming. Electroforming represents a major drawback of memristor technology because of the possibility of permanent electrical shorting induced during the electroforming through e.g. overheating. Memristors with insulating layers of organic and inorganic materials have been found to be relatively stable against such failure during electroforming.

Chapter 2 is an explanatory review on electroforming and unipolar switching of memristor diodes with bilayer architecture comprising an inorganic Al_2O_3 layer and a layer of an organic semiconducting polymer. The chapter starts with an overview of experimental results on Al_2O_3 / polymer diodes. The electroforming process is described in terms of formation of defects that organize into conductive filaments. The resistive switching and the associated electrical bistability are qualitatively interpreted in terms of coexistence of neutral and conductive phases in the memristor.

Electroforming of metal-insulator-metal (MIM) diodes where the insulator

consists of a layer of Al_2O_3 or alkali halide combined with a layer of semiconducting polymer is investigated throughout the chapters 3 to 6. The overall electroforming process is found to occur as a sequence of steps. The initial steps are still reversible, the final step is irreversible.

Chapter 3 and 4 describe the early stage of electroforming in MIM diodes. In the early stage, at low voltages, accumulation and trapping of electrons at the organic / inorganic interface occurs. Trapping of charges inside the MIM structure induces a redistribution of the applied electrical potential difference over the organic and inorganic layers. The trapping of electrons injected initially into the polymer layer, brings most of the applied voltage across the inorganic layers and initiates the electroforming. The charge carrier accumulation at the Al_2O_3 / polymer internal interface, studied in chapter 3, was followed by means of the quasi-static capacitance-voltage technique. As described in chapter 4, the initial reversible step of the electroforming of LiF / polymer diodes, also involves accumulation of electrons at the LiF / polymer internal interface.

In chapter 4, electrical and optical characterization of the diodes shows that formation of positively charged defects in the LiF occurs subsequent to electron trapping. Estimated densities of positively charged defects in the LiF, just before the final irreversible stage of electroforming are on the order of $10^{19} / \text{cm}^3$, in the vicinity of the internal LiF / polymer interface, which is close to the critical density expected for the insulator-to-metal transition.

Chapter 5 and 6 focus on the later stages of electroforming of LiF / alkali halide diodes, occurring at voltages higher than used in Chapter 3 and 4. In Chapter 5, electroforming is found to occur at voltages around 15 V, almost independent of the thickness of the LiF layer. Electroforming is found to be associated with electroluminescence from the light-emitting polymer layer, indicating the injection of holes via the LiF layer. We found that electroforming is essentially a minority carrier effect involving hole injection into a dielectric that becomes progressively filled with defects. Electroluminescence from the light-emitting polymer is found to be a sensitive method to detect minority carrier injection.

Chapter 6 focuses on the electroforming of 7 different alkali halides contained in a bilayer MIM stack with spirofluorene polymer. The voltage needed to induce electroforming was found to vary for the different alkali halides and correlates with the energy of their valence band edge. Optical measurements indicate the formation of defects in the alkali halide during electroforming that are identified as color centers with absorption in the 700 to 1400 nm spectral region. Within the series of selected alkali halides, the voltage corresponding to the onset of defect formation was also found to correlate with the energy of the valence band edge. Electroluminescence originating from the semiconducting polymer was observed during the electroforming process. This is explained by the accumulation of holes in the alkali halide that eventually are injected into the light-emitting polymer and can be detected through electroluminescence. This confirms that electroforming is related to hole injection into the alkali halide and the

voltage needed for electroforming correlates with the injection barrier expected for holes.

Chapter 7 describes experimental evidence for formation of quasi-Ohmic contacts for both holes and electrons with the same LiF layer. Electroluminescence was observed from an organic light-emitting diode under both positive and negative applied bias voltages. Pre-conditioning of the LiF layer by high bias voltage stress was found to induce significant improvements in carrier injection. The formation of quasi-Ohmic contacts is attributed to the formation of charged defects. Non-volatile resistive switching of the diodes is found to occur under both positive and negative write and erase voltage pulses. The memristive behavior is interpreted in terms of voltage induced changes in the ionization state of the defects in the LiF layers. To explain the formation of quasi-Ohmic contacts for both holes and electrons, we argue that both positively and negatively charged defects should exist. High density of positively charged defects near a LiF / metal contact allow for electron injection, and a high density of negatively charged defects allows for hole injection. If now, for instance, defects are predominantly charged negative near the negative electrode, the contact will be blocking. The resistive switching can now be explained in terms of a switch of a contact between a blocking and a quasi-Ohmic configuration, due to changes in ionization state of the defects.

Summarizing the research described in this thesis shows that the organic / inorganic interface in metal / inorganic semiconductor / organic semiconductor / metal electronic devices plays an important role during the electroforming of the initially insulating diodes into an active memristor. Trapping of electrons at this interface initiates a cascade of processes involving accumulation of charged defects in the inorganic semiconductor. The totality of the initial trapping of electrons and the subsequent defect accumulation make up the electroforming. Finally, reversible ionization of defects could be the cause for non-volatile switching of the memory diode resistance. The incorporation of an internal organic / inorganic interface in the memristor structure provides an interesting tool to investigate, manipulate, and stabilize the electroforming process in memristors.

Samenvatting

Elektroformereren en het schakelen van elektrische weerstand in hybride organisch-anorganische geheugens

Sommige diodes vertonen memristieve eigenschappen. Hun elektrische weerstand is schakelbaar en hangt af van eerder aangelegd elektrisch voltage. De elektrische weerstand van memristor diodes hangt dus af van hun geschiedenis. De veranderingen in weerstand zijn vaak reversibel en metastabiel. Hierdoor kunnen memristoren toegepast worden in opslag en verwerking van informatie. De mogelijkheid tot schakeling van de weerstand zorgt ervoor dat de memristor programmeerbaar is in verschillende afzonderlijke weerstandstoestanden. Voor het programmeren worden voltagepulsen met verschillende amplitudes gebruikt. Bij laag voltage treedt het schakelen vaak niet meer op en kan de toestand van het geheugen uitgelezen worden zonder dat de opgeslagen informatie gelijk vernietigd wordt.

Er is een grote verscheidenheid aan materialen die memristieve effecten kunnen laten zien wanneer ze worden verwerkt als actieve laag in een diode, bijvoorbeeld metaaloxides en alkalihalogeniden. Het mechanisme van het schakelen van de weerstand is nog grotendeels onbekend.

Om een diode te krijgen waarvan de weerstand schakelbaar is, moet de diode vaak eerst éénmalig aan een hoge elektrische spanning blootgesteld worden. De elektrische velden in de diode komen dan dicht bij de kritische grens voor diëlektrische doorslag. Dit proces om de diode om te vormen tot geheugencel staat ook wel bekend als elektroformereren. Elektroformereren komt voor in veel elektrische componenten als ze aan (te hoge) spanning blootgesteld worden en verlaagt de stabiliteit en levensduur van o.a. transistoren, condensatoren en lichtgevende diodes.

Het doel van dit proefschrift is het onderzoeken van het elektroformereren in organische-anorganische hybride diodes met als einddoel een betere controle te verkrijgen over de schakeling van de weerstand en degradatie van diodes.

Hoofdstuk 1 van dit proefschrift geeft een inleiding in de uitdaging van de moderne elektronische geheugentechnologie. De beperkingen van de huidige NAND flash technologie die nu in USB sticks gebruikt wordt, worden eerst besproken. Vervolgens wordt gekeken of memristor technologie een alternatief kan bieden voor NAND flash. De opbouw van de memristor en de materialen die daarvoor gebruikt kunnen worden passeren vervolgens de revue. Zoals hierboven besproken, moeten memristoren eerst geactiveerd worden d.m.v. elektroformereren voordat hun weerstand schakelbaar is. Het elektroformereren is een groot nadeel van memristor technologie doordat er tijdens het elektroformereren er altijd een zeker risico bestaat op het ontstaan van een permanente elektrische kortsluiting door de hoge spanningen die daarbij gebruikt worden. Deze permanente kortsluiting kan ontstaan door bijv. oververhitting.

Memristoren met hybride actieve laag van organische en anorganische materialen blijken relatief goed bestand te zijn tegen zulke permanente kortsluitingen tijdens het elektroformer.

Hoofdstuk 2 geeft een overzicht van het elektroformer van memristor diodes met een tweelaagsstructuur, bestaande uit een anorganische Al_2O_3 laag en een laag van organisch, halfgeleidend polymeer. Het schakelen van de weerstand van deze memristoren van hoog naar laag en van laag naar hoog kan met voltage pulsen van dezelfde polariteit. Het hoofdstuk begint met een overzicht van experimentele resultaten van Al_2O_3 / polymeer diodes. Het elektroformer wordt toegeschreven aan het ontstaan van defecten die zich organiseren tot elektrisch geleidende filamenten. De schakelbaarheid van de weerstand en de bijbehorende elektrische bistabiliteit worden kwalitatief geïnterpreteerd door een coëxistentie van neutrale en geleidende fases in de memristor.

Het elektroformer van metaal-isolator-metaal (MIM) diodes waarbij de isolator bestaat uit een laag van Al_2O_3 of alkalihalogenide gecombineerd met een laag halfgeleidend polymeer wordt onderzocht in hoofdstuk 3 tot en met 6. Het blijkt dat het elektroformeerproces als geheel onderverdeeld kan worden in een aantal deelstappen die elkaar in de tijd opvolgen. De initiële processen blijken nog grotendeels reversibel, terwijl de laatste stap in het elektroformeerproces onomkeerbaar is.

Hoofdstuk 3 en 4 beschrijven het beginstadium van het elektroformer in MIM diodes. In het vroegste stadium, waarbij de aangelegde spanning nog laag is, vindt ophoping van elektronen aan het organisch / anorganisch grensvlak plaats. De elektronen worden hier ingevangen door toestanden met laag energieniveau. Het feit dat er ingevangen ladingen binnenin de MIM structuur zitten, induceert een herverdeling van het aangelegde elektrische potentiaalverschil over de organische en anorganische lagen. De gevangen elektronen die aan het begin geïnjecteerd werden in de polymeer laag, zorgen ervoor dat de aangelegde spanningsverschil nu grotendeels over de anorganische laag valt. Dit initieert de elektrische vorming. De ladingsdrager ophoping bij het Al_2O_3 / polymeer grensvlak, beschreven in hoofdstuk 3, werd gemeten met de quasi-statische capaciteits-voltage techniek.

Ook in van LiF / polymeer diodes bestaat de initiële, reversibele stap in het elektroformer uit het ophopen van elektronen bij het interne anorganisch / organisch grensvlak van de diode. Hoofdstuk 4 bespreekt de elektrische en optische karakterisatie van LiF / polymeer diodes tijdens het elektroformer. Na het invangen van elektronen in de diepe toestanden aan het polymeer/alkalihalogenide grensvlak ontstaan er positief geladen defecten in het LiF. De dichtheid van positief geladen defecten in het LiF in de buurt van het LiF / polymeer grensvlak kort voor de laatste irreversibele stap van het elektroformer, schatten we op $10^{19} / \text{cm}^3$. Deze waarde voor de defectconcentratie ligt dicht bij de kritische dichtheid die verwacht wordt voor een isolator-naar-metaal overgang.

In hoofdstuk 5 en 6 ligt de nadruk op de latere stadia van het elektroformeerproces van LiF / polymeer, die geïnduceerd worden door voltages hoger dan de voltages nodig voor de initiële stappen van het elektroformer en besproken in hoofdstuk 3 en 4.

In hoofdstuk 5 laten we zien dat de finale stap van het elektroformer in LiF / polymeer diodes zich voltrekt bij 15 V. Het benodigde voltage blijkt nagenoeg onafhankelijk te zijn van de dikte van de LiF laag. Het elektroformer blijkt bovendien nauw samen te hangen met elektroluminescentie van de licht-emitterende polymeer laag. Deze correlatie tussen elektroformer en elektroluminescentie wijst erop dat elektroformer verband houdt met de injectie van positieve ladingsdragers in de LiF laag. Onder de gegeven omstandigheden lijken de geïnjecteerde gaten in de minderheid ten opzichte van de geïnjecteerde elektronen. Elektroluminescentie van het licht-emitterende polymeer blijkt een gevoelige methode te zijn om de injectie van de minderheidsladingsdragers te detecteren.

In hoofdstuk 6 wordt de chemische structuur van het alkalihalogenide in de hybride diodes gevarieerd. Het elektroformer van zeven verschillende alkalihalogeniden wordt onderzocht in diodes met een spirofluoreen polymeer. Het voltage dat nodig is voor het volledig elektroformer blijkt te correleren met de energie van het hoogste gevulde elektronenniveau in het alkalihalogenide. Optische metingen wijzen op het ontstaan van defecten in de alkalihalogenides gedurende het elektroformer. Deze defecten vertonen overeenkomsten met de zgn. kleurcentra in alkalihalogenides. Kleurcentra bestaan uit halogenide vacatures in het rooster en vertonen karakteristieke absorptiebanden in het ultraviolette en zichtbare gedeelte van het spectrum. In de homologe reeks van alkalihalogeniden vinden we een correlatie van het voltage dat nodig is om kleurcentra te induceren met de energie van de hoogste kant van de valentieband. Samen met de elektroluminescentie van het halfgeleidende polymeer, duidt deze correlatie erop dat het elektroformer samenhangt met injectie van positieve ladingsdragers (gaten) in het alkalihalogenide.

Hoofdstuk 7 beschrijft het experimentele bewijs voor het ontstaan van quasi-ohmse contacten voor zowel gaten als elektronen van de polymerfase met dezelfde LiF laag. Op het eerste gezicht druist de vorming van ohmse contacten van eenzelfde materiaal voor zowel gaten als elektronen, in tegen de algemene verwachting. Waarneming van elektroluminescentie voor zowel positief als negatief voltage vormt echter direct experimenteel bewijs. Een mogelijke verklaring voor dit tegen-intuïtieve gegeven wordt ingegeven door de additionele waarneming dat de LiF lagen geruime tijd blootgesteld moeten worden aan een hoog spanningsverschil voordat ze ohmse karakteristieken gaan vertonen krijgen. Het ontstaan van quasi-ohmse contacten schrijven we daarom toe aan het ontstaan van geladen defecten. De omschakeling van een LiF laag van gaten injectie naar elektronen injectie kan verklaard worden door verandering van de ionisatie toestand van de defecten. Interessanterwijze vertonen de LiF/ polymeer diodes met de schakelbare ohmse contacten ook geheugen eigenschappen. Dit leidt ons tot de

stelling dat het schakelen van de elektrische weerstand in hybride organisch-anorganische geheugens het gevolg is van veranderingen in de ionisatie toestand van defecten in de anorganische component. Als de defecten hoofdzakelijk negatief geladen zijn, zouden we efficiënte injectie van gaten mogen verwachten, zijn de defecten daarentegen negatief geladen dat zou elektronen injectiegaten kunnen domineren. Een diode met LiF / polymeer / LiF structuur en beide LiF lagen gedoteerd met negatief geladen defecten zou al bij lage spanning een grote gatenstroom kunnen laten zien. Schakelt nu één van de lagen om naar overwegend positief geladen defecten, dan verwachten we een diode met veel hogere weerstand bij lage spanning.

Samenvattend, het onderzoek beschreven in dit proefschrift laat zien dat het organisch / anorganisch grensvlak in metaal / anorganische halfgeleider / organische halfgeleider / metaal diodes een cruciale rol speelt tijdens het elektroformer van de aanvankelijk isolerende diodes tot actieve memristoren. Elektronen die ingevangen worden in toestanden met lage energie aan het anorganisch / organisch grensvlak, initiëren een cascade aan processen waarbij geladen defecten zich gaan ophopen in de anorganische halfgeleider. De ophoping van geladen defect leidt tot de uiteindelijke geëlektroformeerde toestand met programmeerbare elektronische eigenschappen. In deze geformeerde toestand kan reversibele verandering van de ionisatietoestand van de defecten, de elektrische eigenschappen van de diode drastische veranderen. De verandering van ionisatietoestand kan aanleiding geven tot een schakelbare elektrische weerstand en een niet-vluchtig geheugen effect in de memristor. Het inbouwen van een organisch / anorganisch grensvlak in een memristor biedt dus interessante handvatten om het elektroformeerproces in memristors te bestuderen, manipuleren, en te stabiliseren.

Résumé

Electroformation et commutation de résistance de mémoires organique-inorganique

La commutation de résistance est un effet memristif qui fait appel à la dépendance de la résistance électrique d'une diode en fonction de la tension appliquée précédemment, i. e. en fonction de l'histoire électrique de la diode. Les changements de résistance sont souvent réversible et métastables, envisageant l'application des diodes à memristance pour le stockage ou le traitement de données. La commutation de résistance permet la programmation du memristor en états résistifs distincts par l'application de tensions ayant des amplitudes bien définies. De basses tensions sont utilisées pour la lecture de l'état dans lequel se trouve la mémoire.

Une grande variété de matériaux peuvent montrer un effet memristif lorsqu'ils sont intégrés comme couche active d'une diode, e. g. oxydes métalliques et composés halogénés alcalins. Le mécanisme physique de commutation de résistance réversible est en grande partie inconnu.

Souvent, l'application d'un haut champ électrique, proche de la tension de claquage du matériau de la couche active, est nécessaire pour permettre la commutation de résistance. L'effet initiateur produit par l'application d'un haut champ électrique est communément appelé électroformation. L'électroformation est rencontrée dans une multitude de composants électriques, affectant ainsi la stabilité et la durée de vie de fonctionnement de transistors, condensateurs et diodes électroluminescentes, comprenant aussi celles organiques et à base petites molécules et de polymères.

Le but de cette thèse consiste en l'étude de l'électroformation de diodes hybrides organiques-inorganiques avec le but ultime d'acquérir un meilleur contrôle sur la commutation de résistance et le claquage de ces diodes.

Le chapitre 1 de cette thèse donne une introduction à propos du défi technologique des mémoires. Les limitations et l'actuel état de l'art de la technologie flash NAND sont présentés et discutés. La technologie alternative des memristors est introduite et comparée à la NAND flash. La structure du memristor ainsi que les matériaux sont définis. Les memristors ont besoin d'être activés par électroformation. L'électroformation représente un sérieux inconvénient de la technologie des memristors à cause de la possibilité de court-circuit électrique permanent provoqué durant l'électroformation à travers une surchauffe. Les memristors ayant des couches isolantes organiques et inorganiques ont démontré être relativement résistants au risque de court-circuit électrique durant l'électroformation.

Le chapitre 2 est une revue explicative à propos de l'électroformation et de la commutation unipolaire des diodes memristors ayant une architecture comprenant une couche inorganique d' Al_2O_3 ainsi qu'une couche organique de polymère semi-conducteur.

Le chapitre commence par une vue d'ensemble des résultats expérimentaux des diodes Al_2O_3 / polymère. Le processus d'électroformation est décrit en terme de formation de défauts qui s'organisent en filaments conducteurs. La commutation de résistance ainsi que la bistabilité qui lui est associée sont interprétées qualitativement par la coexistence de phases neutre et conductrice dans le memristor.

L'électroformation de diodes métal-isolant-métal (MIM) avec un isolant pouvant être soit une couche d' Al_2O_3 , soit de composés halogénés alcalins en combinaison d'une couche de polymère semi-conducteur est étudiée à travers les chapitres 3 à 6. Le processus d'ensemble de l'électroformation est constaté se produisant en une séquence d'étapes. Les étapes initiales restent réversibles alors que l'étape finale est quand elle irréversible.

Les chapitres 3 et 4 décrivent l'électroformation de diodes MIM durant les étapes initiales. Initialement, à basse tension, se produit l'accumulation et le piégeage d'électrons à l'interface organique / inorganique. Le piégeage de charges à l'intérieur même de la structure MIM provoque la redistribution de la différence de potentiel électrique sur les couches organique et inorganique. Le piégeage d'électrons initialement injectés dans la couche de polymère, transfère une grande partie du voltage appliqué à la couche inorganique, ce qui a pour effet d'initier l'électroformation. L'accumulation de porteurs de charge à l'interface interne des couches organique / inorganique, est étudiée dans le chapitre 3 au moyen de la technique quasi-statique de mesure de la caractéristique capacité-voltage. L'état initial réversible de l'électroformation des diodes fluorure de lithium (LiF) / polymère, tel que décrit dans le chapitre 4, implique également l'accumulation d'électrons à l'interface interne LiF / polymère.

Dans le chapitre 4, les caractérisations électriques et optiques de ces diodes apportent l'évidence de la formation de défauts chargés positivement dans le LiF qui se produisent après le piégeage d'électrons. L'estimation de la densité de défauts chargés positivement dans le LiF, juste avant que se produise l'étape finale et irréversible de l'électroformation, est de l'ordre de 10^{19} / cm^3 à proximité de l'interface interne LiF / polymère, ce qui est proche de la densité critique attendue pour la transition métal-isolant.

Les chapitres 5 et 6 portent sur les étapes plus avancées de l'électroformation des diodes comprenant du LiF ainsi que d'autres composés halogénés alcalins. Ces étapes se produisent à des tensions plus élevées que celles utilisées dans les chapitres 3 et 4. Dans le chapitre 5, l'électroformation est trouvée se produire à des tensions d'environ 15 V, pratiquement indépendamment de l'épaisseur de la couche de LiF. L'électroformation est associée à l'électroluminescence de la couche de polymère semi-conducteur et émetteur de lumière, ce qui indique l'injection de trous via la couche de LiF. Nous avons trouvé que l'électroformation est essentiellement un effet mettant en jeu les porteurs minoritaires, impliquant l'injection de trous dans un matériau diélectrique qui devient progressivement rempli de défauts. L'électroluminescence du polymère émetteur de lumière se trouve être une méthode sensible pour détecter l'injection de porteurs minoritaires.

Le chapitre 6 est basé sur l'électroformation de 7 composés halogénés alcalins insérés dans la structure MIM en association avec le polymère spirofluorène. La

différence de potentiel requise pour provoquer l'électroformation montre des variations pour les différents composés halogénés alcalins qui sont en corrélation avec l'énergie de leur bande de valence respective. Des mesures optiques indiquent la formation de défauts dans le composé halogéné alcalin pendant l'électroformation qui sont identifiés étant des centres colorés avec une absorption spectrale comprise entre 700 et 1400 nm. Parmi la série des composés halogéné alcalins sélectionnés, le voltage correspondant au commencement de la formation de défauts a aussi été trouvé être en corrélation avec l'énergie de leur bande de valence respective. L'électroluminescence provenant du polymère émetteur de lumière a pu être observé durant le processus d'électroformation. Cela peut-être expliqué par l'accumulation de trous dans le composé halogéné alcalin qui sont éventuellement injectés dans le polymère émetteur de lumière, ce qui peut être détecté grâce à son électroluminescence. Cela confirme que l'électroformation est liée à l'injection de trous dans le composé halogéné alcalin et que la différence de potentiel nécessaire à l'électroformation est en corrélation avec la barrière d'injection attendu pour les trous.

Le chapitre 7 décrit expérimentalement l'évidence de la formation de contacts quasi-Ohmiques pour trous et électrons à partir de la même couche de LiF. L'électroluminescence du polymère émetteur de lumière a ainsi pu être observée sous des voltages appliqués positif et négatif. Le pré-conditionnement de la couche de LiF, soumis à un voltage élevé, a montré une amélioration considérable de l'injection de porteurs. La formation d'un contact quasi-Ohmique est attribué à la formation de défauts chargés. La commutation de résistance non-volatile de ces diodes est trouvé se produire sous des tensions pulsées d'écriture et d'effacement positives et négatives. Le comportement memristif est interprété en termes de changements induits par un voltage de l'état d'ionisation des défauts dans les couches de LiF. Pour expliquer la formation de contacts quasi-Ohmique pour trous et électrons, nous affirmons que des défauts chargés positivement et négativement doivent exister. Une haute densité de défauts chargés positivement proche du contact LiF / métal permet l'injection d'électrons ainsi qu'une haute densité de défauts chargés négativement permet l'injection de trous. Admettons, par exemple que les défauts sont principalement chargés négativement à proximité de l'électrode négative, alors le contact sera bloquant. La commutation de résistance peut maintenant être expliquée en terme de commutation de la configuration du contact entre bloquant et quasi-Ohmique, provoqué par le changements de l'état d'ionisation des défauts.

En résumé, la recherche décrite dans cette thèse montre que l'interface organique / inorganique dans des diodes électroniques du type métal / semi-conducteur inorganique / semi-conducteur organique / métal joue un rôle important pendant l'électroformation de la diode initialement isolante en un memristor actif. Le piégeage d'électron à l'interface initie une cascade de processus mettant en jeu l'accumulation de défauts chargés dans le semi-conducteur inorganique. L'ensemble constitué du piégeage initial d'électrons ainsi que l'accumulation de défauts qui s'en suit produit l'électroformation. Finalement,

l'ionisation réversible des défauts pourrait être la cause de la commutation de résistance non-volatile de la diode a mémoire. L'incorporation d'une interface interne organique / inorganique dans la structure du memristor procure un outil intéressant pout l'investigation, la manipulation et la stabilisation du processus d'électroformation des memristors.

Curriculum Vitae



Benjamin Bory was born on May 14th 1985 in Grenoble, France. After finishing his high school studies by obtaining his scientific baccalaureate in 2003 at Lycée Champollion in Grenoble, he started technical studies in physical characterization at the Institut Universitaire de Technologie of the Université Joseph Fourier in Grenoble. He then moved to the Université Paul Cézanne in Marseille, France, to broaden his knowledge in materials science where he obtained his bachelor degree in 2006. He started a master in materials science at the Université Claude Bernard in Lyon, France. His master project was carried out in apprenticeship at ParexLanko, Saint-Quentin-Fallavier, France, where he studied the blending of polymeric super-plasticizers in mortar formulations. He obtained his master degree in 2008. In 2009, he moved to TNO Science and Industry, Eindhoven, The Netherlands, to work on fabricating piezoelectric composites with tailored properties. In 2010, he started his PhD project at the Eindhoven University of Technology in the group ‘Molecular Materials and Nanosystems’ under the supervision of Prof. René Janssen, Dr. Stefan Meskers, and Prof. Dago de Leeuw. His doctoral research project forms part of the Dutch Polymer Institute (DPI) research program, the most important results are presented in this dissertation.

List of publications

Macromolecular memories, Bory B.F., and Meskers S.C.J., to appear in: Emerging Nanoelectronic Devices (Publisher: John Wiley & Sons, Ltd).

Electroforming and resistive switching in unipolar memristors, B.F. Bory, Q. Chen, A. Kiazadeh, P.R.F. Rocha, D.M. Taylor, H.L. Gomes, D.M. de Leeuw, and S.C.J. Meskers, submitted.

Role of Hole Injection in Electroforming of LiF-Polymer Memory Diodes, B.F. Bory, H.L. Gomes, R.A.J. Janssen, D.M. de Leeuw, S.C.J. Meskers, *J. Phys. Chem. C* **2012**, *116*, 12443-12447.

Opto-electronic characterization of electron traps upon forming polymer oxide memory diodes, Q. Chen, B.F. Bory, A. Kiazadeh, P.R.F. Rocha, H.L. Gomes, F. Verbakel, D.M. de Leeuw, S.C.J. Meskers, *Appl. Phys. Lett.* **2011**, *99*, 083305.

Trapping of electrons in metal oxide-polymer memory diodes in the initial stage of electroforming, B.F. Bory, S.C.J. Meskers, R.A.J. Janssen, H.L. Gomes, D.M. de Leeuw, *Appl. Phys. Lett.* **2010**, *97*, 222106.

Improving the d(33) and g(33) properties of 0-3 piezoelectric composites by dielectrophoresis, D.A. van den Ende, B.F. Bory, W.A. Groen, S. van der Zwaag, *J. Appl. Phys.* **2010**, *107*, 024107.

Properties of Quasi 1-3 Piezoelectric PZT-epoxy Composites Obtained by Dielectrophoresis, D.A. van den Ende, B.F. Bory, W.A. Groen, S. van der Zwaag, *Integr. Ferroelectr.* **2010**, *114*, 108-118.

Acknowledgements

The last page is to thank many people...

My first acknowledgement goes to my first promotor René Janssen. You gave me the opportunity to accomplish my PhD in your excellent group. I am very grateful of working with you and I really appreciated your guidance and wise comments. The daily supervision of Stefan Meskers was a crucial contribution for me. I have learned so much aside you. Stefan, thank you for being so patient and for explaining me your latest idea or novel interpretation. You always guided me such that I could express my opinion and I very much appreciated your involvement in the project. I really enjoyed your company when going to DPI meetings, trips to Faro, or conferences. Finally, Dago de Leeuw, thank you for your determination and confidence in our work and for being the second promotor. I very much enjoyed our meetings and learned from your experience and perspectives. Your pragmatism made these meetings always fruitful. I wish you all the best with your new challenges in Mainz.

I sincerely acknowledge dr. Henrique Gomes, prof. dr. Pim Groen, and prof. dr. Bert de With for taking part in the PhD committee. Henrique, thank you for your contributions to the project. You have always brought new ideas and excellent comments. Thank you also for your very warm welcoming during our visits in Faro. Pim, I really enjoyed my experience at TNO and I am very grateful to you for accepting me in your group and then for recommending me for my PhD position. I really appreciate you accepted to be in my PhD committee.

I sincerely acknowledge the Dutch Polymer Institute for the funding the research and for always providing an excellent environment for the review and annual meetings. John van Haare, thank you for always supporting our research and for making DPI meetings very pleasant. In the DPI project I had the opportunity to collaborate with Paulo, Qian, and Asal. Paulo I really enjoyed meeting you. I remember some great times spent in Faro and during DPI meetings, especially in Arnhem. I wish you all the best in your future career. I would also like to thank Frank Verbakel for following the project with his experience and his global view on the subject. I have been very glad to follow up on the topic you have initiated.

Special words to Daan van den Ende who welcomed me at TNO and gave me the opportunity to work with him on his project. This experience gave me the motivation to do a PhD in the Netherlands. I am very grateful to Olavio who welcomed me and introduced me to Eindhoven. Bart and Marcel I am glad I have met you and wish a lot of good things.

I would like to warmly thank the secretaries of SMO: Carine, Patricia, Joke, Nora, Jolanda and Martina for making complicated things easy. I enjoyed sharing my office with my officemates: Bastiaan, Renaud, Julia, Véronique, Dominique, Mindaugas, Rafa, Serkan, Tom, and Mike. Tom is sincerely acknowledged for the translation of my summary into Dutch. Véronique, thanks your good mood, for bringing cakes, and explaining about Dutch specialties. Mindaugas I enjoyed sharing the office, some trappists, and meals with you. Serkan thank you for your good mood, and willingness to do funny things, your other officemates should be glad to have you.

Daniele, I think we understand each other's quite well. Our trip into Death Valley was extremely pleasant, the time spent in San Francisco as well! I am glad you enjoy your new

experience in England and don't forget that it is all about doping! Dominique I really liked your company and especially to annoy you. I wish you many good things with Anastasia and all your cats. Dhritiman, I appreciate your honesty and broad knowledge on many topics. I wish you a bright career. Jingxin, thank you for helping to get some last results for my thesis. I am sure you will write a very good and interesting report.

Many group members are thanked for their daily help and sharing the facilities: Ratheesh, Sandra, Alice, Nic, Gijs, Koen, Hans, Stefan O., and Martijn. Bas and Jolanda are acknowledged for taking care of our safety in the lab. Henk, thank you for making the best coffee in the Netherlands. I also enjoyed discussing or collaborating with Miguel, Jessica, Sacha, and Andrey.

I would like to thank the people with whom I have spent some unforgettable moments. Camille D, thank you for being so unique and always in a creative mood. I am looking forward to meeting with you again and again, together with Dario. Matthieu, still I have never been to Berlin; maybe now is the time to get there! Thank you for always inviting me for chat and beers. Camille C, I enjoyed sharing meals and drinks with you. Sami, Christophe, Romain, and Olivier, thank you for your French support. Raf thank you for your advised rugby expertise and for your Alsatian mood.

Ivelina you are a great person. Everywhere you will settle down with Nico and Gabi, I wish you all the best. Gosia we had some unforgettable snowboard experience. You were the only person I met that could talk about biathlon as a professional. Thank you for your creativity and for always being special! I am looking forward to your defense! Ola, thank you for always being in for parties. Isabelle, I hope we will stay in touch; Belgium is not that big so we might be able to see each other.

Many other people that I have enjoyed meeting and from who I have learn something about food, culture, science, geopolitics... Sabriye, Hans, Bahar, Martin F., Gozde, Seda, Alberto P., Alberto C., Evert, Attila, Ard, Ece, Fabian, Natalia, Baris, Delei, Beulah, Marcos, Vladimir, Gorkan, Mauricio, Kartik, Donglin, J.-P., Domenico, Bruno, Valentino, Pedro, Brenda, Can, Anna, Théo, Sam, Penny, Maria, and Jorge...

I enjoyed playing voetbal with my teammates Miguel, Esteban, Joost, Tom, Wilco, Miran, Slavisa, Evgeniy, Mark, and Carlos in the following teams: de Vlackers, Superstars, Spartak SPC. The mathematicians, Botond, Martin, Susana, Stella, and Paulo are thanked for the nice times spent together.

All my friends from Grenoble with whom I could not spend much time with during the past 4 years but with whom I have great fun meeting them. Specifically acknowledged those who dared to come and visit me (for Queen's day): Bob Bob, Joppy (x2), Momone (x2), Youyou, Chloé, Trivet, and Marion, but I also thank Paté, Nathalie, Dada, Anne-Laure, Tof, Flopette, Niam, Gluglu, Juju, Rav'chou, Vince, Guitou, and Frigo for their friendship.

I would like to acknowledge my parents, brothers, and family that have always supported me in all of my choices. Bernadette and Virginie are thanked for their warm welcoming in the Belgian Ardennes.

My last words go to Florence with whom I am extremely happy to share so much. Thank you for your patience, generosity, and happiness. Merci.